

# **Environmentally friendly baths for Cu-Sn co-electrodeposition: cyanide-free aqueous bath and deep eutectic solvents**

**Sujie Xing**



---

October 2014



## **Abstract**

This thesis describes the work of my Ph.D studies in Industrial Engineering during past three years. It regards preparation of copper-tin alloys from green solvents for decorative purposes. Actual industrial process involves cyanide based complex bath in order to produce white bronze layers and they often contain lead as brightener and whitener. The aim of the thesis is to develop a more environmental friendly process for white bronze electrodeposition. Two different electrolytes were considered as eligible candidates: one involves a simple organic acid aqueous solution as bulk electrolyte, and the other one is a new deep eutectic solvent bath.

The investigation of electrodeposition using methanesulfonic acid as complexing agent considered a commercial bath and its optimization in order to be used in the decorative industry. The focus of the study was on the optimization of deposition parameters and verification of bath and deposit stability which was very important from industrial point of view. Obvious improvements on deposits quality and bath stability can be realized by replacement on anode material and utilization of pulse current.

Contrary to that, research on electrodeposition from deep eutectic system was quite new and few relevant studies can be referred especially in the field of alloys. As a result, this work started from deposition of single metal for better understanding of behaviors of mixtures between choline chloride and ethylene glycol or urea. Successful deposition of copper-tin alloys can be carried out under warmed conditions and variation on film composition can be controlled by changing concentrations of metallic salts in the bath. Pulse current acted as an effective tool to refine microstructure of deposits in a similar way as in aqueous solvents. Since no brightener was added, reduced luster was observed here and working mechanism of additives was found to be rather different from that in conventional baths.

In summary, operation parameters including temperature, salt concentration, anode material and supporting electrolytes influence the resultant properties of deposits in great extent. Deposit quality from both solvents can be improved by using pulse current with proper frequency.

## **Acknowledgments**

It is a pleasure to thank all the people who made this thesis possible.

First I would like to express my deep gratitude to my supervisors Professor Flavio Deflorian and Dr. Caterina Zanella for their guidance, support and approachability throughout my PhD. Their friendly and easygoing nature made my stay in Italy an excellent and unforgettable memory. I have learnt a great deal from our legendary long discussions and will count them as a huge influence on my future career. Their generosity and continuous support helped me go through my most important three years in my life. Each time I met difficulty either in life or in research, their considerate and guidance turned to be the strongest encouragements to me. Meanwhile their rigorous and careful spirit on science will influence my whole life. I learnt various experimental skills and research thoughts from their liberating attitude towards scientific innovation realization.

I gratefully acknowledge Mr. Luca Benedetti for his kind help in SEM analysis and essential advice in the experimental set-up. I would like to thank all lovely colleagues in the Corrosion Control Laboratory, Professor Stefano Rossi, Luizgustavo Ecco, Annalisa Cataldi and Michele Fedel who made this lab a big and warm family. I appreciate all the time with all of you, from the congress trips, annual dinners, snack breaks to everyday work, there were so many memorable moments and joys. I will treasure the friendship with you and miss you in the future.

I would also like to thank Professor Alberto Quaranta for his help in ultraviolet microscopy measurements and Dr. Devid Maniglio in Laser Confocal Microscopy.

A special thank goes to the coating company of “Safilo Group” for the invaluable help and financial supports.

# Contents

Abstract .....	i
Acknowledgments .....	iii
Contents .....	v
1 Introduction.....	1
1.1 Electrodeposition of Cu-Sn from $CN^-$ based bath.....	3
1.2 Electrodeposition of Cu-Sn from alternative baths .....	5
1.3 Introduction of Ionic Liquids .....	7
1.3.1 History of Ionic Liquids.....	8
1.3.2 Deep Eutectic Solvents .....	10
1.3.3 Deposition of metals from eutectic mixtures based on choline chloride.....	14
1.3.4 Synthesis of Ionic Liquids.....	18
1.3.5 Physical Properties.....	19
1.3.6 Industrial Applications of Ionic Liquids .....	24
1.4 Electrodeposition from ethaline .....	26
1.4.1 Electrodeposition of Cu from ethaline and reline .....	26
1.4.2 Electrodeposition of Sn from ethaline .....	28
1.4.3 Electrodeposition of Cu-Sn from ethaline .....	30
1.5 Pulse plating .....	30
1.6 Project aims .....	32
1.7 References .....	34
2 The Electrodeposition of Copper-Tin Alloys using Aqueous Solvents....	47
2.1 Effect of direct current density on the composition of deposited coatings.....	48
2.2 Effect of anode on the stability of the bath .....	55
2.3 Effect of pulse frequency on the composition.....	61

2.4	Microstructure and electrochemical properties of deposited coatings	62
2.5	Conclusions .....	69
2.6	References .....	71
3	Electrodeposition of Copper from Deep Eutectic Solvent based on mixture of Choline Chloride and Ethylene Glycol.....	73
3.1	Physical properties .....	74
3.2	Speciation of $\text{Cu}^{2+}$ .....	79
3.3	Cyclic voltammetry .....	83
3.4	Effect of temperature.....	86
3.5	Effect of concentration .....	92
3.6	Galvanic deposition: direct current vs. pulse current .....	98
3.7	Conclusions .....	103
3.8	References .....	105
4	Electrodeposition of Tin from Deep Eutectic Solvent based on mixture of Choline Chloride and Ethylene Glycol .....	107
4.1	Voltammetric behavior.....	108
4.2	Chronoamperometric investigations.....	113
4.3	Potentiostatic deposition.....	116
4.4	Influence of agitation speed .....	117
4.5	Morphology characterization .....	119
4.6	Effect of nicotinic acid additive on the Sn deposition.....	122
4.6.1	Voltammetric behavior .....	123
4.6.2	Chronoamperometric study.....	125
4.6.3	Surface morphology .....	126
4.7	Conclusions .....	128
4.8	References .....	129
5	Electrodeposition of Copper-Tin from Deep Eutectic Solvent based on mixture of Choline Chloride and Ethylene Glycol .....	132
5.1	Cyclic Voltammetry .....	133

5.2 Chronocoulometry .....	135
5.3 Electrodeposition from ethaline containing 0.2 M CuCl <sub>2</sub> +0.2 M SnCl <sub>2</sub> · 2H <sub>2</sub> O .....	138
5.3.1 Galvanostatic deposition .....	138
5.3.2 Surface morphology and composition of deposit .....	140
5.4 Electrodeposition from ethaline containing 0.1 M CuCl <sub>2</sub> +0.3 M SnCl <sub>2</sub> · 2H <sub>2</sub> O .....	144
5.5 Electrodeposition from ethaline containing 0.05 M CuCl <sub>2</sub> +0.3 M SnCl <sub>2</sub> · 2H <sub>2</sub> O .....	148
5.5.1 Galvanostatic deposition .....	150
5.5.2 Pulse deposition .....	152
5.6 Conclusions .....	158
5.7 References .....	160
6 Conclusions and future work .....	161
6.1 Conclusions .....	161
6.2 Future work .....	165



# **1 Introduction**

In decorative applications, nickel is routinely used as an undercoat for noble metal finishes. However, nickel is a known skin allergen and should avoid contacting human skin such as jewelry<sup>[1]</sup>. Bronze coatings, CuSn(Zn), are a known alternative to nickel for their good corrosion resistance, ductility and solderability and therefore are widely used in many different applications<sup>[2]</sup>. As coatings, bronze can be prepared by electrodeposition.

Electrodeposition or electroplating is a process in which metal ions in a bath are stimulated by an electric field to deposit materials on a conductive substrate. The process uses electrical current to reduce metallic cations from a bath and produces a layer of metal or alloy with required physical and chemical properties. The deposited material can give a desired property to a surface that lacks that property. Alloys are materials consisting of two or more elements at least one of which being a metal and all the elements are combined in a way they cannot be readily separated by physical means.

The improved mechanical properties, corrosion resistance and optical characteristics of alloys compared to their pure component elements make them widely applied in industrial productions.

At present, hundreds of alloys are being prepared using electrodeposition. Most widespread are the alloys based on the metals of Fe group, the first group (Cu, Ag, Au), and noble metals. For instance, protective-decorative layers as NiZn<sup>[3]</sup>, NiSn<sup>[4]</sup>, CuSn<sup>[5]</sup>, NiAu<sup>[6]</sup>, corrosion resistant layers as ZnSn<sup>[7]</sup>, CdSn<sup>[8]</sup>, solderable coatings as SnSb<sup>[9]</sup>, SnNi<sup>[10]</sup>, magnetic alloys as NiFeCo<sup>[11]</sup> have been extensively applied by electroplating in engineering. These electrodeposited alloys often feature properties and performance that are much better than individual metal. This is true in particular in regard to wear resistance, hardness and corrosion stability.

The alloy between copper and tin (sometimes a small amount of zinc) is known as bronze. Bronze containing Sn  $\leq$ 12 wt% shows copper color and the alloys containing 12~20 wt% of tin have golden-yellow color<sup>[12]</sup> which are often used as corrosion-protective layers for steel in hot water<sup>[13]</sup>. At higher tin content the alloys turn white in color and exhibit lower porosity and higher hardness<sup>[14]</sup>. They can be used as electrical contacts<sup>[15]</sup> and also as a replacement of nickel in decorative jewelry<sup>[16]</sup>.

The electrocodeposition of Cu-Sn is a more complicated process compared with the deposition of copper or tin since it meets two significant challenges during deposition: first, Sn has more than one oxidation state. In the absence of additives, the bath becomes turbid easily because divalent tin salt in the bath can be readily oxidized to tetravalent tin producing colloidal particles of tin oxide hydrate. In addition, the oxidation of stannous ions may be unavoidable leading to porous and whiskery layers. The stability of stannous ions is very sensitive not only to the presence of additives but also

nature of acid in solution, the anode material and agitation type (mechanic, air flow). Second, electrodeposition of alloys will also become difficult because of the large difference (around 0.5V) between the standard reduction potentials of Cu, +0.34V vs. SHE and tin, -0.14V vs. SHE<sup>[17]</sup>. The co-deposition of Cu-Sn alloys can be facilitated by the inclusion of additives shifting the metal reduction potentials<sup>[18]</sup>. As a consequence, development of suitable electrodeposition bath and optimization of operation parameters is overall a more difficult research issue.

The electrolyte is an ionic conductor, where chemical species of interest are dissolved into a suitable solvent which is most often water, but recently various ionic liquids are being considered<sup>[19]</sup>. This study will be concerned with electrodeposition from both aqueous solutions and ionic liquids.

## **1.1 Electrodeposition of Cu-Sn from CN<sup>-</sup> based bath**

Cyanide compounds were frequently used in plating baths because they are capable of adopting a wide range of electrical current, removing tarnish or other undesirable films from surfaces to be plated<sup>[20]</sup>. They are favorable to lower sensitivity to impurities present in the bath for the metal deposit to obtain an even layer. Metals coatings of cadmium<sup>[21]</sup>, iron<sup>[22]</sup>, gold<sup>[20]</sup>, and zinc<sup>[20]</sup> often use cyanide compounds. Typically cyanide will complex with plating metals, or is added to the bath as sodium cyanide or potassium cyanide.

In the field of alloy electroplating, it has been long that cyanide is used as a complexing agent in baths to allow precious metals to be plated<sup>[23]</sup> and to allow alloy deposition with varying plating potentials<sup>[24]</sup>. For the

preparation of alloys which copper was deposited as a component, cyanide has been adopted to form cyanide-copper complex which allowed the co-deposition of relative nobler Cu with other metals so that alloys can be deposited from cyanide based baths<sup>[25]</sup>. One of the outstanding properties of cyanide copper baths is excellent throwing power and metal distribution ratio, especially for those randomly shaped articles which need to be plated<sup>[25]</sup>.

The electrodeposition of Cu-Sn was also traditionally carried out in cyanide based baths. This is because cyanide can complex copper effectively reducing of its depositing potential. It becomes necessary since copper is a nobler metal which can be more easily deposited compared to tin which shows lower electrode potential. The addition of cyanide ions into the bath can be beneficial to the simultaneous deposition of copper and tin at approximate same potentials<sup>[26]</sup>.

Although cyanide-based baths produce bronze coatings of high quality, they operate at elevated temperatures, display insufficient current efficiency and are high toxic which requires costly industrial wastewater treatment for the correct disposal of cyanide in the environment<sup>[27]</sup>. In addition, these baths are usually alkaline baths that often contain lead compound as grain refiner. This does not make these baths a viable alternative<sup>[1]</sup>.

Moreover, cyanide exposure may cause inhalation, ingestion, or absorption through skin or mucous membranes. Most cyanide compounds are extremely poisonous. Overexposure to these compounds will interfere with the operation of the metabolic system and can cause rapid death. Cyanide cannot be bio-accumulated or stored in humans or animals<sup>[28]</sup>.

## 1.2 Electrodeposition of Cu-Sn from alternative baths

Because of the toxicity of cyanide ions to environment, difficulty in waste treatment and danger in handling, more acceptable electrolytes have been studied for replacement. Since  $\text{Cu}^{2+}$  and  $\text{Sn}^{2+}$  ions can suffer hydrolysis with water at pH higher than  $\sim 4.0$  and  $\sim 1.0$ , respectively and give rise to the occurrence of precipitations<sup>[29]</sup> which makes alkaline solutions impossible to use, except cyanide and pyrophosphate based baths<sup>[30, 31]</sup> since they can complex with copper. However, pyrophosphate based electrolyte has a few disadvantages which make it an unideal option used industrially: the low plating speed which means long plating time and the poor stability of the bath especially the pyrophosphate ions.

Acidic baths have been more widely studied including sulfate<sup>[5, 32, 33]</sup> and methanesulfonate<sup>[18, 34]</sup>. However, the use of sulfuric acid has been severely limited by its inability to stabilize stannous anions and lead to excessive oxidation to stannic anions. In addition, the great difference between the standard reduction potentials of  $\text{Cu}^{2+}$  and  $\text{Sn}^{2+}$  ( $\Delta E=0.4\text{V}$ ) is a major challenge for electrodepositing Cu-Sn alloys. Polarization of Cu deposition to certain degrees can be achieved by the application of organic Cu suppressor in sulfate electrolytes<sup>[5, 32]</sup>.

Recently, EDTA (disodium ethylenediaminetetraacetate) has been found to form ligands with  $\text{Cu}^{2+}$  ions and  $\text{Sn}^{2+}$  ions in less acidic solutions based on sulfuric acid whose pH was adjusted by addition of NaOH (pH=3.4) which can result from  $\sim 27$  wt% to  $\sim 60$  wt% Sn depending on the applied potentials<sup>[14]</sup>.

Methanesulfonic acid, with the chemical formula  $\text{CH}_3\text{SO}_3\text{H}$ , is the simplest form of alkylsulfonic acids. The alkane sulfonic acids form water soluble salts of various metals. The alkane sulfonates do not undergo any appreciable hydrolysis, regardless of the temperature used. Besides, the alkane sulfonates are stable in acidic, neutral and alkaline solutions. Wayne Proell was the first to point out that it was possible to electroplate many metals from alkane sulfonate baths, including cadmium, lead, nickel, silver and zinc<sup>[35, 36]</sup>.

Methanesulfonic acid gained some commercial acceptability after several decades. Currently it becomes an ideal electrolyte for many electrochemical processes, especially those involving tin and lead plating<sup>[37]</sup>. The high solubility of metal methanesulfonates, the conductivity of aqueous methanesulfonic acid solutions and the low toxicity of MSA make MSA a suitable electrolyte for electrodeposition<sup>[38]</sup>. Ease of effluent treatment, acid recovery and salt preparation turn MSA to an environmentally-favorable option. Currently a wide range of materials can be deposited from MSA based baths including  $\text{PbO}_2$  by anodic deposition<sup>[39]</sup>,  $\text{PbO}_2\text{-ZrO}_2$  nanocomposites by pulse electrodeposition<sup>[40]</sup>, Sn-Bi solder in presence of hydroquinone and gelatin<sup>[41]</sup>.

Although MSA is a reducing acid and thus reduces the propensity for stannous oxidation compared to sulfuric acid, oxidation of stannous tin is still a problem in MSA systems. Loss of stannous tin, due to its oxidation to stannic tin, will decrease deposition rate and change the composition of deposited alloys. Sludge builds up when stannic tin accumulates and rough deposits may result. So anti-oxidants are usually included in electroplating baths to inhibit the formation of stannic tin. Pewnim and Roy<sup>[34]</sup> reported that deposits containing 96wt% Sn can be obtained from a methanesulfonic

acid electrolyte (pH=1.17) in presence of commercial additives. C.T.J. Low and F.C. Walsh reported the shift of copper reduction to more negative potentials with respect to the tin deposition potential can be induced by a perfluorinated cationic surfactant<sup>[18, 42]</sup> at optimum surfactant concentration of 0.01 vol%. This facilitated the co-deposition of Cu-Sn alloys. Meanwhile hydrogen evolution during electrodeposition can be effectively suppressed in presence of the surfactant. They also studied the effect of hydroquinone on slowing down the oxidation rate of stannous ion to stannic ion generated on anode<sup>[43]</sup>. To summarize, almost all studied baths have high acidity (pH < 1.0), which cause inconvenience during operations and dispose.

### **1.3 Introduction of Ionic Liquids**

Ionic liquids have gained enormous interest as excellent candidates for industrial applications compared to volatile organic solvents during last decades. There are about 600 conventional solvents used in industry, compared to at least  $10^6$  simple ionic liquids can be easily prepared in laboratory. The physical and chemical properties can be tailored by choosing appropriate cationic and anionic groups for synthesis. They are studied for a wide range of applications, including their use as solvent for organic synthesis and biological reactions due to their low volatility which minimize the risk of atmospheric contamination and reduce associated health concerns<sup>[44]</sup>. One important application related to electrochemistry is electrodeposition. The key advantages of ionic liquids are wide potential windows, high solubility of metallic salts, reduced germination of hydrogen evolution due to low water content in these systems and relatively higher conductivity compared to other non-aqueous solvents.

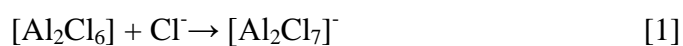
Although it may be not as economically affordable as existing plating systems for common applications, ionic liquids can provide a solution for metals that are difficult to plate. In addition, ionic liquids can be considered as alternatives to replace some hazardous processes by reducing the use of toxic agents.

### 1.3.1 History of Ionic Liquids

Ionic liquid is defined as “salts with a melting temperature below 100°C”, which evolved from traditional high temperature molten salts. The history of ionic liquids began with the synthesis of ethylammonium nitrate ( $C_2H_5N^+H_3NO_3^-$ ) with a melting point of 12 °C reported in 1914 by Walden<sup>[45]</sup>. The next advance in ionic liquid research was after several decades to develop a lower temperature melt eutectic (molten KCl/LiCl) for aluminium electrodeposition which was only available from high temperature molten salts around 1988<sup>[46]</sup>. The decreased melting point of this system compared to pure salts, is due to the formation of bulky chloroaluminate ions (e.g.  $AlCl_4^-$  and  $Al_2Cl_7^-$ ) in the eutectic mixtures. Bulky ions have delocalized charge and this gives rise to a reduction in lattice energy and consequently the melting point of the system<sup>[47]</sup>.

The further reducing of melting point of molten salts by using bulky asymmetric ions was started in 1970s by Osteryoung formed mixture between  $AlCl_3$  and 1-butylpyridinium cation<sup>[48]</sup>. But due to the easy reduction of 1-butylpyridinium cation, 1-ethyl-3-methyl-imidazolium ([EMIM]<sup>+</sup>) cation was soon used as a substituent to mix with  $AlCl_3$ . The mixture has a larger liquid range and lower viscosity with  $AlCl_3$  content between 33 and 67 mol%<sup>[49]</sup>. However, a major limitation of chloroaluminate ionic liquids is they are hygroscopic liquids liberating HCl

and oxo-chloroaluminates due to rapid hydrolysis of  $\text{AlCl}_3$  upon exposure to moisture. Operation in these liquids requires either a strictly controlled inert gas atmosphere or at least closed vessel conditions with limited water concentration. The equations [1]-[3] show various species formed in the chloroaluminate ionic liquids. The Al speciation is altered by the changes in the liquid composition. The relative positions of equilibria depend on the relative concentration of  $\text{AlCl}_3$  in the mixture.



These ionic liquids formed between organic cations and  $\text{AlCl}_3$  were developed from 1905 to around 1995 and are often called “first generation” ionic liquids. Although these liquids were considered to be difficult to handle with and of little practical importance, they have been extensively studied in the electrodeposition of metals and alloys impossible to be deposited other ways as Al-Nb alloy<sup>[50]</sup>, Al-Ti alloy<sup>[51]</sup>, and so on<sup>[52, 53]</sup>.

The second generation of ionic liquids is those composed of discrete ions instead of complex ions formed from  $\text{AlCl}_3$  in first generation ionic liquids. In 1992 Wilkes and Zaworotko described them as the first air and water stable ionic liquids by substituting  $\text{AlCl}_3$  with less reactive tetrafluoroborate  $[\text{BF}_4]^-$  or hexafluorophosphate  $[\text{PF}_6]^-$  anions<sup>[54]</sup>.

The low melting point and stable property of  $[\text{EMIM}][\text{BF}_4]$  have made it a favored ionic liquid in the early adoption. One of the first appeared in 1997<sup>[55]</sup>, reporting the investigation of  $[\text{EMIM}][\text{BF}_4]$  as the electrolyte system for a number of processes, including the electrodeposition of lithium for batteries. The combination of hexafluorophosphate  $[\text{PF}_6]^-$  with analogous 1-butyl-3-methylimidazolium triflate  $[\text{BMIM}]^+$  also produced

room-temperature ionic liquids, reported by Chauvin, Mussmann and Olivier in 1995<sup>[56]</sup>.

This has been followed by majority of studies considering discrete anions as possible components for air and moisture stable ionic liquids. These non-chloroaluminate ionic liquids have the advantages of high thermal and electrochemical stability and ease of handling under ambient, humid condition. However, these systems tend to hydrolyze to generate HF, a corrosive and toxic compound<sup>[57]</sup>. As an improvement, the stability of this class of ionic liquids can be improved by using more hydrophobic anions such as tri-fluoromethanesulphonate  $(\text{CF}_3\text{SO}_3^-)$ (TFO), bis-(trifluoromethanesulphonyl)amide  $[(\text{CF}_3\text{SO}_2)_2\text{N}](\text{Tf}_2\text{N})$ <sup>[58]</sup> and tris-(trifluoromethanesulphonyl)methide  $[(\text{CF}_3\text{SO}_2)_3\text{C}](\text{CTf}_3)$ <sup>[47]</sup>. They have the advantages of large electrochemical window and better tolerance to humidity.

### **1.3.2 Deep Eutectic Solvents**

The melting point of two component mixture is dependent on the interaction between the components. When the components interact strongly with each other, large negative deviations of freezing point can occur. This is presented diagrammatically in Figure 1.1.

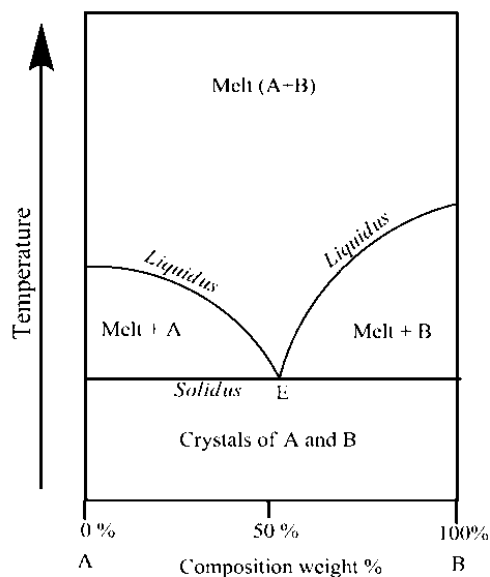


*Figure 1.1 Schematic representation of eutectic mixture formation*

Eutectic mixtures have been extensively used for applications of molten salts to reduce the operating temperature and this is why aluminum based ionic liquids were developed. However due to moisture sensitivity of  $\text{AlCl}_3$  as well as its unsuitability to electrodeposit pure reactive metals such as Si, Ta, Li which can only be obtained as Al co-deposits, methods to replace  $\text{AlCl}_3$  with other metal salts need to be developed.

Around 2000, Abbott<sup>[59, 60]</sup> and Sun<sup>[61, 62]</sup> showed that zinc chloride and quaternary ammonium form mixtures having melting point close to ambient temperature. The principle is that a complexing agent reacts with the anion to effectively delocalize the charge and decrease the interaction with cation. This is shown in Figure 1.2. The general formula of this system can be expressed as  $\text{Cat}^+\text{X}^-\cdot z\text{Y}$ , where  $\text{Cat}^+$  developed so far have been based on pyridinium, imidazolium and quaternary ammonium moieties,  $\text{X}^-$  is generally a halide anion (usually  $\text{Cl}^-$ ), Y is a Lewis or Brønsted acid acting

as a complexing agent and  $z$  is the number of  $Y$  molecules which complex  $X^-$ .

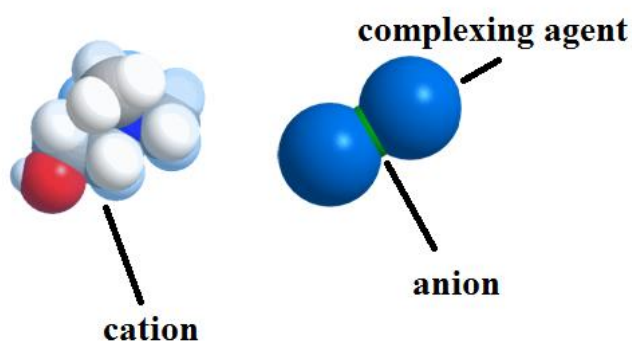


*Figure 1.2 Schematic representation of complexation occurring in eutectic mixtures*

Depending on the nature of complexing agents used, the eutectic solvents can be divided into three types.

Type 1  $Y=MCl_x$ ,  $M=Zn^{[60]}$ ,  $Sn^{[59]}$ ,  $Al^{[63]}$ ,  $Co^{[64]}$

Type 2  $Y=MCl_x \cdot yH_2O$ ,  $M=Cr^{[65]}$

Type 3  $Y=RZ$ ,  $Z=CONH_2$ ,  $COOH$ ,  $OH$

Examples of type 1 eutectics include  $ZnCl_2$  and quaternary ammonium salts<sup>[59-62]</sup>, as well studied chloroaluminate imidazolium melts<sup>[47]</sup>.

The field of first type eutectics can be expanded by using the hydrated metal halides, which are classified as type 2 eutectics. Unlike the anhydrous metal salts, these mixtures are very sensitive to temperature fluctuations. At ambient temperatures they rapidly absorb up to 10wt% water from

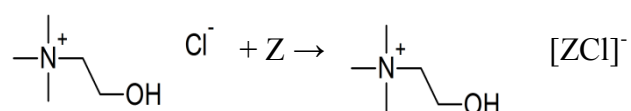
atmosphere. Above certain temperature level the liquids start to lose water and produce a significant change in liquid composition characterized by the color changes. Some metals including Co, Cu, Ni and Fe have been studied on their freezing points with choline chloride<sup>[47]</sup>. They are potential systems but to date only Cr and Co can be electrodeposited from this type of eutectics<sup>[47, 66]</sup>. The authors found that Cr(III) is reduced to Cr(0) via a two-step process involving Cr(II) as the intermediate species. Adherent and crack-free deposit can be obtained without the need of adding any additives. The addition of LiCl to the electrolyte allows obtaining black chromium coatings with nanocrystalline structure<sup>[65]</sup>.

Hydrogen bond donors (HBDs), amide, carboxylic acid and alcohol moiety, have been regarded to complex with choline chloride to form type 3 eutectics. These liquids will be the subject of this thesis. The depression of freezing point for a number of these systems is extremely large, for example the choline chloride-urea system is 178 °C<sup>[47]</sup>. They also exhibit high solubilities to metals and metal oxides<sup>[67]</sup>. Distinguished from conventional ionic liquids these eutectic mixtures contain not only ions but also neutral molecules, the term Deep Eutectic Solvents (DES) and also molecular liquid were adopted. Unlike the room-temperature ionic liquids, these liquids are easy to prepare in pure state and non-reactive to water. They are relatively inexpensive meaning that they can be used for large scale applications.

The freezing point of DESs will be related to the lattice energy as a result of interaction between the salt and HBD. Meanwhile, larger depression of freezing point can be observed when the HBDs have lower molecular weight and take up larger mass fraction in the liquids.

### 1.3.3 Deposition of metals from eutectic mixtures based on choline chloride

Compared with conventional ionic liquids, deep eutectic solvents may represent a “green alternative” for metals and alloys electrodeposition. They consist of eutectic mixtures of quaternary ammonium salt such as choline chloride with a hydrogen bond donor species such as amides, glycols or carboxylic acids. In this case, complexation chemistry in the eutectic solvents formed according to the following reaction<sup>[68]</sup>:



Type I eutectics may be most suitable for Ga, Al and Ge deposition. Type II eutectics are more suitable for Cr deposition and Type III are most often used to deposition Cu, Zn, Sn, Ag and associated alloys. Besides that, Type III is also widely used for electropolishing, metal recovery<sup>[69]</sup> and winning. To date a comprehensive review on electrodeposition from ionic liquids is given by Endres and Abbott et al<sup>[47]</sup>. Figure 1.3 shows some of the metals that have been deposited from Type II and Type III eutectics.

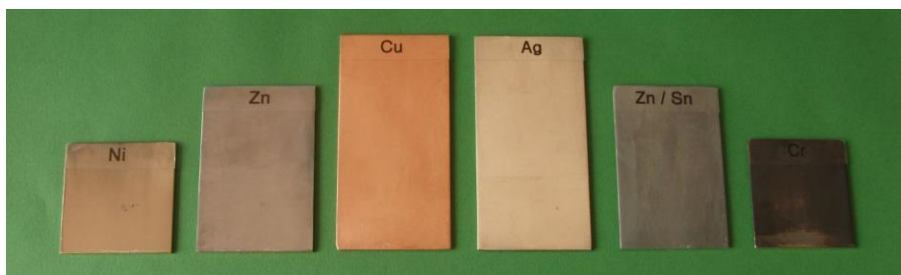


*Figure 1.3 A range of metal and metal alloy coatings deposited electrolytically from type II (Cr far right) and type III (Ni, Cu, Zn, Sn and Ag) choline chloride-based ionic liquids.*

Salome et al.<sup>[70]</sup> studied the influence of different hydrogen bond donors such as urea, ethylene glycol and propylene glycol on the nucleation mechanism of Sn growth and shown that the number of nuclei initially formed were controlled by the OH group adsorption on the GC electrode surface in the order of ethline>propeline>reline. Ghosh et al.<sup>[71]</sup> potentiostatic and galvanostatic deposition of Cu from ethaline containing 0.2 M  $\text{CuCl}_2 \cdot 2\text{H}_2\text{O}$  at room temperature. Long term electrodeposition experiment shows that electroactive species remain the same throughout the plating period. However, the use of inert anode leads to breakdown of DES during copper deposition and the use of soluble anode will produce a brown powder which could be copper based salts and oxides. Anicai et al.<sup>[72]</sup> reported facilitated deposition of Sn from choline chloride-malonic acid eutectic with a significant brightness and a cathodic efficiency higher than 80%. Moreover, the as-deposited Sn coatings showed better corrosion performance compared with those deposited from classical aqueous electrolytes. Li et al.<sup>[73]</sup> investigated the effect of process variables such as cathodic potential and temperature on cathode current density, current efficiency, and morphology of Co deposit. The results showed that current efficiency increase with increasing temperature but non-uniform, dendritic

and cauliflower structure of different sizes deposits were obtained at more negative cathodic potentials and at higher temperatures as shown in Figure 1.4 and Figure 1.5.

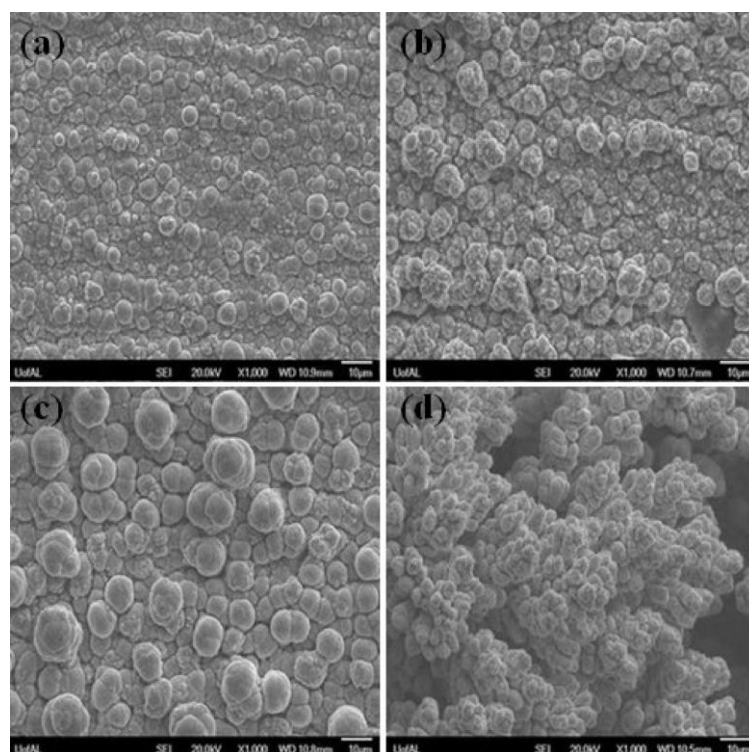


*Figure 1.4 SEM micrographs of cobalt electrodeposits obtained from urea-choline chloride- $\text{CoCl}_2$  (0.05 mol/L) on a copper substrate at different cathodic potentials: (a) -0.80 V, (b) -0.85 V, (c) -0.90 V, and (d) -0.95 V at 373 K.*

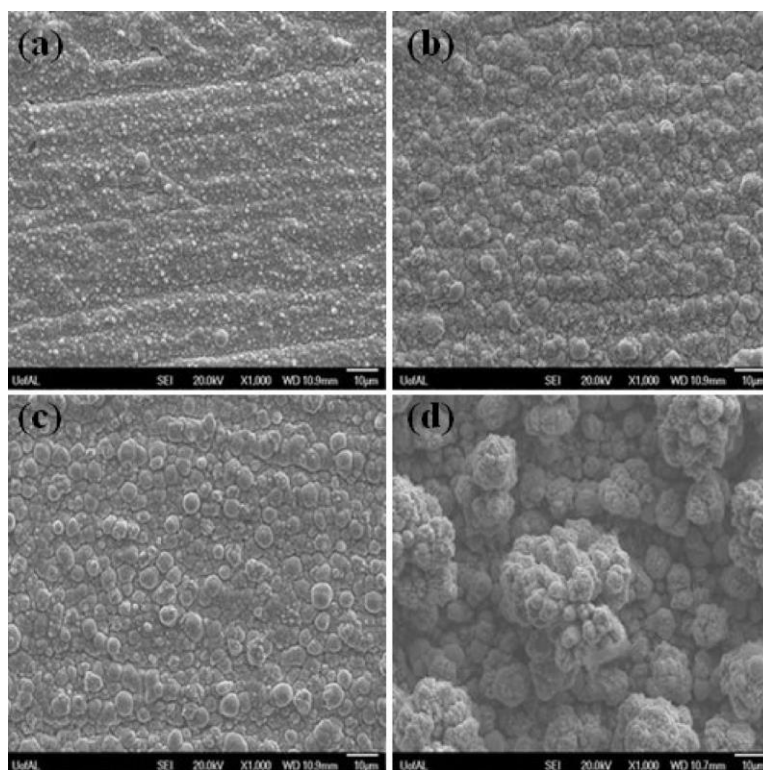
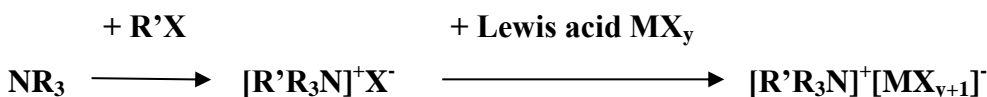


*Figure 1.5 SEM micrographs of cobalt electrodeposits obtained from urea-choline chloride- $\text{CoCl}_2$  (0.05 mol/L) on a copper substrate at different temperatures: (a) 353 K, (b) 363 K, (c) 373 K, and (d) 383 K at -0.80 V.*

Alloys can also be successfully deposited. Wang et al.<sup>[74]</sup> suggested that Ni-Cu co-deposition could be easily achieved in 1:2 ChCl-urea without the addition of complexing agents due to their close onset reduction potentials. Abbott et al.<sup>[75]</sup> discussed great difference of Zn/Sn deposition kinetics and thermodynamics between DES and aqueous solution. De Vreese et al.<sup>[76]</sup> prepared copper-zinc films from a concentrated choline acetate ionic liquid-like electrolyte and improved the morphological stability at longer deposition times by the addition of small concentration of PVA.

### 1.3.4 Synthesis of Ionic Liquids

The synthesis of chloroaluminate-based ionic liquids from halide salts and aluminum Lewis acids (most commonly  $\text{AlX}_3$ ,  $\text{X}=\text{Cl}, \text{Br}$ ) can generally be split into two steps: (i) quaternisation of a haloalkane with a trialkylamine, trialkylphosphine or dialkylsulfide to produce the cationic component, (ii) formation of the chloroaluminate anion by addition of an appropriate aluminum halide to this salt (Scheme 1.1)<sup>[77]</sup>



*Scheme 1.1 General synthesis route to chloroaluminate-based ionic liquids.*

Since ionic liquids have no significant vapor pressure, their purification using conventional methods is difficult. Thus it is necessary to remove as many impurities as possible from starting materials and produce as few side products as possible during synthetic procedures. In addition, all materials should be dried before use and working in a glove box is recommended as the chloride and bromide salts are highly hygroscopic and the chloroaluminate melts are highly moisture sensitive.

The process to produce second generation ionic liquids can be shown in Scheme 1.2. In brief, an organic base is alkylated using a haloalkane to generate an organic halide salt. Then anion exchange is carried out, generally in water, with appropriate acid or metal salt. The ionic liquid can be extracted from the aqueous solution into an organic phase<sup>[77]</sup>.



B= pyridinium, N-methylimidazole, N-methylpyrrolidine, etc.

R= methyl, ethyl, propyl, etc.

X= chloride, bromide, iodide, trifluoromethanesulfonate, etc.

M= H<sup>+</sup> or an alkali metal

A= [BF<sub>4</sub>], [PF<sub>6</sub>], etc.

*Scheme 1.2 General synthetic route to produce air- and moisture- stable ionic liquids*

One of the key advantages of eutectic-based solvents is the ease of preparation. The liquid formation is generally mildly endothermic and requires simply mixing the two components with gentle heating. The liquids based on choline chloride can absorb water with exposure to atmosphere due to hygroscopic property of choline chloride. However, the electrochemical properties of these liquids are insensitive to existing water either naturally adsorbed or deliberately added to the ionic liquids, which is important to practical electroplating process. Since no chemical reactions occur during mixing, they revert to their constituent components upon excessive dilution in water.

## **1.3.5 Physical Properties**

### **1.3.5.1. Thermal properties**

Ionic liquids are different from typical inorganic salts because of their low melting point [T<sub>m</sub>]. [T<sub>m</sub>] of typical inorganic salts is around 1000 °C reflecting their high lattice energies which can be attributed to the strong electrostatic attractive force between ions. The depression of [T<sub>m</sub>] can increase with increasing ion radius because the surface charge density decrease and the separation between ions increase. By replacing Na<sup>+</sup> with

[EMIM]<sup>+</sup> coordinating with Cl<sup>-</sup>, a significant decrease on [T<sub>m</sub>] can be observed, from 808 °C to 87 °C<sup>[78]</sup>. The cations with large ion size in high asymmetry can generate diffused charge which results in reduction of lattice energy and thus a depression in [T<sub>m</sub>] can be obtained. In addition, melting point can also be governed by altering anionic species used. The mixtures formed between [EMIM]<sup>+</sup> and different anions result in great difference in [T<sub>m</sub>] of ionic liquids, [Cl]<sup>-</sup> 89 °C<sup>[79]</sup>, [I]<sup>-</sup> 79 °C<sup>[79]</sup>, [BF<sub>4</sub>]<sup>-</sup> 11 °C<sup>[79]</sup>, [CH<sub>3</sub>COO]<sup>-</sup> 45 °C<sup>[79]</sup>, [CF<sub>3</sub>COO]<sup>-</sup> -14 °C<sup>[80]</sup>. Similar with the effect of cations, larger anions will lower surface charge densities and asymmetric anions generally form ionic liquids with lower [T<sub>m</sub>].

### 1.3.5.2 Conductivity and Viscosity

Conductivities of most room-temperature ionic liquids are within the range of 0.1-18 mS/cm. Generally, ionic liquids based on [EtMeIm]<sup>+</sup> show conductivity around 10 mS/cm, while lower conductivities, between 0.1 and 5 mS/cm are typical of ionic liquids based on tetraalkylammonium, pyrrolidinium, piperidinium and pyridinium cations. Under room temperatures, the conductivity of ionic liquids is almost one order magnitude lower compared with conventional aqueous electrolytes. For example, the specific conductivity of aqueous H<sub>2</sub>SO<sub>4</sub>(30 wt%) is 730 mS/cm. Even the highest room temperature conductivity reported by now for EtNH<sub>3</sub><sup>+</sup>NO<sub>3</sub><sup>-</sup> is about 150 mS/cm at 298K<sup>[81]</sup>. The conductivity of ionic liquids can be greatly influenced by their viscosity, temperature and transference numbers.

First, the relationship between conductivity and viscosity can be expressed by Walden Rule,  $\Lambda\eta = \text{constant}$ , where  $\Lambda$  is the molar conductivity

and  $\eta$  is the viscosity. The viscosity of ionic liquids is typically 10-100 times higher than that of water or organic solvents as a result of strong electrostatic and other interaction forces<sup>[82]</sup> such as by van der Waals forces and hydrogen bonding. For example, fluorinated anions such as  $\text{BF}_4^-$  and  $\text{PF}_6^-$  form viscous liquids due to formation of hydrogen bonding<sup>[83]</sup>.

Second, the changes on temperature have great influence on both conductivity and viscosity of ionic liquids. The “free space model” called also the “hole model” seems the most efficient way to describe the conductivity. The model assumes that the mass transfer is related to the size of ions and the size of voids in liquids<sup>[84]</sup>. The probability of an ion moving through a liquid is dependent on the presence of an adjacent suitably sized hole. Studies have shown the hole size in ionic liquids is smaller than that in aqueous electrolytes while the average ion size is larger. This reduced the ion movement which leads to increase in viscosity and decrease in conductivity. The voids constantly fluctuate in size due to thermal motions. So the fluidity and conductivity can increase as a function of temperature.

The hole theory is valid for not only conventional ionic liquids but also deep eutectic solvents. The physical properties of these molecular liquids are similar to that of ionic liquids. The study carried out by Abbott et.al<sup>[84]</sup> based on eutectic solvents between choline chloride and carboxylic acids showed that a maximum in the conductivity and a minimum in the viscosity are observed at equal molar composition. Conductivity increases approximately linearly with temperature and inversely proportional to the radius of the diffusion ions. In principle the DES should be tunable by varying the hydrogen bond donor and their mole ratio in the mixture.

Third, the conductivity of a classical electrolyte solution is proportional to the number of the number of charge carriers  $N$ . In conventional electrolytes, ions exist in the form of solvate-complexes, so the solvent molecules are parts of mobile ions. Consequently, mobile species consist of not only the flux of ions but also a flux of solvent. Since ionic liquids consist entirely of ions without solvent, it's difficult to determine the number of charge carriers. The charge maybe transported by all the mobile species present in the system, including simple ions and their charged combinations.

### 1.3.5.3 Electrochemical window

The potential range over which the electrolyte is neither reduced nor oxidized at electrode surface corresponds to the electrochemical window, that plays a key role in using ionic liquids for electrodeposition of metals and semiconductors. It is governed by the chemical structure of the materials used, the electrode materials, sweep rate of the potential, temperature, atmosphere, solvent, impurity and so on. Aqueous solutions have narrow electrochemical window of about 1.2V which limits the electrodeposition of certain elements. However, some ionic liquids have significantly larger electrochemical window, especially those based on aliphatic cations such as ammonium cations and piperidinium cations have potential windows around 5V. Also  $[\text{BF}_4]^-$  based ILs have good properties, *e.g.*, 3.5V for  $[\text{BMIM}][\text{BF}_4]$  on a glassy carbon electrode<sup>[85]</sup>, 4.5V for  $[\text{EMIM}][\text{BF}_4]$  on platinum electrode<sup>[86]</sup>. The nature of the anion also influences the electrochemical window. Narrower windows are observed for protic ionic liquids containing chloride, bromide and iodide, as a result of the ease of oxidation compared to  $[\text{BF}_4]^-$ ,  $[\text{PF}_6]^-$  and  $[\text{NTf}_2]^-$ <sup>[87]</sup>. Because of

various reference electrodes used in literatures, it is not easy to compare the values. The enlarged electrochemical window allows ionic liquids to be used for electrodeposition of metals or alloys which were formerly only accessible from high-temperature molten salts, e.g. Na<sup>[88]</sup>, Li<sup>[89]</sup>, Ga<sup>[90]</sup>.

DESs, being inferior to other ionic liquids, have a much narrower window of electrochemical stability, which limits the range of metals that can be deposited. For example, the system based on mixture of ethylene glycol and choline chloride has a potential window of 2.5V on Pt<sup>[91]</sup>, 2V on stainless steel electrode<sup>[92]</sup>. In addition, due to their hygroscopic property, measurements should be carried out in a carefully controlled atmosphere for better reproducibility. The presence of small amount of water will decrease the viscosity of electrolytes but retains their characteristics without leading to decomposition. The mole ratio of water that is compatible with the stability of most DESs at room temperature is close to 0.2, much higher than the mole percentage of water naturally absorbed. However, extend dilution of DES with water will result in the loss of existing hydrogen bonds, and consequently, the disappearance of the special structure of DES<sup>[93]</sup>.

#### **1.3.5.4 Hindrance of hydrogen embrittlement**

The hydrogen embrittlement is a non-neglectable problem in industrial aqueous electroplating. It is often the result of unintentional introduction of hydrogen into susceptible metals, especially high-strength steel, during forming process. The hydrogen embrittlement can induce micro-cracking to metal deposits, which weakens mechanical properties of coatings as well as reduces the current efficiency of electrodeposition. This effect becomes severer when the electrodeposition process is carried out at elevated temperatures for faster kinetic of mass transfer because solubility of

hydrogen often increase with temperature leading to highly-risky hydrogen embrittlement<sup>[94]</sup>.

Due to the wide electrochemical windows combined with large solubility for many metallic salts, ionic liquids have been employed to deposit reactive metals and semiconductors that are not feasible from aqueous solutions due to hydrogen evolution interference. Even for the materials which can be deposited from aqueous solutions, deposition from ionic liquids can be advantageous because the wide potential window can reduce the occurrence of competitive reactions. In addition, because of good thermal stability of ionic liquids, deposition process can be carried out under elevated temperature without significant introduction of hydrogen embrittlement.

### **1.3.6 Industrial Applications of Ionic Liquids**

Great achievements on applications of ionic liquids have been obtained in academic labs including as solvents for electropolishing of stainless steel<sup>[95]</sup>, electrolyte for lithium battery<sup>[96]</sup> and fuel cells<sup>[97]</sup>, metal deposition<sup>[47]</sup> and electrochemical synthesis of nano-particles<sup>[98]</sup>. In past decades, ionic liquids also find their way into a variety of industrial applications proving that handling large quantity of ionic liquid is practical.

Although the basic understanding of ionic liquids was initiated from several decades ago, there was no public hint of industrial applications until the mid-1990s. An industrial academic consortium QUILL(Queen's University Ionic Liquid Laboratories) in Belfast was formed involving sixteen companies in late 1990s, which aimed to develop technologies for ionic liquids applications in industrial scale<sup>[99]</sup>.

The first publicly-announced and most successful process using ionic liquid for commercial application is the BASIL<sup>TM</sup> (Biphasic Acid Scavenging utilizing Ionic Liquids) process induced to BASF Company in 2002. In this process, triethylamine was previously used to scavenge the waste acid during production of alkoxyphenylphosphines, but it was difficult to separate the waste from products. Replacing triethylamine with 1-methylimidazole results in 1-methylimidazolium chloride which is an ionic liquid separated as a discrete phase. The reaction is now carried out at a multi-ton scale, proving that handling large quantities of ionic liquid is practical<sup>[100]</sup>.

Institute Francais du Petrole(IFP) was the first to operate an ionic liquid pilot plant. They used a dimerisation reaction to obtain desired chemicals. The process can be better catalyzed by cationic nickel complex dissolved in hydrocarbons. So the chloroaluminate ionic liquids can be used as solvents for these dimerisation reactions. The activity of nickel catalyst is much higher than in both solvent-free and conventional solvent systems. In addition, the reaction can be performed as a biphasic system between -15 °C and 5 °C as the products can form a discrete phase and the catalysts remain dissolved in ionic liquid phase. This process induced a better use of catalyst with a reduced catalyst disposal and cost<sup>[101]</sup>.

Like BASF, Degussa are developing ionic liquids on several fronts. They used ionic liquids as secondary dispersing agents to reduce the use of volatile organic substances in paintings<sup>[102]</sup>. They also revealed a new air products technology by complexation between reactive gases and ionic liquids. It provides a method to deliver these reactive and hazardous gases in a safer, more efficient and easily handled way compared with traditional method of physical adsorption on solids. The gas can be removed from the

cylinder at sub-atmospheric pressure<sup>[103]</sup> and this technology produces at least twice the performance of that rival process.

Scionix, a research group from the University of Leicester, electroplated chromium based on choline-chromium ionic liquid<sup>[104]</sup>. They also developed a process to electropolish stainless steel in a deep eutectic solvent composed of ethylene glycol and choline chloride. This process has the advantage that high current efficiencies can be obtained with negligible gas evolution at the anode/solution interface<sup>[105]</sup>.

## **1.4 Electrodeposition from ethaline**

### **1.4.1 Electrodeposition of Cu from ethaline and reline**

Although ionic liquids reduce the gaseous emissions compared to aqueous electrolytes, some aspects should be considered before calling them “green solvents”. Maginn et al.<sup>[106]</sup> presented that ionic liquids based on pyridinium and imidazolium are even more toxic than common organic solvents. They found that if all other things being equal, toxicity shows the trend with cation type of ammonium<pyridinium<imidazolium<triazolium<tetrazolium.

Deep eutectic solvent based on choline chloride have advantages that they are biodegradable, easy to prepare, water and air stable and economically suitable in large scale applications. Abbott et al. described different types of ionic liquids based on choline chloride and their applications<sup>[75, 107, 108]</sup>. Especially the mixtures between choline chloride and ethylene glycol or urea, namely ethaline or reline, are characterized by low viscosity, high conductivity and good thermal stability. All the

components are easy to acquire and not harmful to environment and human beings.

Ethaline, mixture between choline chloride and ethylene glycol, is the most popular deep eutectic solvent as a potential bath for electrodeposition of metal and alloys. Ni and its alloys have been successfully deposited from ethaline and it is found that better corrosion resistance of deposited alloys can be obtained with higher Ni content in the film<sup>[109-111]</sup>. Magnetostrictive Fe-Ga thin films can be deposited from ethaline even in the presence of a relatively high content of water and the addition of a small concentration of oxalic acid which improved the microstructure of deposits<sup>[112]</sup>.

The electrodeposition of copper from ethaline was studied in several research groups. Gu et al.<sup>[113]</sup> reported the addition of ethylene diamine can improve the stability of deposition bath containing 0.45 M  $\text{CuCl}_2 \cdot 2\text{H}_2\text{O}$  since it represents a strong nitrogen containing ligand for most transition metal ions. Roy et al.<sup>[71]</sup> obtained smooth Cu deposits at 4.7 mA/cm<sup>2</sup> using 0.2 M  $\text{CuCl}_2 \cdot 2\text{H}_2\text{O}$  at 25 °C generating a current efficiency of (95±5)% at a rotation speed of 700 rpm. The crystalline size is 66±10 nm with an internal strain of 0.2%. They showed that the use of soluble copper anode will produce brown powder and inert anode will lead to the breakdown of DES. Lloyd et al.<sup>[114]</sup> suggested that effect of solution resistance should be taken into consideration during experiment design and a quasi-reversible single electron transfer process occurs between Cu(II) and Cu(I) transition.

Reline is referred to the mixture of choline chloride and urea. The deep eutectic phenomenon occurs for a mixture of choline chloride and urea in a 1:2 mole ratio. Choline chloride has a melting point of 302 °C and that of urea is 133 °C. The eutectic mixture melts as low as 12 °C. Due to its relatively higher viscosity and lower conductivity compared to ethaline,

reline is less popular in the field of electrodeposition. Silver electrodeposition in reline was discussed and proved to follow a nucleation and three dimensional growth governed by diffusion<sup>[115]</sup>. Anodic dissolution of noble metals in reline can be applied to form thin films of nanoparticles such as Au, Ag and Pd<sup>[116]</sup>. Two different additives, ammonia and ethylene diamine, were shown to be effective brighteners for the Zn deposition in reline<sup>[117]</sup>.

Popescu et.al<sup>[118]</sup> investigated the reason of slower diffusion of copper ions in reline than in water was related to the viscosity difference between the two solvents for the first time. Ali et al.<sup>[119]</sup> showed a brown metallic colored copper can be deposited from reline at room temperature with current density of 0.4 mA/cm<sup>2</sup>. Gomez's research group<sup>[120]</sup> have proved that copper deposition corresponds to a nucleation and 3D growth process, diffusion controlled. Up to now, almost all the studies on the copper deposition from reline meet the problem of low deposition current density and porous deposits morphology.

#### **1.4.2 Electrodeposition of Sn from ethaline**

Tin has been widely applied as a coating because it is a non-toxic, ductile and corrosion resistant metal<sup>[121]</sup>. Conventional electrodeposition of tin was carried out in aqueous electrolytes which can be divided into two types, alkali stannate based solutions and acidic stannous salt based solutions<sup>[122-124]</sup>. The alkali stannate solutions can yield satisfactory layers only at high temperatures and requires twice electrical charge to deposit the same mass of tin compared with plating from stannous salt solutions because the tin contained in stannate solution is in the tetravalent form. Deposition from

acidic stannous based solutions is complicated because it needs various additives to improve deposit morphology and adhesion. The organic additives make it more difficult to control the deposition process.

The electrodeposition of tin has also been investigated in some ionic liquids<sup>[125-128]</sup>. Macroporous Sn was direct electrodeposited from a water- and air- stable room temperature ionic liquid, 1-ethyl-3-methylimidazolium-dicyanamide<sup>[129]</sup>. In addition, porous tin-based films can be deposited from ethaline containing  $\text{SnCl}_2 \cdot 2\text{H}_2\text{O}$  without any complexing agent or additive<sup>[130]</sup>. The porous Sn or its alloy would be a good anode candidate for the lithium-ion batteries. The oxidation of Sn(II) to Sn(IV) can be hindered effectively in these solvents.

Fundamental study of electrodeposition of tin was carried out by comparing the mixtures between different hydrogen bond donors and choline chloride<sup>[70]</sup>. They found the choice of hydrogen bond donor does not affect, significantly, the chemistry of tin in solution and tin nucleation on glassy carbon surface occurs through a 3D instantaneous process with growth controlled by diffusion at a concentration of 0.01 M under 75 °C. The SEM image of the deposit obtained from ethaline show the presence of small particles which could indicate a certain degree of progressive nucleation besides parallelepiped crystallites which can hardly cover the entire surface. Hillman A. R. et.al<sup>[131]</sup> applied the combined electrochemical quartz crystal microbalance and probe beam deflection technique to study Sn electrodeposition from ethaline. By slowing the scan rate in the viscous solvent, the probe beam deflection responses reveal the solubility limitations in the Sn system.

### 1.4.3 Electrodeposition of Cu-Sn from ethaline

Several alloys can be deposited from ethaline<sup>[75, 132]</sup> at room temperature. Surface morphology and chemical composite of the films are significantly dependent on the metallic concentrations in the electrolytes. Electrochemical and transport properties of ethaline containing copper and tin chloride separately have been measured by S. Roy group<sup>[133]</sup> covering a temperature range of 20 °C-55 °C. They showed that copper and tin species did not change over the concentration range of their work which reaches 0.2M CuCl<sub>2</sub> and 0.1M SnCl<sub>2</sub>. Mechanism and analysis of Cu-Sn alloys deposition from ethaline was studied in detail in 4<sup>th</sup> chapter of Abubakr Alhaji's Ph.D thesis using acoustic impedance<sup>[134]</sup>. However, due to the low tin concentration (0.1M and 0.03M) adopted in their study, they suffered insufficient current density and low tin content in deposited films.

### 1.5 Pulse plating

Pulsed current electrodeposition has received great attention in recent years for improved mechanical, chemical and electronic properties<sup>[135-137]</sup>. In pulse plating, an interrupted current or potential is applied periodically. Three major different forms in pulse deposition can be classified by wave shapes: (1) rectangular-pulse consisting of rectangular shaped current or potential separated by intervals of zero current or potential; (2) periodic reverse deposition with periodically switched current or potential from cathodic to anodic polarization; (3) superimposed pulse deposition whose waveform is the sum of pulse (ac) wave current and a direct cathodic current (dc). In most commercial processes, rectangular pulse and reversed

pulse on current are more widely used for its ease of control. Rectangular pulse is now more widely used in preparation of alloys and composite materials because the pulse deposition shows obviously positive effects on grain refinement for deposits and adhesion strength improvement between the active materials and the substrate<sup>[40, 138, 139]</sup>. Reversed pulse is more used to improve the deposit uniformity by preferentially dissolving overplated areas during the reverse-time where an anodic current is applied<sup>[140, 141]</sup>. In our study we carried out electrodeposition process using rectangular pulse which is schematically shown in Figure 1.6.

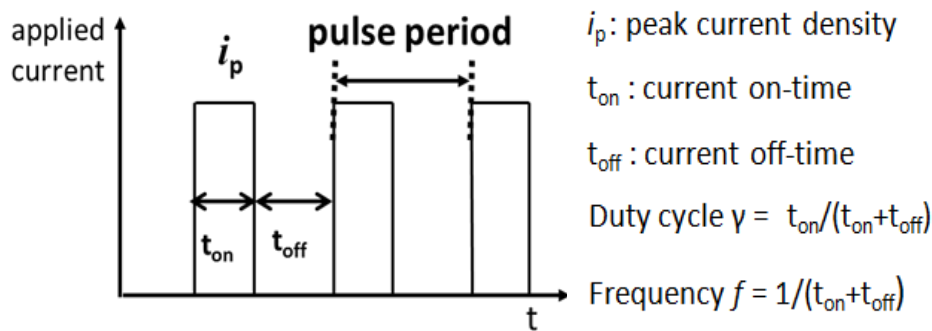


**Figure 1.6** Schematic representation of rectangular-pulse.

Pulse plating can be useful to improve the current distribution<sup>[142]</sup> and to alter the mass transfer conditions<sup>[143]</sup>. It can also be used to control the microstructure<sup>[144]</sup> and composition<sup>[145]</sup> of deposits. Unlike the DC electrodeposition which controls the applied current density or potential as the only variable, pulse current electrodeposition has various operation parameters, such as peak current density  $i_p$ , on-time  $t_{on}$ , off-time  $t_{off}$  and frequency  $f$ , to control the process and produce deposits with desired properties. Landolt and Marlot reported significant effect of pulse plating parameters (PC) on microstructure and composition of metallic coatings depending on the mass transport kinetics of metallic ions in the bath<sup>[146]</sup> and

they also suggested the possible presence of corrosion reactions during off-time. Higher throwing power of copper deposition can be realized by applying pulse plating<sup>[22]</sup>, leading also to deposition on irregular shapes and surfaces that can be effectively leveled up<sup>[10]</sup>. For example, Cha et al.<sup>[135]</sup> performed defect-free Cu gap filling into patterned wafers using a combination of pulse plating and electrochemical oxidation in absence of any additives.

However, previous investigators primarily concentrated on direct current (DC) electrodeposition of Cu-Sn alloys from various acids<sup>[1, 147-160]</sup>, and the effect of various parameters like deposition current density<sup>[158]</sup> or potential<sup>[159]</sup>, additive agents<sup>[1, 149, 150]</sup>, metal concentration<sup>[148, 161]</sup>, annealing conditions<sup>[157]</sup>, substrates<sup>[150]</sup>, electroplating time<sup>[155]</sup> on copper content of the deposit and predictive models were explored<sup>[147, 151]</sup>. A few attempts have been made for the PC electroplating of Cu-Sn alloys<sup>[30, 162]</sup> though they are deposited from pyrophosphate or cyanide based baths. Beattie S.D. et al.<sup>[30]</sup> showed the changes of average stoichiometry and phases present as a function of the position on the substrate foil in a hull cell with low frequencies. Nickchi et al.<sup>[162]</sup> prepared composite coatings containing self-lubricant particles like graphite in bronze film to decrease the coefficient of friction.

## **1.6 Project aims**

Cu-Sn has been successfully electrodeposited from various electrolytes with effort on optimizing processes, additive combination and so on. However few studies have attempted to compare the morphology and

electrochemical behavior of deposits obtained from aqueous and ionic liquid systems. The development of the choline chloride based deep eutectic solvents represents a real opportunity to substitute electrodeposition technologies from aqueous baths. This thesis contains the optimized deposition process of Cu-Sn carried out both in methanesulfonic acid based aqueous solution and in choline chloride-ethylene glycol mixtures. The relationship between bath composition and deposit morphology will be explored. The effect of pulsed current, certain additives and operation parameters will be investigated and physiochemical characterization of the alloys will be presented.

## 1.7 References

- [1] A. Hovestad, R.A. Tacke, H.H.t. Mannelje, *Physica Status Solidi (c)*, 5 (2008) 3506-3509.
- [2] J.-S. Park, V. Shinde, *Journal of Archaeological Science*, 40 (2013) 3811-3821.
- [3] N. Eliaz, K. Venkatakrishna, A.C. Hegde, *Surface and Coatings Technology*, 205 (2010) 1969-1978.
- [4] U. Lačnjevac, B.M. Jović, V.D. Jović, *Journal of The Electrochemical Society*, 159 (2012) D310-D318.
- [5] H. Nakano, S. Oue, D. Yoshihara, H. Fukushima, Y. Saka, S. Sawada, Y. Hattori, *Materials Transactions*, 52 (2011) 1237-1243.
- [6] P. Allongue, L. Cagnon, C. Gomes, A. Gündel, V. Costa, *Surface Science*, 557 (2004) 41-56.
- [7] H. Kazimierzak, P. Ozga, A. Jałowicz, R. Kowalik, *Surface and Coatings Technology*, 240 (2014) 311-319.
- [8] R.D. Srivastava, D. Tripathi, A.K. Agarwal, *Journal of Applied Electrochemistry*, 8 (1978) 71-74.
- [9] G.I. Medvedev, N.Y. Fursova, *Journal of Electrochemistry*, 36 (2000) 796-798.
- [10] J.W. Cuthbertson, N. Parkinson, *Journal of The Electrochemical Society*, 100 (1953) 107-119.
- [11] V.D. Bachvarov, M.H. Arnaudova, R.S. Rashkov, A. Zielonka, *Bulgarian Chemical Communication*, 43 (2011) 115-119.
- [12] A.N. Correia, M.X. Façanha, P. de Lima-Neto, *Surface and Coatings Technology*, 201 (2007) 7216-7221.

- [13] E. García-Marí, M. Gasque, R.P. Gutiérrez-Colomer, F. Ibáñez, P. González-Altozano, *Applied Thermal Engineering*, 61 (2013) 663-669.
- [14] E.P. Barbano, G.M. de Oliveira, M.F. de Carvalho, I.A. Carlos, *Surface and Coatings Technology*, 240 (2014) 14-22.
- [15] J.S. Kang, R.A. Gagliano, G. Ghosh, M.E. Fine, *Journal of Electronic Materials*, 31 (2002) 1238-1243.
- [16] C. Zanella, S. Xing, F. Deflorian, *Surface and Coatings Technology*, 236 (2013) 394-399.
- [17] D.R. Lide, *CRC Handbook of Chemistry and Physics*, CRC Press, Boca Raton, 2005.
- [18] C.T.J. Low, F.C. Walsh, *Surface and Coatings Technology*, 202 (2008) 1339-1349.
- [19] Y.D. Gamburg, Z. Giovanni, *Theory and Practice of Metal Electrodeposition*, pp. 1, Springer, 2011.
- [20] M. Schlesinger, M. Paunovic, *Modern Electroplating*, John Wiley & Sons, Inc., 2010.
- [21] S. Wernick, *The Electrochemical Society*, 60 (1931) 129-142.
- [22] M. Aguilar, X.H. Huang, R.N. Zare, *Journal of Chromatography*, 480 (1989) 427-431.
- [23] B. Bozzini, B. Busson, G.P. De Gaudenzi, L. D'Urzo, C. Mele, A. Tadjeddine, *Journal of Electroanalytical Chemistry*, 602 (2007) 61-69.
- [24] A. Dolati, M. Ghorbani, M.R. Ahmadi, *Journal of Electroanalytical Chemistry*, 577 (2005) 1-8.
- [25] N. Mandich, *Metal Finishing*, 103 (2005) 16-23.

- [26] G. Moretti, F. Guidi, G. Capobianco, R. Tonini, *Journal of Materials Chemistry*, 11 (2001) 922-925.
- [27] A. Survila, Z. Mockus, S. Kanapeckaitė, V. Jasulaitienė, R. Juškėnas, *Electrochimica Acta*, 52 (2007) 3067-3074.
- [28] E. Ronald, *Handbook of Chemical Risk Assessment: Health Hazards to Humans, Plants, and Animals*, CRC Press 2000.
- [29] M. Pourbaix, *Atlas of Electrochemical Equilibria in Aqueous Solutions*, Pergamon Press Ltd., Texas, 1974, pp. 479.
- [30] S.D. Beattie, J.R. Dahn, *Journal of The Electrochemical Society*, 150 (2003) C457-C460.
- [31] S.D. Beattie, J.R. Dahn, *Journal of The Electrochemical Society*, 152 (2005) C542-C548.
- [32] I. Volov, X. Sun, G. Gadikota, P. Shi, A.C. West, *Electrochimica Acta*, 89 (2013) 792-797.
- [33] G.F. Ortiz, M. López, R. Alcántara, J.L. Tirado, 585 (2014) 331-336.
- [34] N. Pewnim, S. Roy, *Electrochimica Acta*, 90 (2013) 498-506.
- [35] W.A. Proell, C.E. Adams, B.H. Shoemaker, *Industrial and Engineering Chemistry*, 40 (1948) 1129-1132.
- [36] W.A. Proell, *Electrodepositing bath and process*, US, 1950.
- [37] C. Rosenstein, *Metal Finishing*, 88 (1990) 17-21.
- [38] M.D. Gernon, M. Wu, T. Buszta, P. Janney, *Green Chemistry*, 1 (1999) 127-140.
- [39] C.T.J. Low, D. Pletcher, F.C. Walsh, *Electrochemistry Communications*, 11 (2009) 1301-1304.

- [40] Y. Yao, M. Zhao, C. Zhao, H. Zhang, *Electrochimica Acta*, 117 (2014) 453-459.
- [41] Y. Goh, A.S.M.A. Haseeb, M.F.M. Sabri, *Electrochimica Acta*, 90 (2013) 265-273.
- [42] C.T.J. Low, F.C. Walsh, *Surface and Coatings Technology*, 202 (2008) 3050-3057.
- [43] C.T.J. Low, F.C. Walsh, *Electrochimica Acta*, 53 (2008) 5280-5286.
- [44] K. Haerens, E. Matthijs, A. Chmielarz, B. Van der Bruggen, *Journal of Environmental Management*, 90 (2009) 3245-3252.
- [45] P. Walden, *Bull. Acad. Imper. Sci., St. Petersburg*, 1914, pp. 405-422.
- [46] F. Lantelme, H. Alexopoulos, M. Chemla, O. Hass, *Electrochimica Acta*, 33 (1988) 761-767.
- [47] F. Endres, D. MacFarlane, A.P. Abbott, *Electrodeposition from Ionic Liquids*, WILEY-VCH Verlag GmbH & Co. KGaA, Weinheim, 2008.
- [48] H.L. Chum, V.R. Koch, L.L. Miller, R.A. Osteryoung, *Journal of the American Chemistry Society*, 97 (1975) 3264-3265.
- [49] J.S. Wilkes, J.A. Levisky, R.A. Wilso, C.L. Hussey, *Inorganic Chemistry*, 21 (1982) 1263-1264.
- [50] G.R. Stafford, G.M. Haarberg, *Plasmas & Ions*, 2 (1999) 35-44.
- [51] G.R. Stafford, *Journal of Electrochemical Society*, 141 (1994) 945-953.
- [52] S. Zein El Abedin, P. Giridhar, P. Schwab, F. Endres, *Electrochemistry Communications*, 12 (2010) 1084-1086.
- [53] G.-B. Pan, W. Freyland, *Electrochimica Acta*, 52 (2007) 7254-7261.
- [54] J.S. Wilkes, M.J. Zaworotko, *Journal of the Chemical Society, Chemical Communications*, (1992) 965-967.

- [55] J. Fuller, R.T. Carlin, R.A. Osteryoung, *J. Electrochem. Soc.*, 144 (1997) 3881-3886.
- [56] Y. Chauvin, L. Mussmann, H. Olivier, *Angewandte Chemie International Edition.*, 34 (1995) 2698-2700.
- [57] C. Villagran, M. Deetlefs, W.R. Pitner, C. Hardacre, *Analytical Chemistry.*, 76 (2004) 2118-2123.
- [58] S. Zein El Abedin, M. Polleth, S.A. Meiss, J. Janek, F. Endres, *Green Chemistry*, 9 (2007) 549-553.
- [59] A.P. Abbott, G. Capper, D.L. Davies, H.L. Munro, R.K. Rasheed, V. Tambyrajah, *Chemical Communications*, 19(2001) 2010-2011.
- [60] A.P. Abbott, G. Capper, D.L. Davies, H. Munro, R. Rasheed, *Inorganic Chemistry*, 43 (2004) 3447-3452.
- [61] S.-I. Hsiu, J.-F. Huang, I.-W. Sun, C.-H. Yuan, J. Shiea, *Electrochimica Acta*, 47 (2002) 4367-4372.
- [62] Y.-F. Lin, I.-W. Sun, *Electrochimica Acta*, 44 (1999) 2771-2777.
- [63] C.L. Aravinda, W. Freyland, *Chemical Communications*, (2004) 2754-2755.
- [64] Y.-T. Hsieh, M.-C. Lai, H.-L. Huang, I.W. Sun, *Electrochimica Acta*, 117 (2014) 217-223.
- [65] A.P. Abbott, G. Capper, D.L. Davies, R.K. Rasheed, J. Archer, *Trans. Inst. Metal Finish*, 82 (2004) 14-17.
- [66] E.S.C. Ferreira, C.M. Pereira, A.F. Silva, *Journal of Electroanalytical Chemistry*, 707 (2013) 52-58.
- [67] A.N. Chiemela, R.J. Lesuer, *J. Phys. Chem. B*, 111 (2007) 13271-13277.
- [68] Shamsuri, *Singapore Journal of Scientific Research*, 8(2011) 1-7.

- [69] A. Mandroyan, M. Mourad-Mahmoud, M.-L. Doche, J.-Y. Hihn, *Ultrasonics Sonochemistry*, 2(2014)111-115.
- [70] S. Salomé, N.M. Pereira, E.S. Ferreira, C.M. Pereira, A.F. Silva, *Journal of Electroanalytical Chemistry*, 703 (2013) 80-87.
- [71] S. Ghosh, S. Roy, *Surface and Coatings Technology*, 238 (2014) 165-173.
- [72] L. Anicai, A. Petica, S. Costovici, P. Prioteasa, T. Visan, *Electrochimica Acta*, 114 (2013) 868-877.
- [73] M. Li, Z. Wang, R.G. Reddy, *Electrochimica Acta*, 123 (2014) 325-331.
- [74] S. Wang, X. Guo, H. Yang, J. Dai, R. Zhu, J. Gong, L. Peng, W. Ding, *Applied Surface Science*, 288 (2014) 530-536.
- [75] A.P. Abbott, G. Capper, K.J. McKenzie, K.S. Ryder, *Journal of Electroanalytical Chemistry*, 599 (2007) 288-294.
- [76] P. De Vreese, A. Skoczylas, E. Matthijs, J. Fransaer, K. Binnemans, *Electrochimica Acta*, 108 (2013) 788-794.
- [77] F. Endres, D. MacFarlane, A. Abbott, *electrodeposition from ionic liquids*, WILEY-VCH Verlag GmbH & Co. KGaA, Weinheim, 2008.
- [78] S. Zhang, N. Sun, X. He, X. Lu, X. Zhang, *Journal of Physical and Chemical Reference Data*, 35 (2006) 1475-1517.
- [79] H.L. Ngo, K. LeCompte, L. Hargens, A.B. McEwen, *Thermochimica Acta*, 357-358 (2000) 97-102.
- [80] P. Bonhote, A.-P. Dias, M. Armand, N. Papageorgiou, K. Kalyanasundaram, M. Gratzel, *Inorganic Chemistry*, 35 (1996) 1168-1178.
- [81] W. Xu, *Science*, 302 (2003) 422-425.
- [82] K.R. Seddon, A. Stark, M.-J. Torres, *American Chemistry Society, Symp. Ser.*, 819 (2002) 34-49.

- [83] P.A.Z. Suarez, S. Einloft, J.E.L. Dullius, R.F. de Souza, J. Dupont, *J. Chim. Phys.*, 95 (1998) 1626-1639.
- [84] A.P. Abbott, D. Boothby, G. Capper, D.L. Davies, R.K. Rasheed, *Journal of American Chemistry Society*, 126 (2004) 9142-9147.
- [85] S. Eugénio, C.M. Rangel, R. Vilar, A.M. Botelho do Rego, *Thin Solid Films*, 519 (2011) 1845-1850.
- [86] J. Fuller, R.T. Carlin, R.A. Osteryoung, *Journal of the Electrochemical Society*, 144 (1997) 3881-3886.
- [87] L.E. Barrosse-Antle, A.M. Bond, R.G. Compton, A.M. Mahony, E.I. Rogers, D.S. Silvester, *Chemistry-An Asian Journal*, 5 (2010) 202-230.
- [88] G.E. Gray, P.A. Kohl, J. Winnick, *Journal of the Electrochemical Society*, 142 (1995) 3636-3642.
- [89] B.J. Piersma, *Journal of the Electrochemical Society*, 94 (1994) 415-419.
- [90] P.-Y. Chen, Y.-F. Lin, I.-W. Sun, *Journal of the Electrochemical Society*, 146 (1999) 3290-3294.
- [91] S. Xing, C. Zanella, F. Deflorian, *Journal of Solid State Electrochemistry*, (2014).
- [92] N.M. Pereira, P.M.V. Fernandes, C.M. Pereira, A. Fernando Silva, *Journal of the Electrochemical Society*, 159 (2012) D501-D506.
- [93] Y.T. Dai, *Natural Deep Eutectic Solvents as new potential media for green technology*, Institute of Biology, Leiden University, Leiden, 2013, pp. 75.
- [94] S. Eugénio, C.M. Rangel, R. Vilar, S. Quaresma, *Electrochimica Acta*, 56 (2011) 10347-10352.

- [95] A.P. Abbott, G. Capper, K.J. McKenzie, K.S. Ryder, *Electrochimica Acta*, 51 (2006) 4420-4425.
- [96] B. Garcia, S. Lavallée, G. Perron, C. Michot, M. Armand, *Electrochimica Acta*, 49 (2004) 4583-4588.
- [97] E.G. Yanes, S.R. Gratz, M.J. Baldwin, *Analytical Chemistry*, 73 (2001) 3838-3844.
- [98] Y. Zhou, M. Antonietti, *Journal of American Chemistry Society*, 125 (2003) 14960-14961.
- [99] K.R. Seddon, *Green Chemistry*, 1 (1999) G58-G59.
- [100] M. Maase, K. Massonne, K. Halbritter, R. Noe, M. Bartsch, W. Siegel, V. Stegmann, M. Flores, O. Huttenloch, M. Becker, W. Pat. (Ed.), 2003.
- [101] Y. Chauvin, *Olefin Metathesis*, *Angewandte Chemie*, 45 (2006) 3740-3747.
- [102] A. Hoff, C. Jost, A. Prodi-Schwab, F.G. Schmidt, B. Weyershausen, *Elements: Degussa Science Newsletter*, 9 (2004) 10-15.
- [103] N.V. Plechkova, K.R. Seddon, *Chemical Society Reviews*, 37 (2008) 123-128.
- [104] A.P. Abbott, G. Capper, D.L. Davies, R.K. Rasheed, J. Archer, C. John, *Transactions of the IMF*, 82 (2004) 14-17.
- [105] A.P. Abbott, G. Capper, B.G. Swain, D.A. Wheeler, *Transactions of the IMF*, 83 (2005) 51-53.
- [106] D.J. Couling, R.J. Bernot, K.M. Docherty, J.K. Dixon, E.J. Maginn, *Green Chemistry*, 8 (2006) 82-90.
- [107] A.P. Abbott, G. Capper, D.L. Davies, R.K. Rasheed, V. Tambyrajah, *Chemical Communications*, (2003) 70-71.

- [108] A.P. Abbott, *ChemPhysChem*, 5 (2004) 1242-1246.
- [109] C.D. Gu, Y.H. You, Y.L. Yu, S.X. Qu, J.P. Tu, *Surface and Coatings Technology*, 205 (2011) 4928-4933.
- [110] Y.H. You, C.D. Gu, X.L. Wang, J.P. Tu, *Surface and Coatings Technology*, 206 (2012) 3632-3638.
- [111] J. Vijayakumar, S. Mohan, S. Anand Kumar, S.R. Suseendiran, S. Pavithra, *International Journal of Hydrogen Energy*, 38 (2013) 10208-10214.
- [112] F. Zhao, S. Franz, A. Vincenzo, M. Bestetti, F. Venturini, P.L. Cavallotti, *Electrochimica Acta*, 114 (2013) 878-888.
- [113] C.D. Gu, Y.H. You, X.L. Wang, J.P. Tu, *Surface and Coatings Technology*, 209 (2012) 117-123.
- [114] D. Lloyd, T. Vainikka, L. Murtomäki, K. Kontturi, E. Ahlberg, *Electrochimica Acta*, 56 (2011) 4942-4948.
- [115] P. Sebastián, E. Vallés, E. Gómez, *Electrochimica Acta*, 112 (2013) 149-158.
- [116] A. Renjith, A. Roy, V. Lakshminarayanan, *Journal of Colloid and Interface Science*, 426 (2014) 270-279.
- [117] A.P. Abbott, J.C. Barron, G. Frisch, K.S. Ryder, A.F. Silva, *Electrochimica Acta*, 56 (2011) 5272-5279.
- [118] A.-M. Popescu, V. Constantin, A. Cojocaru, M. Olteanu, *REV. CHIM.*, 62 (2011) 206-211.
- [119] M.R. Ali, M.Z. Rahman, S. SankarSaha, *Journal of Electrochemistry*, 20 (2014) 139-145.
- [120] P. Sebastián, E. Vallés, E. Gómez, *Electrochimica Acta*, 123 (2014) 285-295.

- [121] R. Sekar, C. Eagammai, S. Jayakrishnan, *Journal of Applied Electrochemistry*, 40 (2009) 49-57.
- [122] A.G. Gray, *Modern Electroplating*, John Willy & Sons, Inc., New York, 1953, pp. 387.
- [123] J.W. Cuthberton, *Tin and Its alloys*, E.S. Hedges (Ed.), Edward Arnold Ltd, London, 1960, pp. 99.
- [124] A. He, Q. Liu, D.G. Ivey, *Journal of Materials Science: Materials in Electronics*, 19 (2007) 553-562.
- [125] X.-H. Hu, C.L. Hussey, *Journal of the Electrochemical Society*, 140 (1993) 618-626.
- [126] J.-F. Huang, I.W. Sun, *Journal of The Electrochemical Society*, 150 (2003) E299-E306.
- [127] M. Morimitsu, Y. Nakahara, Y. Iwaki, M. Matsunaga, *Journal of Mining and Metallurgy*, 39 (2003) 59-67.
- [128] N. Tachikawa, N. Serizawa, Y. Katayama, T. Miura, *Electrochimica Acta*, 53 (2008) 6530-6534.
- [129] M.-J. Deng, T.-I. Leong, I.W. Sun, P.-Y. Chen, J.-K. Chang, W.-T. Tsai, *Electrochemical and Solid-State Letters*, 11 (2008) D85-D88.
- [130] C.D. Gu, Y.J. Mai, J.P. Zhou, Y.H. You, J.P. Tu, *Journal of Power Sources*, 214 (2012) 200-207.
- [131] A.R. Hillman, K.S. Ryder, C.J. Zaleski, V. Ferreira, C.A. Beasley, E. Vieil, *Electrochimica Acta*, 110(2014) 418-427.
- [132] Y.H. You, C.D. Gu, X.L. Wang, *Surface and Coatings Technology*, 17 (2012) 3632-3638.
- [133] S. Ghosh, K. Ryder, S. Roy, *Transaction of the IMF*, 92 (2014) 41-46.

- [134] A. Alhaji, *Electrodeposition of Alloys from Deep Eutectic Solvents*, Department of Chemistry, University of Leicester, Leicester, 2011.
- [135] S.H. Cha, S.-S. Kim, S.K. Cho, J.J. Kim, *Electrochemical and Solid-State Letters*, 10 (2007) D22-D24.
- [136] W.-C. Tsai, C.-C. Wan, Y.-Y. Wang, *Journal of The Electrochemical Society*, 150 (2003) C267-C272.
- [137] H.W. Shim, J.D. Koppers, H. Huang, *Journal of Nanoscience and Nanotechnology*, 8 (2008) 3999-4002.
- [138] M. Uysal, T. Cetinkaya, A. Alp, H. Akbulut, *Applied Surface Science*, 290 (2014) 6-12.
- [139] T. Liu, G. Shao, M. Ji, G. Wang, *Journal of Solid State Chemistry*, 8 (2014) 111-115.
- [140] N. Chaisubanan, N. Tantavichet, *Journal of Alloys and Compounds*, 559 (2013) 69-75.
- [141] H. Surani Yancheshmeh, M. Ghorbani, *Surface and Coatings Technology*, 238 (2014) 158-164.
- [142] H. Fuchs, H. Mecke, M. Ellrodt, *Surface and Coatings Technology*, 98 (1998) 839-844.
- [143] D.-T. Chin, J.Y. Wang, O. Dossenbach, J.-M. Locarnini, A. Numanoglu, *Electrochimica Acta*, 36 (1991) 625-629.
- [144] A. Ul-Hamid, H. Dafalla, A. Quddus, H. Saricimen, L.M. Al-Hadhrami, *Applied Surface Science*, 257 (2011) 9251-9259.
- [145] P. Bala Srinivasan, J. Liang, R.G. Balajeee, C. Blawert, M. Störmer, W. Dietzel, *Applied Surface Science*, 256 (2010) 3928-3935.

- [146] D. Landolt, A. Marlot, *Surface and Coatings Technology*, 169-170 (2003) 8-13.
- [147] K. Subramanian, V.M. Periasamy, M. Pushpavanam, K. Ramasamy, *Journal of Electroanalytical Chemistry*, 648 (2010) 176-183.
- [148] A.P. Abbott, K.J. McKenziea, *Phys. Chem. Chem. Phys.*, 8 (2006) 4265-4279.
- [149] R. Juškėnas, Z. Mockus, S. Kanapeckaitė, G. Stalnionis, A. Survila, *Electrochim Acta*, 52 (2006) 928-935.
- [150] A. Survila, Z. Mockus, S. Kanapeckaitė, V. Jasulaitiene, R. Juskenas, *Electrochimica Acta*, 52 (2007) 3067-3074.
- [151] K. Subramanian, V.M. Periasamy, M. Pushpavanam, K. Ramasamy, *Journal of Electroanalytical Chemistry*, 636 (2009) 30-35.
- [152] R. Balaji, M. Pushpavanam, K.Y. Kumar, K. Subramanian, *Surface and Coatings Technology*, 201 (2006) 3205-3211.
- [153] E. Huttunen-Saarivirta, T. Tiainen, *Journal of Materials Processing Technology*, 170 (2005) 211-219.
- [154] T.-I. Leong, Y.-T. Hsieh, I.W. Sun, *Electrochimica Acta*, 56 (2011) 3941-3946.
- [155] T.N.Vorobyova, V.P. Bobrovskaya, V.V. Sviridov, *Metal Finishing*, 11 (1997) 14, 16-18,20.
- [156] W.J. Boettinger, C.E. Johnson, L.A. Bendersky, K.W. Moon, M.E. Williams, G.R. Stafford, *Acta Materialia*, 53 (2005) 5033-5050.
- [157] E. Huttunensaarivirta, T. Tiainen, *Journal of Materials Processing Technology*, 170 (2005) 211-219.

- [158] Z. Mockus, S. Kanapeckaitė, V. Jasulaitienė, A. Survila, *Protection of Metals*, 42 (2006) 485-490.
- [159] B. Palys, M.I. Borzenko, G.A. Tsirlina, K. Jackowska, E.V. Timofeeva, O.A. Petrii, *Electrochimica Acta*, 50 (2005) 1693-1702.
- [160] K. Subramanian, V.M. Periasamy, M. Pushpavanam, K. Sivakumar, *Journal of Electroanalytical Chemistry*, 648 (2010) 176-183.
- [161] H. Xinkuai, *Transactions of Nonferrous Metals society of China*, 16 (2006) 1379-1385.
- [162] T. Nickchi, M. Ghorbani, *Surface and Coatings Technology*, 203 (2009) 3037-3043.

## **2 The Electrodeposition of Copper-Tin Alloys using Aqueous Solvents**

In this study, electrodeposition of Cu-Sn alloy was performed from MSA based bath by varying peak current density  $i_p$  and frequency  $f$  in the pulsed mode. Besides that, influence of three different anodes on the stability of bath and reproductivity of deposits were studied. The use of two anodes was firstly under investigation which brought improvement to the existing results and is worthy further study on mechanisms in the future.

## 2.1 Effect of direct current density on the composition of deposited coatings

Methanesulfonic acid based bronze electroplating solution containing  $\text{Cu}^{2+}$  6g/l,  $\text{Sn}^{2+}$  3g/l, MSA 300 ml/l (mole ratio Cu:Sn=3.71) was commercially available from Enthone Group and operated at room temperature (25°C). It contains 300 ml/l acid concentrate, 200 ml/l make-up, 3 ml/l brightener, 20 ml/l wetting agent and 10 ml/l additive HG besides the bulk metal salts.

These additives not only are brighteners but also are needed to stabilize tin ions. Other examples of electrodeposition copper-tin alloys from methanesulfonic acid-based bath can be found with different additives, e.g. 200g  $\text{dm}^{-3}$  MSA based bath with addition of primary grain refiner, second grain refiner and brightener was used to electrodeposit 99wt% Sn at a 10A  $\text{dm}^{-2[1]}$  and 2mol  $\text{dm}^{-3}$  MSA based bath with 25ppm MPS and 75ppm PEG to deposit 7% Sn<sup>[2]</sup>.

Distilled water was used throughout. The deposition was carried out in a cell with two electrodes fixed vertically parallel with both direct current as well as square wave current pulses at room temperature. A graphite sheet, a copper plate or a combination of graphite and copper was used as anode material. When two anodes were used, both anodes were circuited with working electrode in a double anodic circuit and current density was assigned as Cu plate: graphite sheet= 4:1. Low alloy steel panels (4cm×4cm) were used as substrates for deposition and were pretreated by polishing with SiC paper (grit 4000) degreasing with acetone, pickled in 0.1M  $\text{H}_2\text{SO}_4$  for 15 minutes and rinsed. When indicated, the steel panels were coated by

bright Cu underlayer layer (5 $\mu$ m). During deposition, bronze bath was kept constantly under mechanical stirring at 350 rpm.

Regarding the deposited coatings, the surface morphology and composition were characterized by Environmental Scanning Electron Microscopy (ESEM, Phips XL30) and energy dispersive X-ray spectroscopy (EDXS).

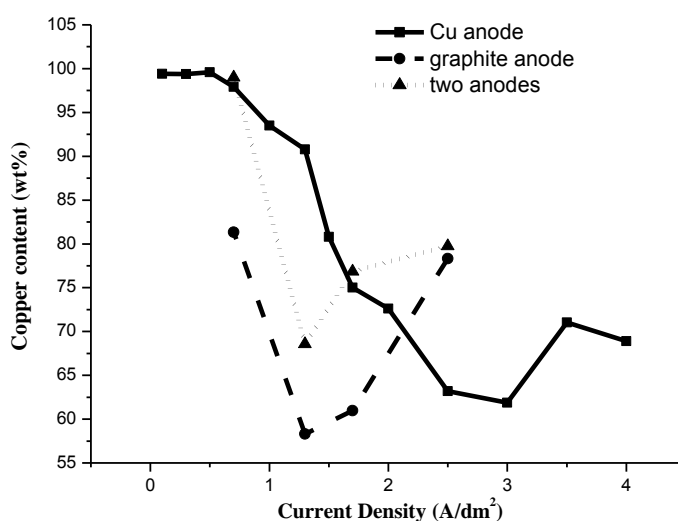


**Figure 2.1** Effect of current density on copper content of films deposited with copper anode (solid line), graphite anode (dashed line) and two anodes (dotted line)

In order to investigate the range of current that is favourable to layers with silver-white color, the films were produced at different current densities from 0 to 4 A/dm<sup>2</sup> with Cu plate as anode. Figure 2.1 showed that copper content of the deposit first decrease and then increase with the increase of current density. The minimum of copper content (60wt %) was obtained at about 3 A/dm<sup>2</sup>. This result can be explained by the fact that

copper deposits at more positive potentials than that of tin<sup>[3, 4]</sup>. The higher the current density, the more negative the potential at the cathode. At very low current densities, the potentials on the cathode are positive enough to deposit only copper, not tin. At higher current densities (more negative potentials), both copper and tin are ready to deposit. Given a 3.71:1 difference between molarities of copper and tin ions in bath, the tin deposition is limited by diffusion and the copper deposition is less limited when sufficiently higher current densities (sufficiently negative potentials) are applied. By visual observations, the deposits show light yellow ( $i < 2 \text{ A/dm}^2$ ) to silver white ( $2 \text{ A/dm}^2 \leq i \leq 3 \text{ A/dm}^2$ ) and then to light yellow ( $i > 3 \text{ A/dm}^2$ ) changing trend corresponding to the composition change. Bright and coherent deposits could be obtained in the range of 2.0-3.0  $\text{A/dm}^2$  with target colour.

As can be seen from microstructure of deposits obtained using copper anode in Figure 2.2, grains tend to grow into larger size when applied current density increased from 0.1  $\text{A/dm}^2$  to 0.5  $\text{A/dm}^2$  despite their comparable composition. Cracks can be clearly distinguished on the deposits when Sn content increased continuously especially when  $i > 2 \text{ A/dm}^2$ . The porosity of deposits prepared under current density of 1.1  $\text{A/dm}^2$  can be ascribed to the lower thickness of the layer than other films and the patterned background may be caused by the slight polish of the substrate before deposition.

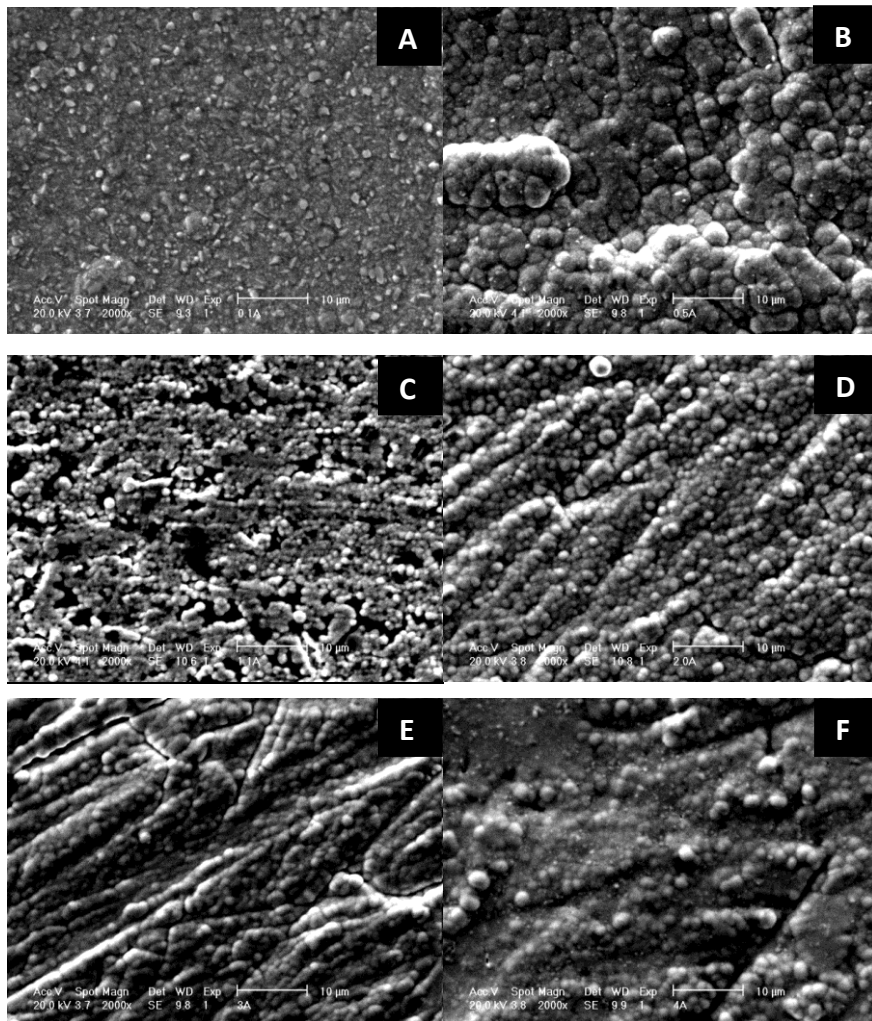


**Figure 2.2** Surface morphology of films deposited with copper anode at current density of (A)  $0.1 \text{ A/dm}^2$ , (B)  $0.5 \text{ A/dm}^2$ , (C)  $1.1 \text{ A/dm}^2$ , (D)  $2.0 \text{ A/dm}^2$ , (E)  $3.0 \text{ A/dm}^2$  and (F)  $4.0 \text{ A/dm}^2$

Graphite anode was also studied in narrower current range shown in Figure 2.1. Comparable composition (57wt% Cu) could be obtained at much lower current density,  $1.3 \text{ A/dm}^2$  since the composition trend seems to be shifted at lower current deposition. Copper content of the layer deposited with graphite anode is lower compared to the deposit obtained at the same

current density value with copper anode when current density is lower than  $2 \text{ A/dm}^2$ . Current efficiency of the deposition processes with both anodes was very high, 95%-98%, covering the whole current range under investigation.

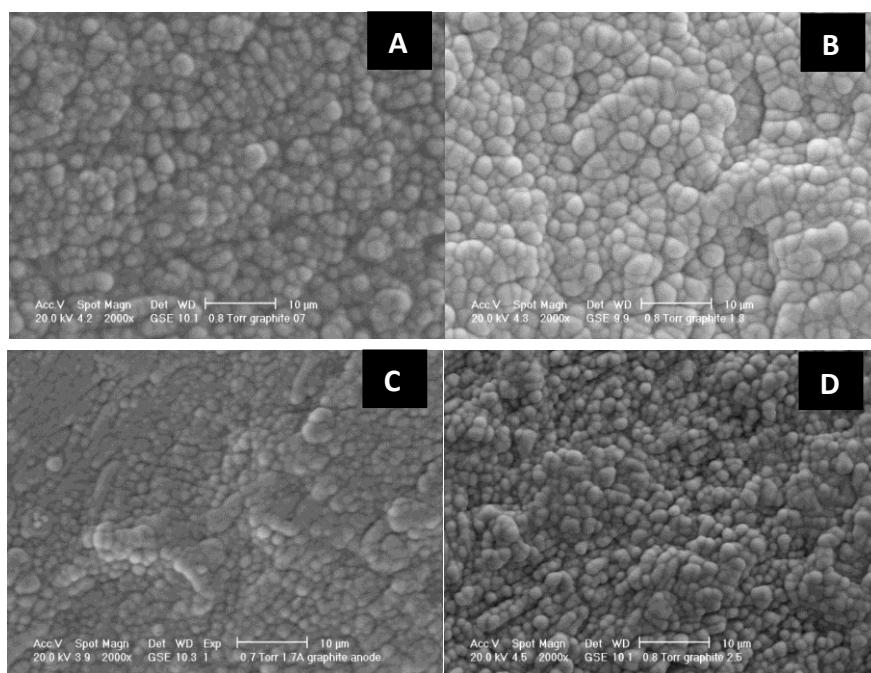


**Figure 2.3** Surface morphology of films deposited with graphite anode at current density of (A)  $0.7 \text{ A/dm}^2$ , (B)  $1.3 \text{ A/dm}^2$ , (C)  $1.7 \text{ A/dm}^2$  and (D)  $2.5 \text{ A/dm}^2$



**Figure 2.4** Photos of deposits with graphite anode at current density of (A)  $0.7 \text{ A/dm}^2$ , (B)  $1.3 \text{ A/dm}^2$ , (C)  $1.7 \text{ A/dm}^2$  and (D)  $2.5 \text{ A/dm}^2$

Compared with the films deposited using copper anode, the layers prepared with graphite anode produced more compact surfaces with regular-shaped grains which were shown in Figure 2.3. No visible cracks can be recognized neither by naked eye nor microscopy observation when graphite anode was adopted. With consecutive increase of applied current density, deposits appeared to have three-dimensional growth perpendicular to substrate composed of smaller grains, which caused developing roughness. This behavior is close to the pure Sn electrodeposition<sup>[5]</sup> which presents increasing roughness with rising currents. Pure tin layer shows porous surfaces in high currents while alloy film can remain compact even the tin content reaches approximately 40 wt%.

The visual appearance of deposits is obviously different emerging from the varied composition, as shown in Figure 2.4. The film prepared using 0.7 A/dm<sup>2</sup> has typical color of copper; the alloy deposited at 1.3A/dm<sup>2</sup> shows silver color with attractive gloss while that obtained at 1.7 A/dm<sup>2</sup> is mat; the deposit resulted at 2.5 A/dm<sup>2</sup> turned to be grey in color and darker in reflection.

The composition of the films deposited using two anodes was also studied. The changing trend was fairly different from those using copper anode while it was similar with that with graphite anode covering the same current range. As the current density was as low as 0.5 A/dm<sup>2</sup>, deposited alloy shows the same composition as that obtained by copper anode. This is due to low overpotentials on both circuits consisting copper and graphite as anode materials under low currents. While the current density increased to 1.3 A/dm<sup>2</sup>, tin content increased to 30 wt% in the film presenting silver color. The copper content increased with continuous current growing which is not unexpected since the difference of concentrations between copper and

tin ions in the solvent played a major role under mass-transfer controlled condition.

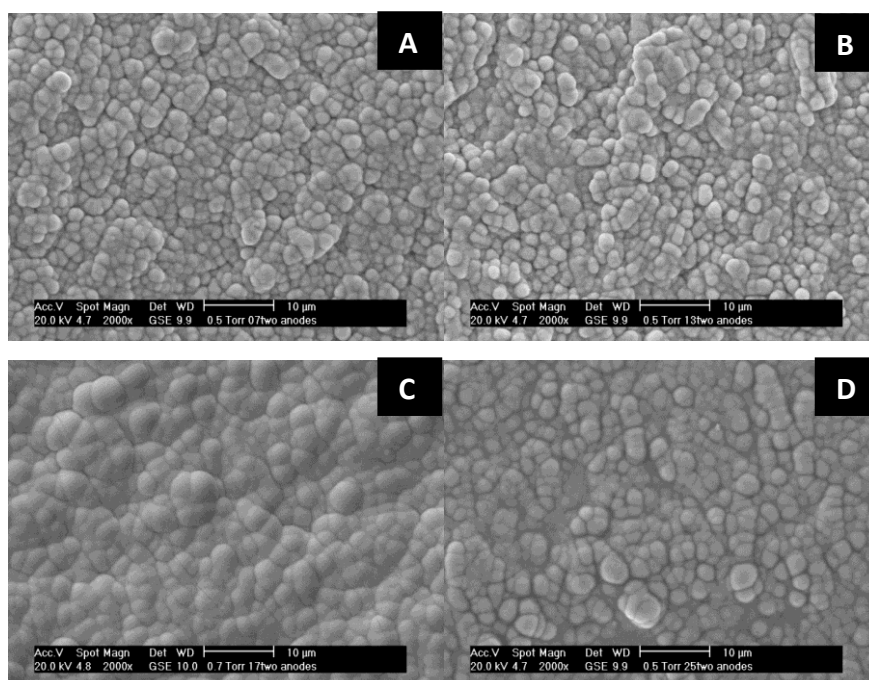


**Figure 2.5** Surface morphology of films deposited with two anodes at a total current density of (A)  $0.7 A/dm^2$ , (B)  $1.3 A/dm^2$ , (C)  $1.7 A/dm^2$  and (D)  $2.5 A/dm^2$

It can be shown in Figure 2.5 that deposits prepared with two anodes exhibits similar surface morphology with those obtained using graphite anode.

The improvement on surface microstructure by adopting graphite or two anodes instead of copper can be proved by the reduced roughness determined by a surface profilometer. The substrate was polished until the surface roughness  $R_a$  was around  $1.03 \pm 0.11 \mu m$ , the layers deposited in presence of graphite anode show a roughness of  $0.22 \pm 0.02 \mu m$  and two

anodes  $0.20 \pm 0.03 \mu\text{m}$  while the films deposited using copper as anode had a surface roughness of  $0.96 \pm 0.12 \mu\text{m}$ .

## 2.2 Effect of anode on the stability of the bath

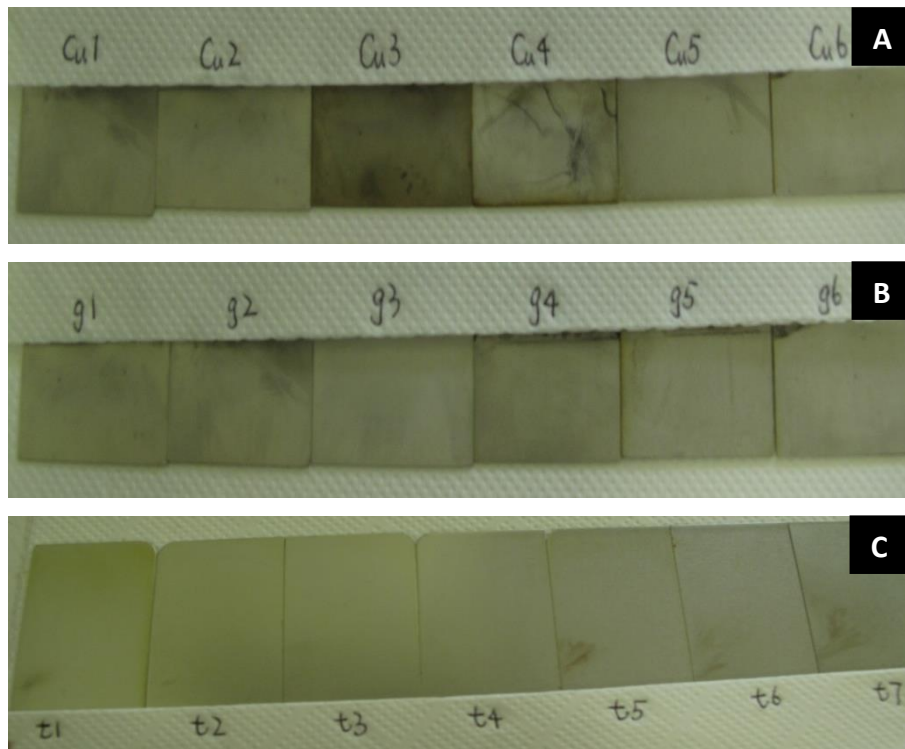


**Figure 2.6** Photos of films continuously deposited with (A) copper anode, (B) graphite anode and (C) two anodes at current density of  $1.3 \text{ A/dm}^2$

A copper plate, a graphite sheet and the mixed two anodes were adopted as anode material to check its influence on stability of composition of deposited films and lifetime of the bath. Continuous depositions on separate substrates were carried out in three equally prepared baths. Current density was fixed at  $1.3 \text{ A/dm}^2$  under DC and deposited films were controlled with  $5 \mu\text{m}$  thickness. Each deposit requires approximately 200C (0.056Ah) to accomplish. With the increase of electrical quantity passed in the bath,

deposited samples with copper anode experienced color change from silver white to light yellow at first three samples, then return to silver white while color of the bath shows slightly turbid after several samples. On the contrary, deposited films with graphite anode or joined two anodes keep rather stable colour, silver white, during the whole process and also bath does not show any visual change in colour. The changing trends of deposits are compared in Figure 2.6.

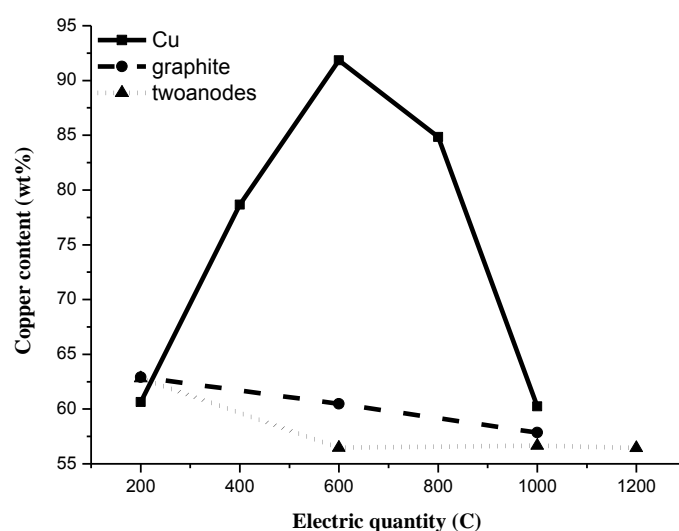


**Figure 2.7** Copper content of continuously deposited films with copper anode (solid line), graphite anode (dotted line) and two anodes (dotted line) obtained from EDX analysis

To verify the result, composition analysis was carried out on the samples with different ageing time as shown in Figure 2.7. It can be seen that copper content reached a maximum around after 600 C (0.167Ah), i.e. the third sample. Even the second and fourth samples show distinct different composition compared to the first one. On the contrary, samples resulted

from graphite maintain constant composition with only slight changes and deposits prepared with combined two anodes reached a minimum copper content at consumed electric quantity of 600C followed by a steady composition in subsequent deposits. This clarified that the adoption of two anodes can be beneficial to better reproducibility of samples deposited.

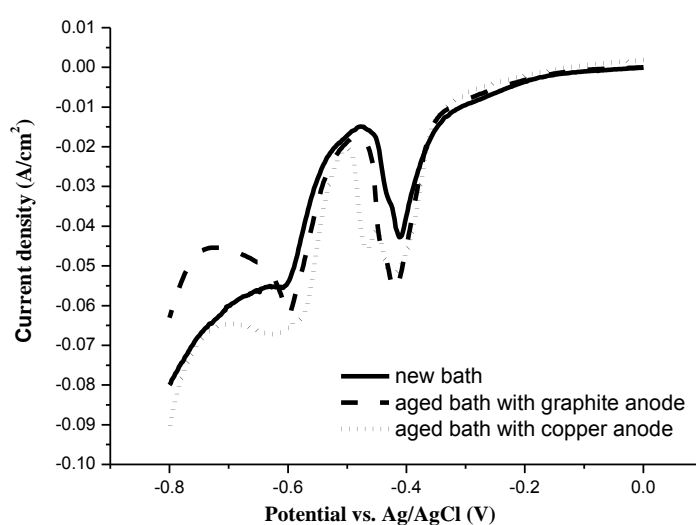


**Figure 2.8** Linear scanning curves in new bath (solid line), aged bath with graphite anode (dashed line) and aged bath with copper anode (dotted line)

To find out the reason leading to deposits changes, linear scanning voltammetry was carried out to show the redox species changes of baths which are new-prepared or have accomplished several electroplating processes, as shown in Figure 2.8.

The linear scanning voltammetry was carried out in a 3 electrode cell by a PAR potentiostat model 273. Platinum plate was used as working electrode, platinum foil as counter electrode and the potential was swept from 0 to -0.8 V vs. Ag/AgCl/3M KCl at a scan rate of 10 mV/s.

The reduction process initiates at a potential of approximately -0.17V vs. Ag/AgCl which locates at the same value for copper deposition as reported in Ref<sup>[6]</sup>. The solid line presents the linear scanning voltammetry of new bath. The two well-defined peaks with a maximum located at -0.4V and -0.62V in the fresh bath represent the reduction of Cu(II) and Sn(II), separately. The transition of Cu(II) to Cu(0) occurs at the same potential even after the bath was aged by deposition with either copper or graphite anode. The reduction of Sn(II) ions to Sn metal starts to occur at -0.5V both in fresh and in old baths although the peak shape is slightly steeper for old ones. With the change of anode material, the reduction potential remains at -0.5V showing that anode material did not alter the tin deposition potential. This is in agreement with work carried out by other researchers<sup>[6, 7]</sup>. As the potential became more negative, the current density reached a plateau followed by an increase. The appearance of plateau can be associated with the complete consumption of metallic ions at the electrode surface due to mass transport control of the reduction. The further increases in current density, at a potential more negative than -0.7 V, are attributable to hydrogen evolution as a secondary reaction<sup>[8]</sup>. The hydrogen reaction starts at more negative potential and lower rate in aged bath with graphite anode compared to both new bath and the old one adopting copper anode. However, a new peak emerges at -0.48 V vs. Ag|AgCl which help prove the occurrence of Sn(IV) during the electroplating process with copper anode after 600C (0.167Ah) of ageing. This new peak is assumed to be related to the existence of Sn<sup>4+</sup> due to oxidation from Sn<sup>2+</sup>. The bath aged using graphite anode on the contrary does not show differences in peaks compared to initial bath, which states that the oxidation of Sn<sup>2+</sup> can be accelerated with copper anode more easily compared to graphite. Similar behavior with

graphite anode can be observed when two materials were used as anode, which is not shown in this figure for better clarity. This can be explained by the fact that  $\text{Sn}^{2+}$  shows less noble oxidation potential than  $\text{Cu}^0$ . As a result  $\text{Sn}^{2+}$  contained in the bath has the tendency to be oxidized on the copper anode surface. Slight increase of reduction peak of  $\text{Cu}^{2+}$  can be attributed to the higher ratio of Cu/Sn.

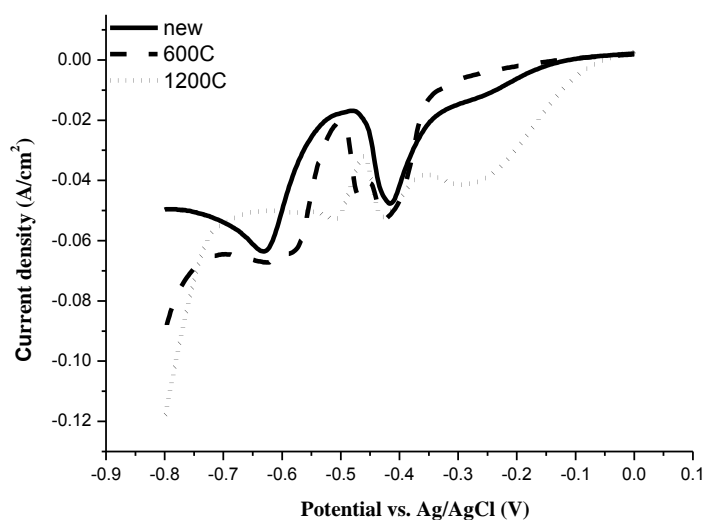


**Figure 2.9** Linear scanning curves in new bath (solid line), aged bath consumed 600C (dashed line) and aged bath consumed 1200C (dotted line) operated with copper anode

The species change in the same bath with continuous deposition using copper anode have been investigated as shown in Figure 2.9. With longer ageing time of the bath, not only a new peak appears indicating the reduction from  $\text{Sn}^{4+}$  to  $\text{Sn}^{2+}$  but also the three peaks according to the reduction of  $\text{Cu}^{2+}$ ,  $\text{Sn}^{4+}$  and  $\text{Sn}^{2+}$  have been moved to more positive potentials and peak currents of  $\text{Cu}^{2+}$  and  $\text{Sn}^{4+}$  reduction increased. The

volatility of the potential positions can be ascribed to the decomposition of surfactants in the bath which may be accelerated by copper anode<sup>[6]</sup>. Also it is due to increase of  $\text{Cu}^{2+}$  and  $\text{Sn}^{4+}$  concentration throughout the process. The increase and broaden of  $\text{Cu}^{2+}$  reduction peak can be resulted from the dissolution of copper anode during deposition process and more copper complexes existing in the solvent. Meanwhile, hydrogen evolution occurs in higher extent with the increase of aging time due to the varied composition of the solvents.

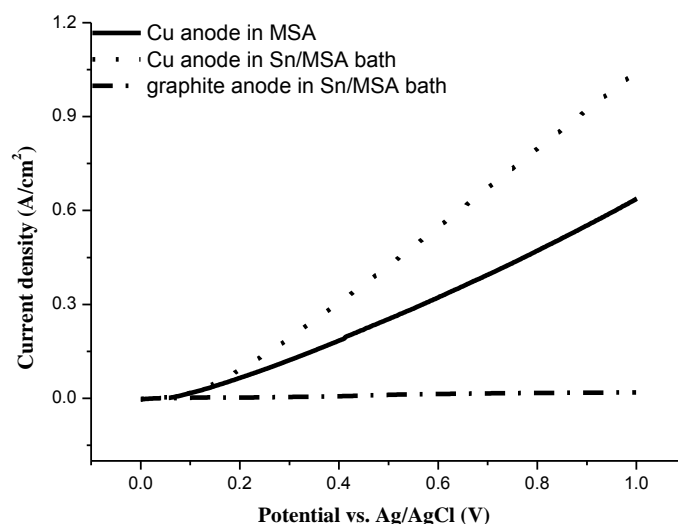


**Figure 2.10** Anodic polarization curves for copper anode in MSA electrolyte (solid line), copper anode in MSA electrolyte containing Sn salts (dotted line) and graphite anode in MSA containing Sn salts (dash-dotted line)

In order to understand if oxidation extent of  $\text{Sn}^{2+}$  is different on two materials: copper and graphite, the anodic polarization curves (Figure 2.10) of these two anodes are carried out in baths containing either tin or without

metallic ions. Copper anode exhibits much greater currents when polarized positively than that of graphite anode due to the continuous dissolution of bulk material when oxidized. Therefore it is difficult to extrapolate the current intensity due to  $\text{Sn}^{2+}$  oxidation, the difference between the current recorded in Sn-contained bath and in blank bath can give an estimation of the oxidation of stannous ions. The increasing disparity in current with potential increase is significantly larger than the one of graphite which shows very limited currents in the same conditions.

### 2.3 Effect of pulse frequency on the composition

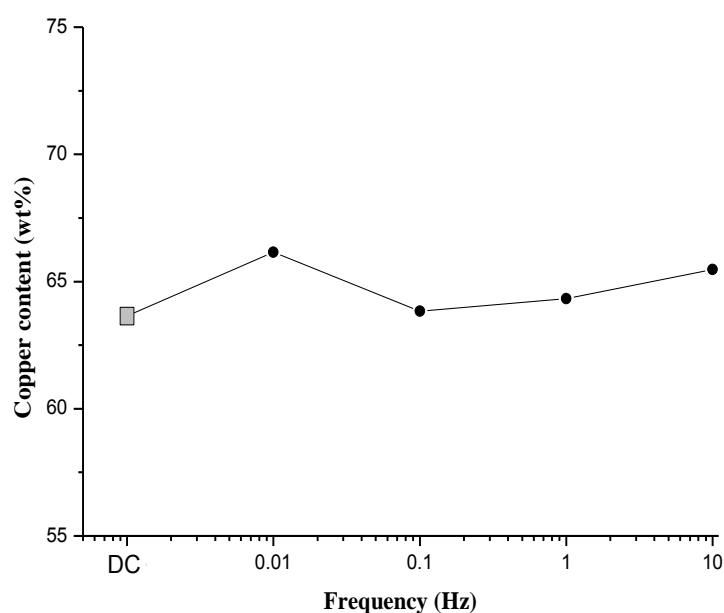


**Figure 2.11** Effect of frequency on copper content of films deposited with graphite anode at current density of  $1.3\text{A}/\text{dm}^2$  and duty cycle of 0.5.

The deposition with pulse current was carried out varying the current density between  $2.6 \text{ A/dm}^2$  (on-time) and zero (off-time) with a square wave pulse and a duty cycle of 50%, while different frequencies were applied from 0.01 to 10 Hz. Deposition time was varied according to actual current density in order to obtain constant thickness of  $5 \mu\text{m}$ .

For the PC deposition the graphite anode was used and the applied current is cycled between  $2.6 \text{ A/dm}^2$  and zero at fixed duty cycle of 0.5. This results an average current density of  $1.3 \text{ A/dm}^2$  which remains the same as in that direct current mode. Copper content, reported in Figure 2.11, is slightly higher in the entire range studied than that deposited with DC. Despite small increase of copper content, the appearance of films remains silver-colored. The higher copper content is likely due to the copper ion exchanges with the plated tin during the off pulse according to the reaction  $\text{Cu}^{+2}(\text{aq}) + \text{Sn}(\text{s}) \rightarrow \text{Cu}(\text{s}) + \text{Sn}^{+2}(\text{aq})$ <sup>[9]</sup>. Such a behavior has been verified experimentally for Ni-Cu and Co-Cu alloys<sup>[10, 11]</sup>. The change of alloy composition resulting from pulse plating has been numerically modeled by some studies<sup>[12, 13]</sup>.

## **2.4 Microstructure and electrochemical properties of deposited coatings**

SEM micrographs revealed the nodular growth morphology of the as-deposited surface of Cu-Sn layers coating under DC and PC plated conditions. In Figure 2.12, representative PC samples are presented. Prior to deposition, the substrate was slightly polished to a surface roughness Ra of around  $1.029 \mu\text{m}$ . The average roughness of the layers deposited under PC

is  $0.12 \pm 0.2 \mu\text{m}$  which is lower than its DC counterparts ( $0.22 \mu\text{m}$ ). The increasing frequency shows no obvious influence on surface roughness of resulting layers.

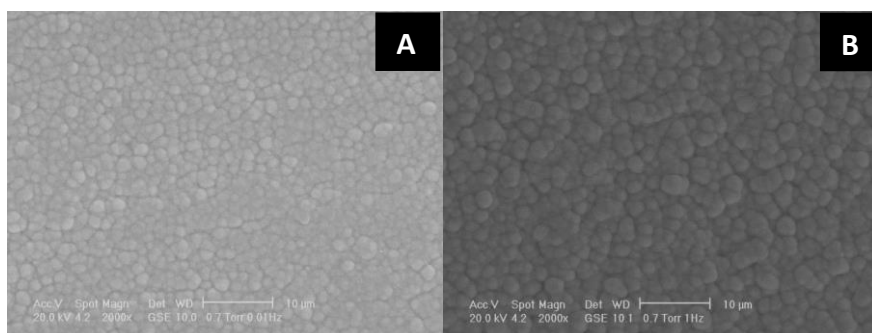


**Figure 2.12** Secondary electron micrographs of Cu-Sn alloys prepared with pulse plating with frequency of (A) 0.01 Hz and (B) 1 Hz with graphite anode at current density of  $1.3 \text{ A/dm}^2$  and duty cycle of 0.5.

Electron microscopy observation of the layer electrodeposited with pulse current shows a nodular microstructure irrespective of the applied frequency. Also, significantly peak broadening of the XRD peaks was observed.

The X-ray diffraction (XRD) spectra were collected using a powder diffractometer (Rigaku D-max), employing  $\text{CuK}\alpha$  radiation and a graphite monochromator in the diffracted beam; typical scans were performed in the  $2\theta$   $10 - 110^\circ$  range, with a sampling range of  $0.05^\circ$  and 6 s counting time.

The nodules in the SEM images together with the broadened XRD peaks are evidence for a nanocrystalline coating morphology. However, increasing the deposition frequency nodule structure and size seems to slightly increase and in this case aggregate in bigger granules.

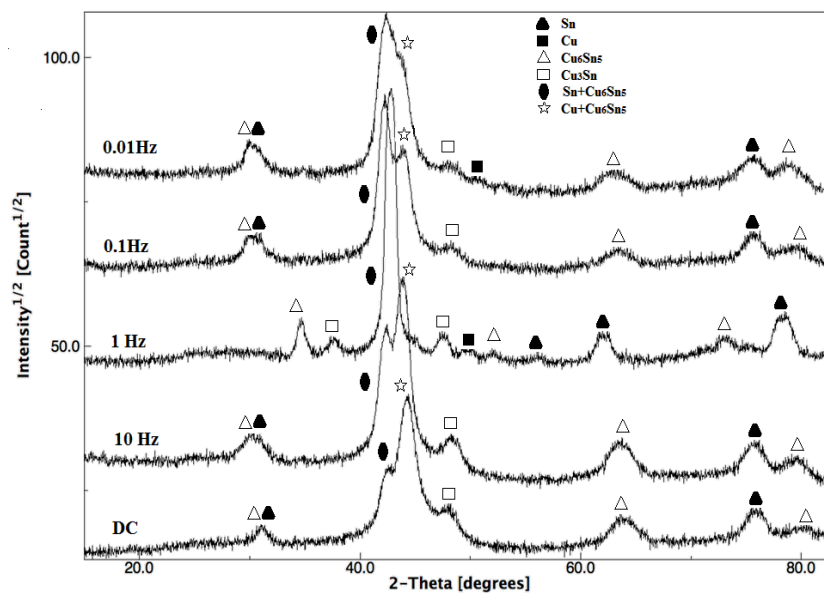


**Figure 2.13** Characteristic XRD patterns obtained for Cu–Sn alloy deposited at current density of  $1.3 \text{ A/dm}^2$  and duty cycle of 0.5 at indicated frequencies or DC

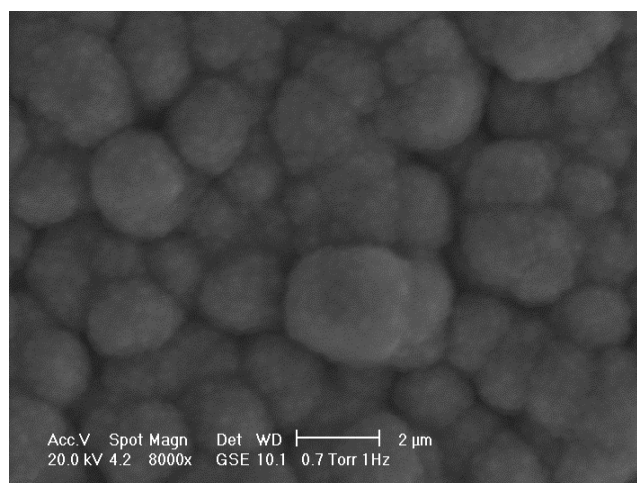


**Figure 2.14** Magnified secondary electron micrograph of Cu-Sn alloys deposited at 1Hz with graphite anode at current density of  $1.3 \text{ A/dm}^2$  and duty cycle of 0.5.

Further investigation on microstructure was carried out by analysis on X-ray diffraction patterns of deposits obtained under different deposition conditions reported in Figure 2.13. The broad peaks may also due to the fact Cu-Sn layers were relatively thin (5  $\mu\text{m}$ ) besides their nanocrystalline microstructure<sup>[14]</sup> which can be distinguished from the magnified image in Figure 2.14.

Peak intensity analysis was carried out by comparison with XRD patterns in other investigations related to bronze coatings<sup>[4, 14-16]</sup>. It shows that the deposit is mostly tin, copper with  $\text{Cu}_6\text{Sn}_5$  and  $\text{Cu}_3\text{Sn}$  intermetallics. With increasing the applied frequency from 0.01 Hz to 10 Hz, Cu is achieving higher portion in bi-phase deposit while Sn is reduced in content by comparing the two significant peaks arising between 40-45°. This result is compatible with the composition analysis of Cu (~65wt%) and Sn (~35wt%) obtained by EDXS, where the total copper content comes from the signal of  $\text{Cu}_6\text{Sn}_5$  alloy whose composition is ~40wt% Cu and 60 wt% Sn, plus dissolution of pure copper<sup>[17, 18]</sup>. In other studies, copper-tin alloys can also be obtained via, e.g. heat treatment for 24 hours to produce hexagonal  $\text{Cu}_6\text{Sn}_5$  and cubic  $\text{Cu}_3\text{Sn}$ <sup>[19]</sup> and chemical reduction to produce 20-40nm  $\text{Cu}_6\text{Sn}_5$ <sup>[20]</sup>. The diffraction line of 1Hz is not easy assigned to specific metallic phase with shifted peaks. The two peaks appeared around 35° can be assumed to the existence of meta-stable phases of the intermetallics,  $\text{Cu}_6\text{Sn}_5$  and  $\text{Cu}_3\text{Sn}$ , which is similar with the results obtained by aging alloys above 300 °C<sup>[21]</sup>.

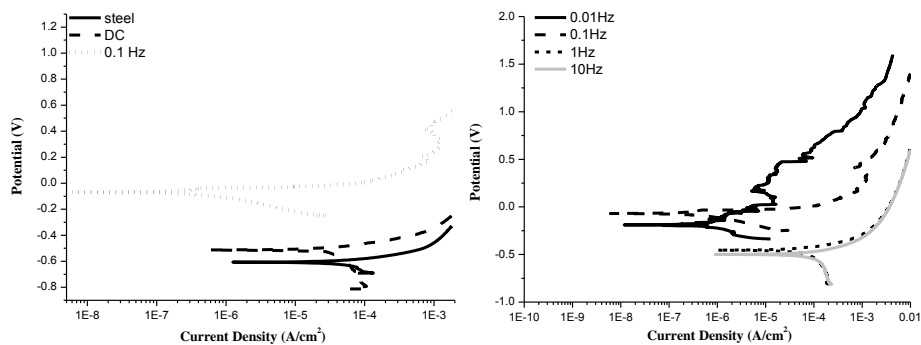


**Figure 2.15** Polarization curves of bronze films deposited on steel plate in 0.1M NaCl solution

Deposited layers	Anodic			
	Tafel slope ( $\beta_a$ , mV)	Cathodic Tafel slope ( $\beta_c$ , mV)	Eoc (mV vs. SCE)	Exchange current density ( $\text{mA cm}^{-2}$ )
Steel substrate	23.3	20.3	-607.2	7.164
DC deposited Cu-Sn	23.0	19.5	-513.0	3.561
PC deposited Cu-Sn 0.01Hz	18.8	19.5	-188.8	0.066
PC deposited Cu-Sn 0.1Hz	22.8	19.2	-72.26	0.048
PC deposited Cu-Sn 1Hz	27.3	16.7	-454.5	5.718
PC deposited Cu-Sn 10Hz	24.1	22.9	-498.8	5.974

**Table 2.1** Tafel data of different Cu-Sn layers deposited on steel substrate in 0.1M NaCl

In term of corrosion protection, coatings were deposited both on steel substrate and copper underlayer in order to evaluate the electrochemical behavior by potentiodynamic polarization measurements in 0.1 M NaCl aqueous solution.

Electrochemical behaviors of the deposits were characterized by potentiodynamic polarization curves using a Princeton Applied Research PARSTAT 2273 potentiostat. A three-electrode cell was used with  $1\text{cm}^2$  deposits as working electrode, Ag/AgCl/3M KCl as reference electrode and platinum foil as counter electrode. The anodic polarization was performed in 0.1M NaCl solution (pH=6.5) in the range of -0.3V vs. OCP to 1V vs. Ag/AgCl at a scan rate of 0.2 mV/s at room temperature.

For better clarity, comparison on polarization curve of between deposits obtained by DC, 0.1Hz and substrate was presented in Figure 2.15(A), and layers prepared with different frequencies was compared in Figure 2.15(B). Detailed data has been shown in Tables. Bronze layers are expected to increase the corrosion potential of substrate and lower the corrosion currents. However, as shown in Figure 2.15 and Table 2.1, the DC-deposited ones show poor improvement indicating the defective films caused by porous structure. On the contrary, the PC indeed improves the layers showing more compact surface compared to DC. On the other hand, passive behavior can be hardly observed on the film deposited on steel plate even using pulse current, due to relatively high porosity.

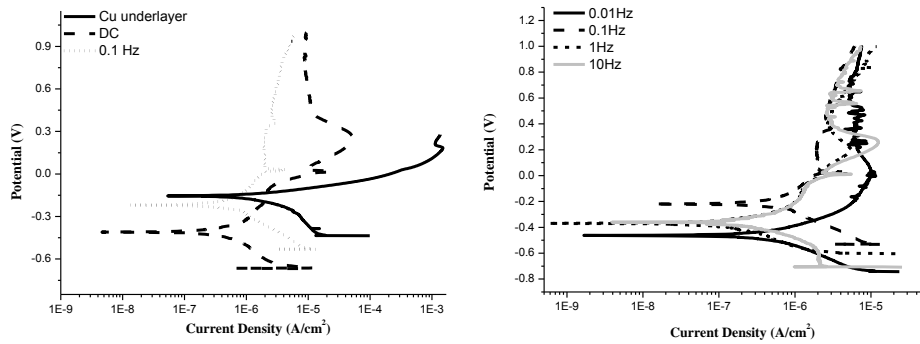


**Figure 2.16** Polarization curves of bronze films deposited on Cu underlayer (5µm) in 0.1M NaCl solution

Deposited layers	Anodic Tafel slope ( $\beta_a$ , mV)	Cathodic Tafel slope ( $\beta_c$ , mV)	Eoc (mV vs. SCE)	Exchange current density ( $\text{mA cm}^{-2}$ )
Cu underlayer	21.3	24.0	-154.5	0.167
DC deposited Cu-Sn	31.0	16.6	-410.1	0.037
PC deposited Cu-Sn 0.01Hz	26.2	18.4	-384.8	0.147
PC deposited Cu-Sn 0.1Hz	26.6	27.2	-284.4	0.036
PC deposited Cu-Sn 1Hz	27.3	15.4	-369.7	0.012
PC deposited Cu-Sn 10Hz	46.3	30.3	-360.0	0.045

**Table 2.2** Tafel data of different Cu-Sn layers deposited on copper underlayer in 0.1M NaCl

However, in the practical application, copper underlayer is deposited on the substrate in order to provide a bright surface and retain the attractive appearance as well as improve the coating's adhesion to the surface<sup>[22]</sup>. Figure 2.16 and Table 2.2 showed the corrosion behavior of bronze deposited on copper layer. As shown, copper underlayer shows significantly lower corrosion potential and reduced corrosion rate compared to steel substrate proving it is a protective coating free of pores. Passive behavior

can be observed on the bronze deposits on copper underlayer suggesting that copper-tin co-deposits exhibits better protective function than pure copper. The addition of tin to the co-deposition can decrease the corrosion potential of copper. The deposition of bronze coating on copper reduces the cathodic Tafel slope and shifts corrosion current density towards lower values, thereby resulting in a reduced corrosion rate. By comparing the deposits produced with direct current and pulse current, the film obtained by pulse plating can exhibit lower corrosion rate within the passive region. It can be concluded that corrosion potential is proportional to copper content in bronze layers from the fact that PC-deposited layers have higher corrosion potentials.

## **2.5 Conclusions**

The deposition of Cu-Sn coatings from a methanesulfonic based bath for decorative purposes was studied and process parameter was optimized in order to obtain layers with expected composition and high stability. In this part of our work, three electrodeposition parameters - choice on anode material, current density under direct condition and frequency values under pulsed condition - were varied to control the physical and chemical characteristics of the deposits obtained from the described bath. First, effect of current density on Cu content was studied by DC method in order to cover the wide range of compositions with lustrous appearance in silver-like color. Then, the use of only copper, only graphite and simultaneous use of these two materials were compared as anode options to achieve longer working time of the bath. The change of anode from copper to graphite or two anodes has been beneficial to both life time of the bath and appearance

of deposits. Ultimately, to obtain better microstructure and corrosion resistance behavior compared to DC, different frequencies under PC deposition were investigated. Satisfying results can be achieved under optimized conditions since the employment of pulsed current during electrodeposition process can reduce the grain size and introduce new crystal structures. In term of corrosion protection direct deposition on steel leads to the formation of defects and accordingly non protective coatings, while a copper underlayer can solve this problem leading to a protective coating.

## 2.6 References

- [1] C. Doyle, N. Brown, M. Bardizeh, *Metal Finishing*, 1 (2002) 10-12, 14-17.
- [2] I.-Chia Hsu Chang, P. C. Andricacos, Jean Horkans, H. Deligianni, *Journal of the Electrochemical Society*, 142 (1995) 3779-3785.
- [3] S.D. Beattie, J.R. Dahn, *Journal of the Electrochemical Society*, 150 (2003) C457-C460.
- [4] S.D. Beattie, J.R. Dahn, *Journal of the Electrochemical Society*, 150 (2003) A894-A898.
- [5] A. Sharma, S. Bhattacharya, R. Sen, B.S.B. Reddy, H.J. Fecht, K. Das, S. Das, *Materials Characterization*, 68 (2012) 22-32.
- [6] C.T.J. Low, F.C. Walsh, *Surface and Coatings Technology*, 202 (2008) 1339-1349.
- [7] N.M. Martyak, R. Seefeldt, *Electrochimica Acta*, 49 (2004) 4303-4311.
- [8] A. Hovestad, R.A. Tacke, H.H.t. Mannelje, *Physica status solidi (c)*, 5 (2008) 3506-3509.
- [9] D. Landolt, A. Marlot, *Surface and Coatings Technology*, 8-13 (2003) 169-170.
- [10] P.E. Bradley, D. Landolt, *Electrochim Acta*, 45 (1999) 1077-1087.
- [11] P.E. Bradley, D. Landolt, *Electrochim Acta*, 42 (1997) 993-1003.
- [12] S. Roy, *Journal of Applied Electrochemistry*, 27 (1997) 299-307.
- [13] S. Roy, D. Landolt, *Journal of the Electrochemistry Society*, 142 (1995) 3021-3027.
- [14] N. Pownim, S. Roy, *Electrochimica Acta*, 90 (2013) 498-506.
- [15] C.T.J. Low, F.C. Walsh, *Surface and Coatings Technology*, 202 (2008) 1339-1349.

- [16] R. Juškėnas, Z. Mockus, S. Kanapeckaitė, G. Stalnionis, A. Survila, *Electrochimica Acta*, 52 (2006) 928-935.
- [17] I.A. Carlos, C.A.C. Souza, E.M.J.A. Pallone, R.H.P. Francisco, V. Cardoso, *Journal of Applied Electrochemistry*, 30 (2000) 987-994.
- [18] M.Hansen, K. Anderko, *Constitution of Binary Alloys*, McGraw Hill, New York, 1958.
- [19] R.O. Noriyuki Tamura, F. Masahisa, F. Shin, *Journal of Power Sources*, 107 (2002) 48-55.
- [20] C.-H. Wu, F.-Y. Hung, T.-S. Lui, L.-H. Chen, *Materials Transactions*, 50 (2009) 381-387.
- [21] N.F. Kennon, D.P. Dunne, L. Middleton, *Metall. Trans. A*, 13A (1982) 551.
- [22] K. Weitershaus, European Patent Office, Buckley, Guy Julian, European, 2013.

### **3 Electrodeposition of Copper from Deep Eutectic Solvent based on mixture of Choline Chloride and Ethylene Glycol**

In this part of our study, we investigated the deposition of copper from both ethaline and reline at elevated temperature for higher available applied current and better quality of deposits. Copper salts with different anions, comparison of diffusion coefficient in two solvents, operation temperature and metallic salts concentrations were studied for optimized set-up. In latter part, pulse current was chosen to improve the current efficiency of deposition process and it proved to refine grain size as well as improve the throwing power.

### 3.1 Physical properties

Choline chloride [ $\text{HOC}_2\text{H}_4\text{N}(\text{CH}_3)_3\text{Cl}$ ] (ChCl) (Aldrich 98%), Urea [ $\text{CO}(\text{NH}_2)_2$ ] (Aldrich 99%) and ethylene glycol [ $\text{HOCH}_2\text{CH}_2\text{OH}$ ] (EG) (Aldrich 99%) were used as received. The mixture was formed by stirring the two components together at 1:2 molar ratio of ChCl: hydrogen bond donor at 80 °C until a homogeneous, colorless liquid formed. The copper salts,  $\text{CuCl}_2 \cdot 2\text{H}_2\text{O}$  (Aldrich  $\geq 98\%$ ) and  $\text{CuSO}_4 \cdot 5\text{H}_2\text{O}$  (Aldrich  $\geq 98\%$ ), were used as received.

The physical properties, viscosity and conductivity, were compared between neat eutectic solvents and the ones with various concentrations of  $\text{CuCl}_2 \cdot 2\text{H}_2\text{O}$  or  $\text{CuSO}_4 \cdot 5\text{H}_2\text{O}$  at various temperatures. The viscosity was measured using a Brookfield DV-E Viscometer fitted with a thermostatic jacket. The conductivity was determined by Crison conductimeter 525. Complete dissolution of salts was aided by gentle stirring for 10 min before each measurement.

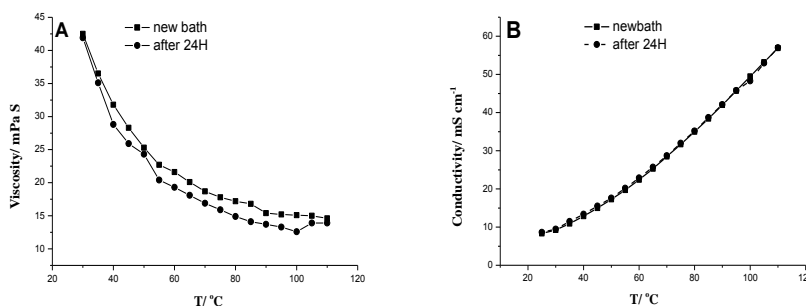


**Figure 3.1** The (A) viscosity and (B) conductivity of neat ethaline as a function of temperature

Due to the hygroscopic property of choline chloride, it's essential to study the influence of water uptake on the physical properties of eutectic solvents after a period of exposure to atmosphere. As shown in Figure 3.1, generally, viscosity decreased and conductivity increased significantly with elevating temperature. The value that viscosity reaches at 80 °C (9.8 mPa S) is almost three times lower than that under room temperature. The conductivity at 80 °C (32.5 mS cm<sup>-1</sup>) is much higher than that of conventional ionic liquids<sup>[1]</sup>. After 24 hours' placing of ethaline in natural environment, conductivity kept unchanged while viscosity decreased slightly indicating the existence of low content water adsorbed during exposure.

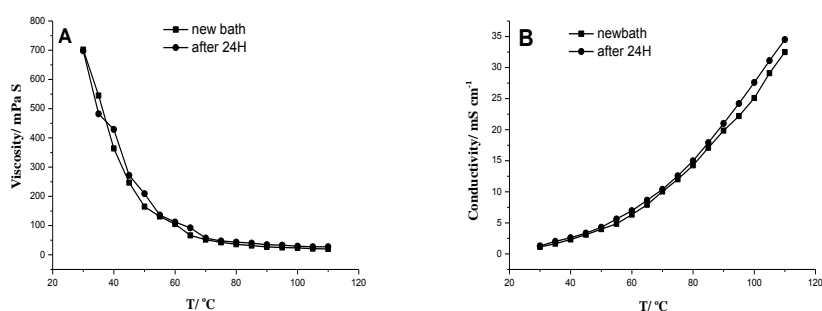


**Figure 3.2** The (A) viscosity and (B) conductivity of neat reline as a function of temperature

Similar behaviors can be observed for reline shown in Figure 3.2. Compared to ethaline, reline shows more than 10 times higher viscosity and almost half conductivity. This can be explained by the stronger interaction between choline chloride with urea than with ethylene glycol<sup>[2]</sup>. This also result in different freezing temperature of ethaline (-10 °C) and reline (12 °C).

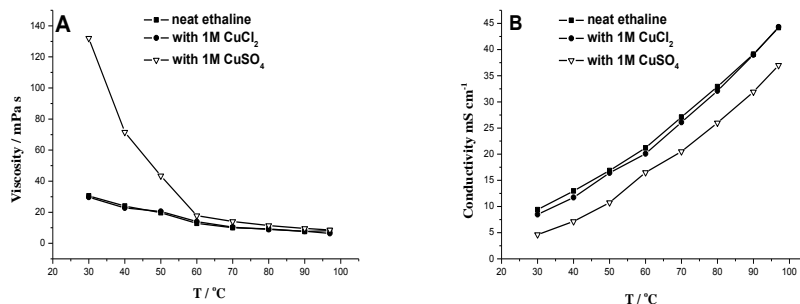


**Figure 3.3** The (A) viscosity and (B) conductivity of neat ethaline (-■-), with addition of 1 M  $\text{CuCl}_2 \cdot 2\text{H}_2\text{O}$  (-●-) and with addition of 1 M  $\text{CuSO}_4 \cdot 5\text{H}_2\text{O}$  (-▽-) as a function of temperature

In the majority of ionic liquid electrodeposition studies to date, little consideration has been given to the effect of metallic ions upon the physical properties of the solvent. However, cation/anion effects have been proved to influence the crystal growth, thus alter the morphology of deposits. It is imperative that any discussion of electrodeposition from these system gives due consideration to the effect on physical properties of the inclusion of a solute with specific ion structure.

To check if the addition of metal salts with different anions will influence the physical properties of bulk ethaline, 1 M  $\text{CuCl}_2 \cdot 2\text{H}_2\text{O}$  and 1 M  $\text{CuSO}_4 \cdot 5\text{H}_2\text{O}$  were add into ethaline respectively and variation of physical properties with temperature were recorded. Figure 3.3 demonstrates that the addition of 1 M  $\text{CuCl}_2 \cdot 2\text{H}_2\text{O}$  has no obvious effect on the viscosity and conductivity of ethaline from 30 °C to 100 °C. Figure 3.3(A) shows that viscosity of the electrolytes decrease with elevated temperatures despite the addition of copper salts. The conductivity of ethaline shown in Figure 3.3(B) is, in an analogous manner to the viscosity, insensitive to  $\text{CuCl}_2$  addition and increases linearly with temperature.

This is due to the fact that chloride anion is the principle migration species as it is smaller than the choline cation or ethylene glycol molecule<sup>[3]</sup>. The addition of  $\text{CuCl}_2$  increases the molar concentration of chloride anions as well as copper cations which hinder the ions migration. The two effects counterbalance each other resulting in negligible changes. In this case, the conductivity remains rather stable with addition of 1 M of salts, while in aqueous solutions conductivity is generally observed to increase dramatically as the concentration of electrolyte is increased<sup>[4]</sup>.

Figure 3.3(A) and (B) also demonstrate that the addition of equal concentration of  $\text{CuSO}_4$  have significant different effect on the viscosity and conductivity of ethaline almost covering the whole temperature range studied. Figure 3.3(A) shows that 1 M  $\text{CuSO}_4$  has greatly increased the viscosity especially when temperature is lower than 60 °C, with a 300% increase at 30 °C. The increased viscosity at relatively lower temperature maybe due to the incomplete dissolution of 1 M  $\text{CuSO}_4$  with redundant salt stabilized in bulk solvent as crystals generating from reduced solubility. 0.01 M of  $\text{CuSO}_4 \cdot 5\text{H}_2\text{O}$  causes opposite effect by slightly decreasing the viscosity due to the liberated water from metallic salts.

The different effect of Cu salts on the mass transport properties could be due to either a difference in Cu salts solubility or a lattice disruption effect. From the lattice point of view, since ethylene glycol acts as relatively weak hydrogen bonding donor, the mixture of ethylene glycol and choline chloride already contains a high proportion of larger voids which can be evidenced by the relative low fluidity<sup>[5]</sup>. The addition of both salts may act to disrupt the hydrogen bonding network in the solvent leading to a change in average void magnitude and hence a change in mass transport. Since  $\text{CuCl}_2$  contains the same anion as solvent, the solvent would be less

susceptible to disruption upon the addition while  $\text{SO}_4^{2-}$  has a much larger size and greater charge than chloride anion which can be regarded as a distinct barrier for mass transport. This influences similarly the decrease of conductivity.

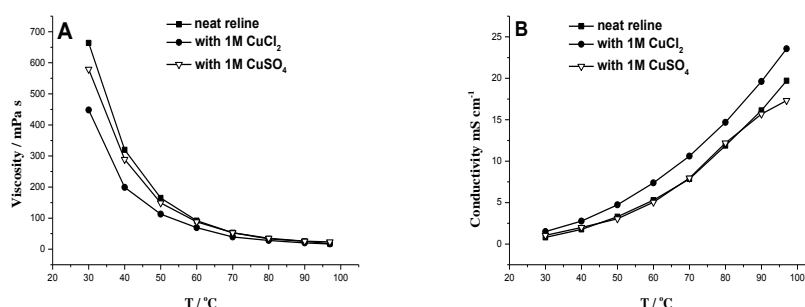


**Figure 3.4** The (A) viscosity and (B) conductivity of neat reline (-■-), with addition of 1 M  $\text{CuCl}_2 \cdot 2\text{H}_2\text{O}$  (-●-) and with addition of 1 M  $\text{CuSO}_4 \cdot 5\text{H}_2\text{O}$  (-▽-) as a function of temperature

Figure 3.4 shows how reline reacts to the addition of Cu salts. The results are significantly different from ethaline. The addition of  $\text{CuCl}_2$  and  $\text{CuSO}_4$  both decrease the viscosity of solvent and  $\text{CuCl}_2 \cdot 2\text{H}_2\text{O}$  shows more significant influence. Similar effect on conductivity can be observed from the addition of equal concentration of copper salts into reline.

Since reline has rather low density of voids which could be inferred from its sticky property, the addition of exotic ions will increase the possibility of vacancy. However, chloride anion is more active migration specie than sulfate ion, so the resulting viscosity is comparatively lower with conductivity increased.

A model which has been demonstrated to accurately predict the viscosities and conductivities of DESs is hole theory<sup>[6]</sup>. The central assumption of hole theory is that as a solid melts, voids of random size and

orientation are formed. The probability of ion motion can be considered to be a product of the size of the ions in consideration and the relative population of suitably sized holes. Mass transport in ionic liquids, which contain bulky asymmetric ions, is primarily controlled by the availability of suitably sized holes. It is assumed that with the addition of mass  $\text{CuSO}_4$ , strong hydrogen bonding will form between H from hydrogen donor and O from  $\text{SO}_4^{2-}$  group which results in more stable complexion state than existing form in ethaline. This faint network lowers the mass transport i.e. increase viscosity and decrease conductivity. However, with temperature increasing, the bonding effect has been weakened as mobility of ions increases. That helps to decrease the percentage of mass transport variations. While in reline, hydrogen bond donor tends to form strong bonding with choline chloride instead of with  $\text{CuSO}_4$ . In addition, the relatively larger sized  $\text{SO}_4^{2-}$  disturbs the bonding network in the system and increase the possibility of suitable vacancies.

### **3.2 Speciation of $\text{Cu}^{2+}$**

Since the addition of different copper salts influenced the physical properties of bulk solvent in distinct extent, it is necessary to study the speciation of  $\text{Cu}^{2+}$  after complete dissolution of  $\text{CuCl}_2 \cdot 2\text{H}_2\text{O}$  or  $\text{CuSO}_4 \cdot 5\text{H}_2\text{O}$  in the two solvents. UV-VIS spectra of two Cu salts in two solvents were determined by diluting both samples to a concentration of 0.5 mM in ethaline and 1 mM in reline with appropriate color intensity and measuring in a 1cm path length quartz cuvette. Measurements were carried out by Jasco model V-570 and Jasco FP-6300 spectrophotometers ultraviolet-visible and fluorescent spectroscopy analysis. Values for  $\lambda_{\text{max}}$

were determined using the spectrophotometer's built-in peak-pick feature, using uv-probe software.

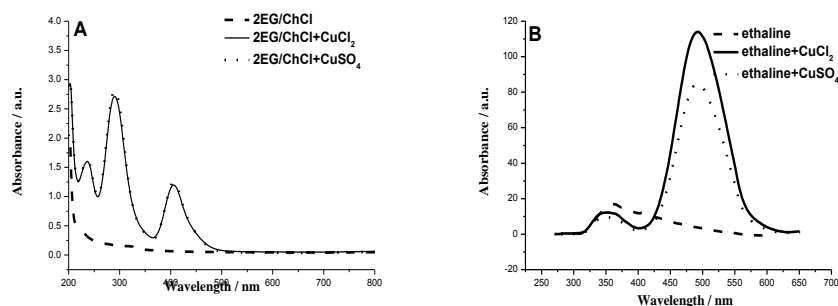


**Figure 3.5** (A) UV-VIS spectra of electrolytes in ethaline (B) the fluorescent spectra excited at 266 nm, both determined with 0.5 mM of corresponding copper salts

The UV-vis spectra in Figure 3.5 have provided some useful insight. In Figure 3.5(A), the spectra of 0.5 mM solutions of both  $[\text{CuCl}_2 \cdot 2\text{H}_2\text{O}]$  and  $[\text{CuSO}_4 \cdot 5\text{H}_2\text{O}]$  in the ethaline can be compared with the pure solvent. The spectra of mixture shows three charge transfer bands at 405 nm, 290 nm and 236 nm. The results are in agreement with data reported by Abbot et al.<sup>[7]</sup>. The location of these peaks demonstrates the presence of the  $[\text{CuCl}_4]^{2-}$  copper complex, as reported by Amuli et.al<sup>[8]</sup>. The following spectrum is the fluorescence spectrum excited at 266 nm to confirm the existence of Cu (I) since only Cu (I) complex in this mixture has fluorescence property. The addition of different salts into same solvent results in same complex form which states that  $\text{SO}_4^{2-}$  is displaced from the coordination sphere of the  $\text{Cu}^{2+}$  ion upon dissolution in the ionic liquid. This is not surprising since the relative concentration of chloride ion is much higher than that of Cu complex.

For the purpose to compare deposits obtained under different conditions, the surface morphology and elemental compositions of Cu deposits were characterized by Low Vacuum Scanning Electron Microscopy (SEM) (Philips XL 30), equipped with energy dispersive X-ray spectrometry (EDXS).

This conjecture is verified by images from scanning electron microscopy shown in Figure 3.6. Samples deposited from 0.01 M  $\text{CuCl}_2$  and 0.01 M  $\text{CuSO}_4$  show similar morphology. The fluorescence spectra excited at 266nm shows Cu (I) complex formed in comparable concentrations from both copper salts. Since Cu (II) doesn't show fluorescence property, the transition ratio from Cu (II) to Cu (I) can't be measured.

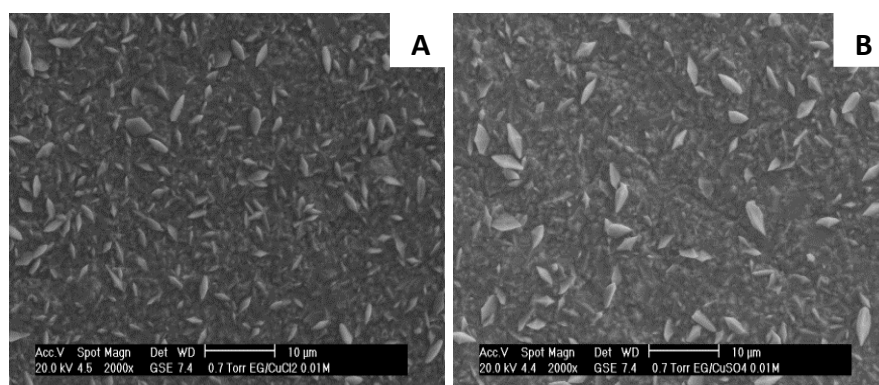


**Figure 3.6** Scanning electron micrograph obtained by the electrolysis of (A) 0.01 M  $\text{CuCl}_2$  and (B) 0.01 M  $\text{CuSO}_4$  in ethaline plated onto copper foil at a potential of -1.1 V at a current density of  $0.2 \text{ mA/cm}^2$  for 3 h at  $60^\circ\text{C}$

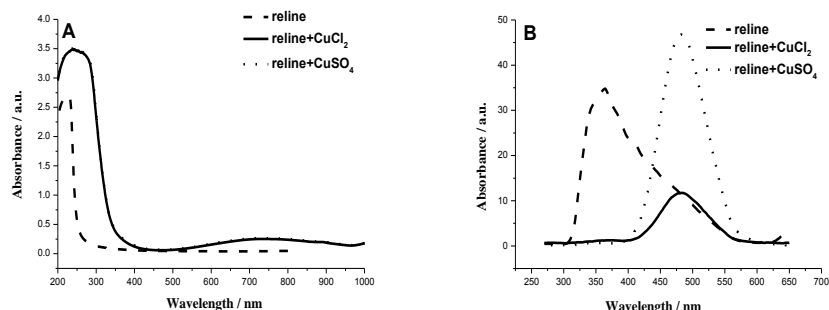


**Figure 3.7** (A) UV-VIS spectra of electrolytes in reline (B) the fluorescent spectra excited at 266 nm, both determined with 1 mM of corresponding copper salts

As for reline, the large peak at approximately 250 nm in Figure 3.7(A) is possibly due to the conjugate effect formed between carbonyl and amino in urea<sup>[9]</sup>. When heated or hydrolysis occurs, urea tends to release ammonia on account of its instability<sup>[10]</sup>. The broad peak at 760 nm may due to the formation of  $[\text{Cu}(\text{NH}_3)_4]^{2+}$ . Though we are not sure about the existence of the mentioned complex since no report can be referred so far, the test states that the resulting complex in both solvent is the same which would be sufficient for following studies. The fluorescence peak at 350 nm can be ascribed to choline. The reason why this peak remains in ethaline with addition of salts while disappears in reline is assumed to be a chemical equilibrium effect. With addition of copper salt into reline, urea molecule tend to form complex  $[\text{Cu}(\text{NH}_3)_4]^{2+}$  instead of conjugating with choline cation resulting in a diminution of the peak in 350 nm.

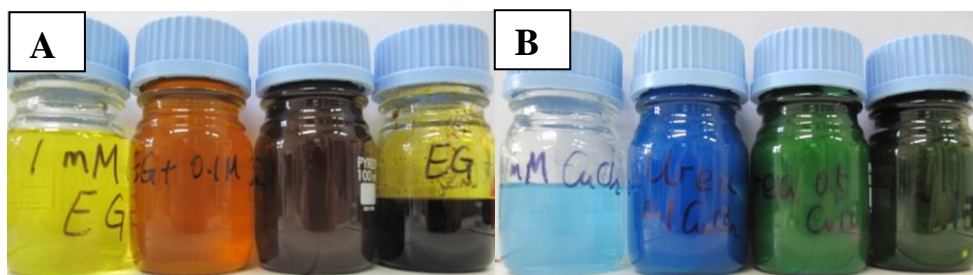


**Figure 3.8** Photos of  $\text{CuCl}_2 \cdot 2\text{H}_2\text{O}$  dissolved in (A) ethaline and (B) reline at concentrations of 1 mM, 0.1 M, 0.5 M and 1 M (from left to right).

The different coordination effect occurs in the two solvents can be further confirmed by the visual appearance of eutectics containing metallic salts shown in Figure 3.8. The existence of  $\text{CuCl}_2 \cdot 2\text{H}_2\text{O}$  altered the colorless solvent into different appearances. Ethaline changed from light yellow to orange and then to brown with increasing concentration  $[\text{CuCl}_4]^{2-}$  copper complex. Reline changed from light blue which a typical color of  $[\text{Cu}(\text{H}_2\text{O})_6]^{2+}$  and then to dark blue indicating the increased concentration of  $[\text{Cu}(\text{H}_2\text{O})_6]^{2+}$ . When the added  $\text{CuCl}_2 \cdot 2\text{H}_2\text{O}$  reached 0.5M, the generated mixture showed green color which is typical for  $[\text{Cu}(\text{NH}_3)_4]^{2+}$  compound.

### 3.3 Cyclic voltammetry

To optimize temperature and concentration, cyclic voltammetry (CV) was conducted using a PAR model 273A potentiostat/galvanostat (Princeton applied research) connected to a PC for data acquisition and control. The cell set-up consists of three electrodes, Pt plate (area=6  $\text{cm}^2$ ) as working electrode, a Pt wire as quasi-reference and a Pt plate as counter electrode. The electrodes were polished until mirror-like surfaces were obtained and cleaned by ultrasound for 10 min in distilled water and acetone and then dried with  $\text{N}_2$  prior to each experiment. Voltammograms were performed at

10 mV/s (if not diversely stated) at various temperatures (30 °C, 60 °C, 80 °C) and different copper salts concentrations (0.01 M, 0.1 M, 0.5 M, 1 M).

The electrochemical window of the neat ethaline was found to be narrower than other ionic liquids<sup>[11-14]</sup>. However, in this case the electrochemical window of neat solvent, +0.7V~-1.8V(vs. Pt), can covers well the redox peaks of Cu (II)/Cu (I) and Cu (I)/Cu (0). The cyclic voltammetry shown in Figure 3.9 exhibited two pairs of well-defined redox peaks: (I) corresponds to the Cu (II)/Cu (I) redox couple and (II) corresponding to the Cu (I)/Cu (0) couple.

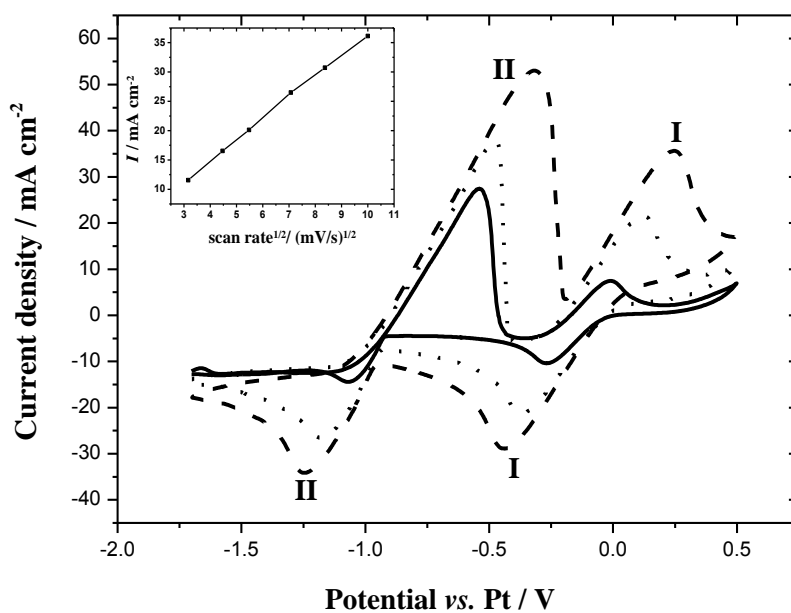


**Figure 3.9** Cyclic voltammetry of ethaline containing 0.1 M CuCl<sub>2</sub>·2H<sub>2</sub>O obtained at scan rate of 10 mV/s (solid line), 50 mV/s (dotted line) and 100 mV/s (dashed line) at 80 °C. Inset is the plot of reduction current density of peak (II) versus the root of scan rate

A voltammetric study was performed in order to study in more detail the deposition kinetics and to determine the diffusion coefficient of  $\text{Cu}^{2+}$  in the solvent. The impact of the potential scanning rate ( $v$ ) on the voltammograms of the electrolyte is presented in Figure 3.9. The cathodic current density of peak (II) varied linearly with  $v^{1/2}$  (inset of Figure 3.9), indicating that the deposition process is diffusion controlled. However, according to Table 3.1, the difference  $|E_{\text{pa}}^{\text{II}} - E_{\text{pc}}^{\text{II}}|$  ( $\Delta E_{\text{p}}^{\text{II}}$ ) increases with  $v$  and is larger than the value typically found for reversible reactions<sup>[15]</sup>. The large peak separation between anodic peak and cathodic peak for the same process indicates a mixed diffusion and kinetic controlled electrolyte system<sup>[16]</sup>. The large value of  $\Delta E_{\text{p}}$  is usually indicative of a high solution resistance, which is often characteristic of ionic liquid-based electrolyte<sup>[17]</sup>. This can be explained by the slow kinetics of the reaction and thus the equilibria cannot establish in-time compared to the voltage scan rate. Moreover, in this situation the linearity does not go through the origin also suggesting a quasi-reversible system.

The relation between the peak current density  $i_{\text{p}}$  and the potential scanning rate ( $v$ ) for an irreversible reaction (also for quasi-reversible reaction) is:

$$i_{\text{p}} = \frac{0.282\pi^{1/2}F^{3/2}}{(RT)^{1/2}} n(\alpha n_{\alpha})^{1/2} D^{1/2} C_0 v^{1/2}$$

Where  $F$  is the Faraday constant ( $96485 \text{ C mol}^{-1}$ ),  $R$  is the ideal gas constant ( $8.31 \text{ J mol}^{-1} \text{ K}^{-1}$ ),  $T$  is the temperature (K),  $n$  is the number of electrons transferred,  $\alpha$  the charge coefficient,  $n_{\alpha}$  is number of electrons transferred in the rate-determining step,  $D$  the diffusion coefficient ( $\text{cm}^2 \text{ s}^{-1}$ ) and  $C_0$  the  $\text{Cu}^{2+}$  concentration ( $\text{mol cm}^{-3}$ ),  $(\alpha n_{\alpha})$  is given by the equation

$$|E_{\text{p}} - E_{\text{P}/2}| = \frac{1.857RT}{\alpha n_{\alpha} F}$$

Scan rate $v$ $\text{mV s}^{-1}$	$E_{\text{pa}}^{\text{II}}$ V	$E_{\text{pc}}^{\text{II}}$ V	$ E_{\text{pa}}^{\text{II}} - E_{\text{pc}}^{\text{II}} $ V	Diffusion coefficient $\text{cm}^2 \text{s}^{-1}$ $\times 10^{-2}$
10	-0.54	-1.07	0.53	4.54
50	-0.48	-1.17	0.69	6.06
100	-0.32	-1.24	0.92	11.52

**Table 3.1** Potential disparity between reduction and oxidation process of Cu (I)/Cu (0) under different scan rates analyzed from Figure 3.9

### 3.4 Effect of temperature

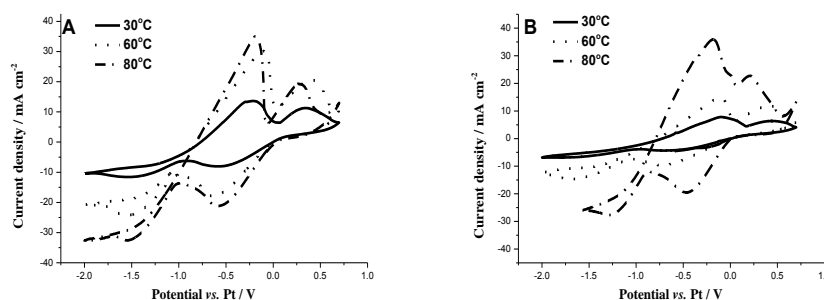


**Figure 3.10** Cyclic voltammograms of (A) 1 M  $\text{CuCl}_2 \cdot 2\text{H}_2\text{O}$  (B) 1 M  $\text{CuSO}_4 \cdot 5\text{H}_2\text{O}$  in ethaline (Potential versus Pt disk quasi-reference electrode)

It was proved that the anion of the metal salt has a significant effect on the mass transport in both DESs. The anions of metal salt can also change the trend in Cu (II)/Cu (I) redox with respect to that of the Cu (I)/Cu (0) couple<sup>[18]</sup>. The resulting cyclic voltammograms of the ethaline containing 0.01 M  $\text{CuCl}_2$  and 0.01 M  $\text{CuSO}_4$  as a function of temperatures share exact the same outcome (not shown) while differ a bit with 1M concentration in Figure 3.10. From Figure 3.10(A) and (B), we can see that reduction potential which causes deposition of copper lies near -1.5 V versus Pt. With

temperature increase, current density of  $\text{CuCl}_2$  increases linearly while potential position stays stable. The elevated currents can be ascribed to an increase of the mobility of electroactive species toward the electrode surface resulting in a reduced nucleation overvoltage at elevated temperature.

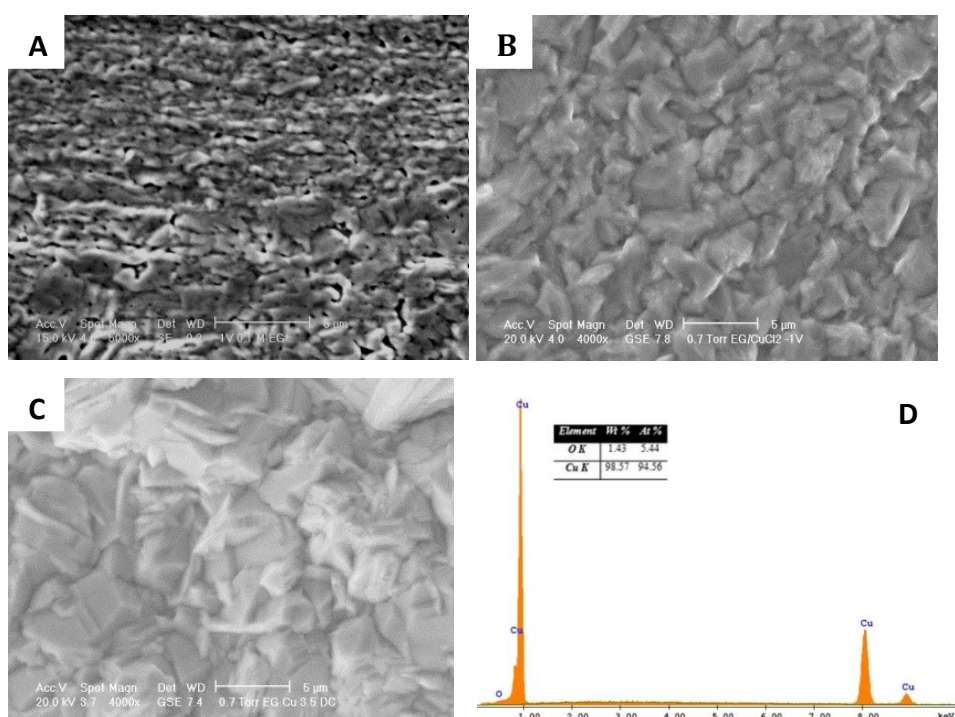


**Figure 3.11** SEM images of layer deposited from 0.1 M  $\text{CuCl}_2$  in ethaline at (A) 30 °C (B) 60 °C (C) 80 °C (D) EDS mapping analysis of the film corresponding to Figure 3.11 C deposited at 80 °C

Figure 3.11 gives the surface morphologies of the as-deposited Cu films corresponded three different temperatures under the 0.1 M concentration. Significant difference between samples prepared under 30 °C and 60 °C (80 °C) can be clearly observed under the SEM observations. Due to the increased current densities, resulted changing temperature from 30 °C to

60 °C, the as-deposited surface of the Cu film becomes very compact without any obvious colony structures, which is different from the porous appearance observed under lower temperature. At 80 °C, grains grow into even larger size and form smoother surface. To confirm the eventual film deposited is composed of pure copper, EDS analysis was carried out as shown in Figure 3.11(D) which indicates that the film is mainly composed of Cu and the residually small amount of O species. The oxygen might be from the partial oxidation of Cu surface. By comparing the actual deposited weight with the theoretical value calculated according to Faraday's law, the current efficiency is between 30%-50% for the three deposits shown in Figure 3.11. In this result range, current efficiency decreased with increasing temperature. This can be related to the electrochemical stability of solvent. Decomposition of choline chloride based ionic liquid analogues over long periods of electrolysis was investigated and side-reaction can be observed on both electrodes<sup>[19]</sup>. Several decomposition products such as 2-methyl-1,3-dioxolane and a range of chlorinated products can be formed in ethaline due to two possible reasons: a reaction on either anode or cathode; consecutive reactions of reaction products formed at both electrodes.

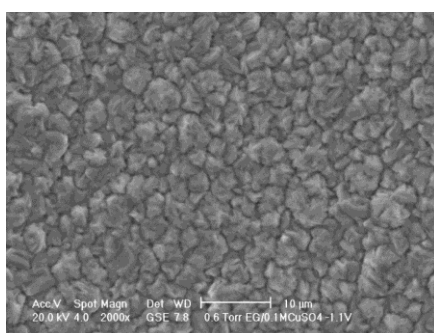


**Figure 3.12** SEM image of layer deposited in reline containing 0.1M  $\text{CuSO}_4 \cdot 5\text{H}_2\text{O}$  at 60 °C

The increasing temperature leads to rather different electrochemical response on  $\text{CuSO}_4$  (Figure 3.10B). With heating up, the reduction potential slightly moves to positive direction, which we assume is related to two possible reasons: the formation of a new complex formed between  $\text{Cu}^{2+}$ ,  $\text{Cl}^-$  and  $\text{SO}_4^{2-}$  with relatively higher concentration of  $\text{SO}_4^{2-}$ ; change of temperature according to Nernst equation. By comparing the deposits obtained from ethaline containing  $\text{CuCl}_2$  and  $\text{CuSO}_4$  in Figure 3.11(B) and Figure 3.12, we can assume that existing  $\text{SO}_4^{2-}$  is beneficial to smaller grain size and more compact morphology.

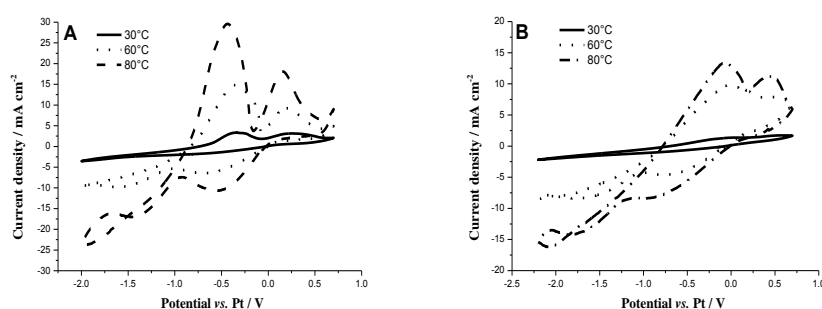


**Figure 3.13** Cyclic voltammograms of (A) 1 M  $\text{CuCl}_2 \cdot 2\text{H}_2\text{O}$  (B) 1 M  $\text{CuSO}_4 \cdot 5\text{H}_2\text{O}$  in reline (Potential versus Pt disk quasi-reference electrode)

Figure 3.13 shows electrochemical responses of 1M  $\text{CuCl}_2$  and 1M  $\text{CuSO}_4$  in reline at 60 °C. It can be seen that nucleation can hardly proceed near room temperature (30°C) probably because of the low mobility under relatively low temperature and a couple of hours of deposition time was essential to finish 1 $\mu\text{m}$  thick film. The difference between the two electrolytes is that the peak current on both reduction processes in reline are

relatively lower compared to that of ethaline. Potentials have little changes in positions.

Similar morphology can be observed on the deposits prepared in reline and ethaline containing same concentration of copper salts when operation temperature is 60 °C or 80 °C.

A

	30 °C		60 °C		80 °C	
	$i_p/m$	$\eta/mPa$	$i_p/mA$	$\eta/m$	$i_p/mA$	$\eta/m$
	A $cm^{-2}$	s	$cm^{-2}$	Pa s	$cm^{-2}$	Pa s
2ethaline+1 M $CuCl_2$	11.6	29.7	24.35	14.0	32.55	8.9
2reline+1 M $CuCl_2$	2.67	448	9.75	69.5	16.95	28.2
$a=i_p(\text{ethaline})/i_p(\text{reline})$	4.34		2.50		1.92	
b=	3.88		2.23		1.78	
$\sqrt{\eta(\text{reline})/\eta(\text{ethaline})}$						
Ratio b/a	89.40%		89.20%		90.72%	

B

	30 °C		60 °C		80 °C	
	$i_p/mA$	$\eta/m$	$i_p/mA$	$\eta/m$	$i_p/mA$	$\eta/m$
	$cm^{-2}$	Pa s	$cm^{-2}$	Pa s	$cm^{-2}$	Pa s
2ethaline+1 M $CuSO_4$	6.88	132	14.68	17.8	27.7	11.4
2reline+1 M $CuSO_4$	1.71	579	8.40	88	14.3	35.4
$a=i_p(\text{ethaline})/i_p(\text{reline})$	4.01		1.75		1.94	
b=	2.09		2.22		1.76	
$\sqrt{\eta(\text{reline})/\eta(\text{ethaline})}$						
Ratio b/a	52.12%		126.86%		90.72%	

**Table 3.2** Comparison between diffusion coefficients obtained from (a) peak currents and (b) viscosity values respect for addition of (A)  $CuCl_2$  and (B)  $CuSO_4$

Comparing the peak current of Cu (I)/Cu (0) between the two solvents, we can obtain Table 3.2 suggesting significantly different reduction currents despite the similar concentration. For example the ratio of cathodic peak currents for Cu (I)/Cu (0),  $i_p(\text{EG})/i_p(\text{urea})$ , observed during cyclic voltammograms shows a ratio of approximately 4 at 30°C. The magnitude of this ratio can be explained by the difference in viscosity,  $\eta$ , of the two mixtures. These viscosities are related to the diffusion coefficients,  $D$ , of reacting species by *Walden's Rule*, where the subscripts 1, 2 denote the viscosities and diffusion coefficients of a reacting species in two differing media.

$$D_1 \eta_1 \approx D_2 \eta_2$$

It can be easily shown for a diffusion-controlled process in a linear sweep voltammogram that the corresponding ratio of peak currents for Cu (I) reduction in the two media is given by the expression:

$$\frac{i_p(\text{ethaline})}{i_p(\text{reline})} = \sqrt{\frac{D(\text{ethaline})}{D(\text{reline})}} = \sqrt{\frac{\eta(\text{reline})}{\eta(\text{ethaline})}}$$

Inserting the ratio of diffusion coefficients derived from the viscosity values (*Walden's Rule*) into this expression gives a value for the ratio  $i_p(\text{ethaline})/i_p(\text{reline})$  of 3.88 for  $\text{CuCl}_2$ . The comparison of this value to the theoretical one of 4 indicates that viscosity influence almost account for 90% of the observed difference. The remaining discrepancy could be accounted for differences in deposition kinetics.

The impact factor of viscosity on diffusion is rather stable with slight increase when heated for  $\text{CuCl}_2$  containing media while shows a dramatic fluctuation for  $\text{CuSO}_4$  containing ones. This fact shows that deposition for  $\text{CuCl}_2$  salts is “mainly” diffusion controlled process. In order to obtain high currents which could be appropriate for commercial applications, reduced

viscosity seems to be essential. Since for  $\text{CuSO}_4$ , no fixed trend can be observed. Diffusion is not the controlling factor. The different  $\text{Cu}^{2+}$  complexations take place along with reduction can be considered as a possibility.

From the comparison between diffusion coefficients of  $\text{CuCl}_2$  and  $\text{CuSO}_4$  in same media in Table 3.2, we can conclude that no great difference can be observed between the two especially under relatively high temperatures. The block effect of  $\text{SO}_4^{2-}$  relative to  $\text{Cl}^-$  can be intensified with low mobility under low temperatures which could be adopted to explain the fact greater difference shown between the two in  $30^\circ\text{C}$ .

### 3.5 Effect of concentration

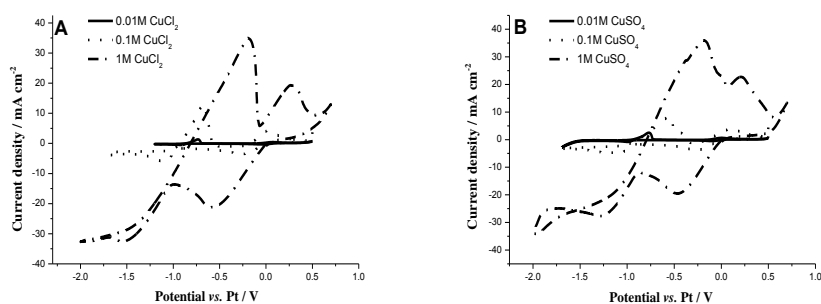


**Figure 3.14** Cyclic voltammograms of (A)  $\text{CuCl}_2 \cdot 2\text{H}_2\text{O}$  (B)  $\text{CuSO}_4 \cdot 5\text{H}_2\text{O}$  in ethaline

Effect of Cu salt concentration was studied at  $80^\circ\text{C}$  since this condition can stimulate mass transfer with reduced solution viscosity. The results from Figure 3.14 have the similar trend: increasing the concentration, both reduction peaks move to negative direction. Nucleation of copper in ethaline and reline both follow a three-dimensional instantaneous

mechanism<sup>[2]</sup>. However, at longer time scales, the mechanism changes to a three-dimensional progressive nucleation. Solvents containing copper salt with concentration higher than 0.01M result in a bright deposit while at lower copper concentration the deposition results in a black deposit.

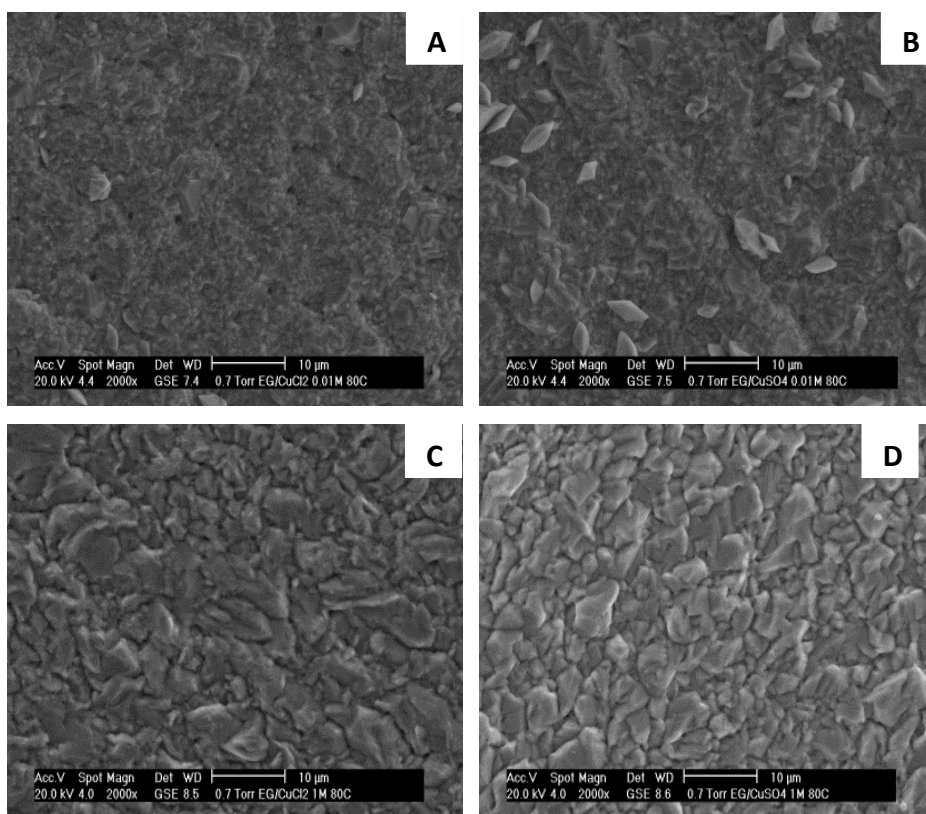


**Figure 3.15** Scanning electron micrograph obtained by the electrolysis of (A) 0.01M CuCl<sub>2</sub> (B) 0.01M CuSO<sub>4</sub> (C) 1 M CuCl<sub>2</sub> (D) 1 M CuSO<sub>4</sub> in ethaline at 80 °C under plated onto brass foil at peak potentials

Potentiostatic deposition was carried out from ethaline and reline with various concentrations of CuCl<sub>2</sub>.2H<sub>2</sub>O at various temperatures. The deposition was carried out under unstirred conditions between two parallel vertical electrodes immersed in a cell warmed by thermostatic jacket.

Potentials was chosen at reduction peak of Cu(I) to Cu(0) on cyclic voltammograms, which was -1.1 V, in our condition. The deposition time can be evaluated by average resulting current density to reach thickness of around 1  $\mu\text{m}$  of the layer according to Faraday's law.

The copper deposition was performed on brass foil (area=10  $\text{cm}^2$ ). A surface cleaning treatment of the brass substrate was conducted to remove the industrial oil from the surface by ultrasound cleaning and deionized water rinsing. Before the plating process, the substrate was dried with  $\text{N}_2$ . The counter electrode for the deposition process was a Pt plate to avoid any impurity and the quasi-reference electrode was a Pt wire to keep the working potential stable. The final deposits were sequentially rinsed with sufficient deionized water and dried with flowing air.

From results reported in Figure 3.15, Cu layers deposited at -1.1 V vs. Pt from baths containing different concentration of  $\text{CuCl}_2 \cdot 2\text{H}_2\text{O}$ , a rough surface composed by randomly distributed pores and particles is obtained at 0.01 M. When increasing concentration to 1 M, grains tend to grow in larger size. Deposit obtained from bath containing 1 M  $\text{CuCl}_2 \cdot 2\text{H}_2\text{O}$  shows inhomogeneous color distribution and can hardly be regarded as a coating. So it can be assumed that low concentration of Cu salts favors tridimensional growth. While at higher concentration, crystal growth tends to level up surface and to increase the dimension of grains. This result seems true for both additions of  $\text{CuCl}_2$  and  $\text{CuSO}_4$  into ethaline which indicates similar deposition kinetics. Under this condition, the highest concentration available to deposit uniform colored layers is 0.5 M. Unfortunately, the current efficiency of deposition carried out at 80  $^\circ\text{C}$  and 0.5 M remains rather poor, around 50% for both solvents.

In ethaline, current density tends to increase linearly with concentration until 0.5 M when the same reduction potential was applied, as shown in Figure 3.16.

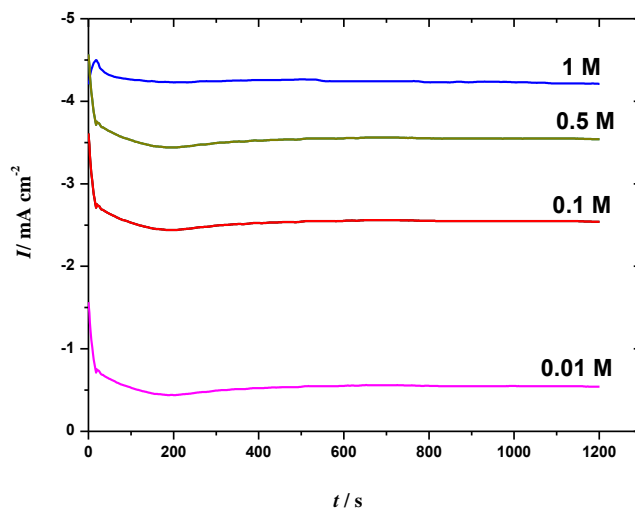


**Figure 3.16** Resulting current density versus time deposited from bath containing indicated concentrations of  $\text{CuCl}_2 \cdot 2\text{H}_2\text{O}$  at  $80^\circ\text{C}$

Surface deposited from reline showed rather flat morphology even in low concentrations. This is not surprising because since reline is much more viscous than ethaline, the growth of the crystallites perpendicularly to the surface is in this case inhibited and the overlapping and spreading across the surface produce smooth layers on the microscopic scale.

By the comparison between Figure 3.15 and Figure 3.17, the fact that both solvents can be applied to deposit surfaces with similar morphology can be observed. This states that elevated temperature can greatly reduce the relative difference in viscosity reflected by comparable current density at  $80^\circ\text{C}$  and generates surfaces identical in appearance.

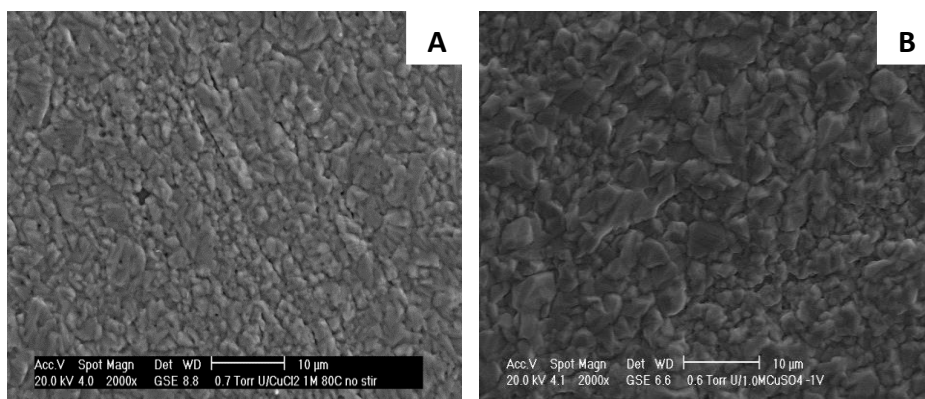


**Figure 3.17** Scanning electron micrograph obtained by the electrolysis of (A) 1 M  $\text{CuCl}_2$  (B) 1 M  $\text{CuSO}_4$  in reline at  $80^\circ\text{C}$  under plated onto copper foil at peak potentials

Same trend between current and concentration can be observed in reline solvent at  $80^\circ\text{C}$  while the value of deposition current density at same applied potential was almost 10 times lower than that in ethaline especially when the concentration of  $\text{CuCl}_2 \cdot 2\text{H}_2\text{O}$  is low, as recorded in Table 3.3 carried out at  $80^\circ\text{C}$ . Accordingly 10 times longer time is needed to deposit same thickness of layer in reline. In addition, current efficiency of deposition carried out in reline shows similar values as in ethaline due to electrochemical decomposition of both urea<sup>[10, 20]</sup> and choline chloride<sup>[19]</sup>. It is reasonable to assume that deposition from ethaline is more time-efficient than from reline. Meanwhile, deposits obtained from two solvents show rather similar morphology. As a result, ethaline was chosen as solvent for subsequent pulse deposition studies.

	Current density (mA/cm <sup>2</sup> )	Theoretical time to deposit 1 $\mu$ m (min) IF C.E.=100%
<b>0.01M CuCl<sub>2</sub> in Ethaline</b>	0.5	90
<b>0.1M CuCl<sub>2</sub> in Ethaline</b>	2.5	20
<b>0.5M CuCl<sub>2</sub> in Ethaline</b>	3.5	12
<b>0.01M CuCl<sub>2</sub> in Reline</b>	0.05	900
<b>0.1M CuCl<sub>2</sub> in Reline</b>	0.35	120
<b>0.5M CuCl<sub>2</sub> in Reline</b>	1	45

**Table 3.3** Current densities recorded during potentiostatic deposition containing indicated concentrations of CuCl<sub>2</sub>.2H<sub>2</sub>O and the theoretical time to deposit 1  $\mu$ m film

The results presented in these two sections (3.1.3.4&3.1.3.5) indicate both temperature and concentration play important roles in manipulating the surface topography of the deposits. Higher temperature can decrease the viscosity of the ionic liquid and thus increase ion species mobility, which would favor the Cu nucleation and deposition process. In the meanwhile, moderate increase in concentration can be beneficial for Cu<sup>2+</sup> to gain more active sites for crystalline nucleation which result smoother surface. Elevated temperature and concentration reduce the difference between solvent effects from ethaline and reline on the deposition process, which tends to yield similar morphology of deposits. While deposition in ethaline is significantly more rapid than in reline which can be regarded as an obvious advantage for practical productions. As a result, 80 °C, 0.5 M and

operation in ethaline has been chosen as optimized parameters for electrodeposition.

The difference of anions of copper salts added show rather slight influence on physical properties of bulk eutectics. However the resulting morphology of deposits from two copper salts was comparable especially carried out in high concentrations which can be explained by the weakened effect from solvent. So  $\text{CuCl}_2 \cdot 2\text{H}_2\text{O}$  was used for better availability of the solvent.

### **3.6 Galvanic deposition: direct current vs. pulse current**

To simulate the deposition process carried out in practical production which commonly adopts galvanic mode and for better kinetics control, constant current was applied to deposit Cu film to replace potentiostatic mode employed in previous sections. Galvanic deposition was performed under optimized conditions applying the average current density measured by potentiostatic process. Deposition time was calculated using applied current density to obtain 1  $\mu\text{m}$  thickness. Current efficiency was obtained by actual deposited weight divided by theoretical weight.

Improved deposition results were obtained by optimizing conditions such as temperature, concentration as described above, current efficiency calculated from Faraday's law is as high as 56% which is far from satisfying. This may be explained by the fact that the electrodeposition is predominantly mass controlled and at initial stage of nucleation requires a relatively larger overpotential. The resulting current efficiency of deposited Cu film with 1  $\mu\text{m}$  thickness in direct current mode is as low as 56%, which

can be hardly acceptable in industrial production. So pulse plating was adopted to improve the current efficiency as well as to refine the microstructure.

Pulse plating was applied to study its effect on process and deposited layer using the same experimental set-up as that of direct current deposition. The schematic diagram of the wave shape of PC was introduced in 2<sup>nd</sup> chapter, in the squared waveform pulse plating,  $i_p$  refers to the normal pulse current density,  $t_{on}/t_{off}$  denote the on-time/off-time of the normal pulse. The duty cycle ( $\theta$ ) is given by  $t_{on}/(t_{on}+t_{off})$  and frequency ( $f$ ) equals to  $1/(t_{on}+t_{off})$ . The average current density ( $i_{av}$ ) in pulse plating is defined as  $i_{av}=\text{peak current } (i_p) \times \text{duty cycle } (\theta)$ . Since duty cycle in our study was fixed at 0.5 and average current keeps the same as direct plating,  $i_p$  was two times the value of direct one. Varied frequencies (0.005 Hz, 0.5 Hz and 50 Hz) were attempted to investigate its influence on the deposits morphology. To obtain deposits with the same thickness as that of direct current, total time ( $t_{on}+t_{off}$ ) was kept the same as direct deposition.

The value employed as on-time deposition current was set as 7 mA/cm<sup>2</sup>. It was doubled the value which was determined when constant potential (-1.1 V vs Pt) was applied at 80 °C from bath containing 0.5 M CuCl<sub>2</sub> · 2H<sub>2</sub>O. The specific setup parameters for each electrodeposition were stated as in Table 3.4.

	Pulse frequency, Hz			current density, mA cm <sup>-2</sup>	
	0.005	0.5	50	Peak	Average
Duty cycle, %	Pulse times (on-off), sec				
50	100-100	1-1	0.01-0.01	7	3.5

**Table 3.4** Details of Pulse Conditions

As a result, pulse plating was proved to improve the poor current efficiency. Interestingly, the resulting current efficiencies by applying pulse current were as high as 90%-98% covering all the three frequencies.

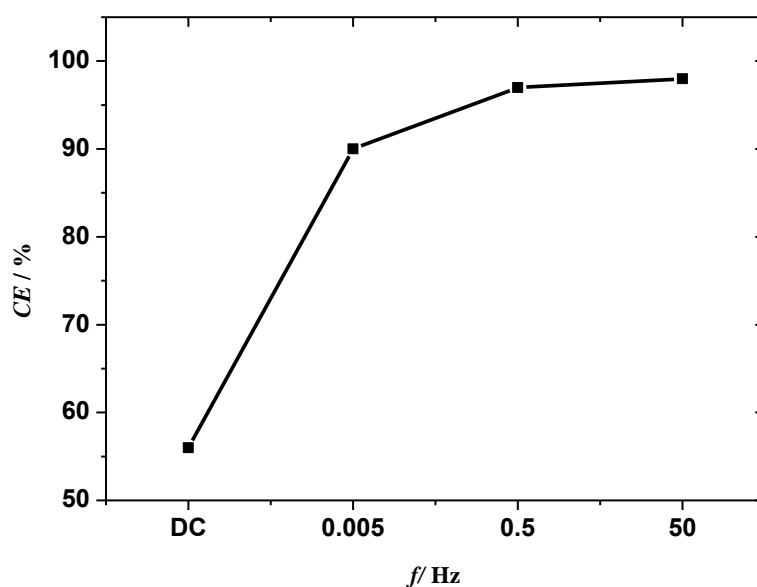


**Figure 3.18** Effect of frequency on current efficiency of films deposited at current density of 3.5 mA/cm<sup>2</sup> under direct current and 7.0 mA/cm<sup>2</sup> under pulse current with duty cycle of 0.5

As shown in Figure 3.18, current efficiency shows a drastic increase when the direct current was replaced by pulse current, which can be considered a result of in-time supply of  $\text{Cu}^{2+}$  during off-time. Even in the comparison in pulse range, current efficiency tends to increase with frequency until reaches a maximum at 50 Hz. Shorter cycle time under higher frequency favors the formation of thinner diffusion layer near the electrode surface, which is more beneficial to the efficient replenishment of copper ions during off-time. This result confirmed the diffusion-controlled deposition process as mentioned before and the lack of copper ions near to the surface that is the main cause of the low efficiency under DC<sup>[21]</sup>. So taking great advantage of improved current efficiency, time needed to deposit 1  $\mu\text{m}$  Cu film can be reduced to 12 minutes under pulsed mode from 23 minutes under DC condition. Layers deposited at different frequencies show rather comparable surface morphology.

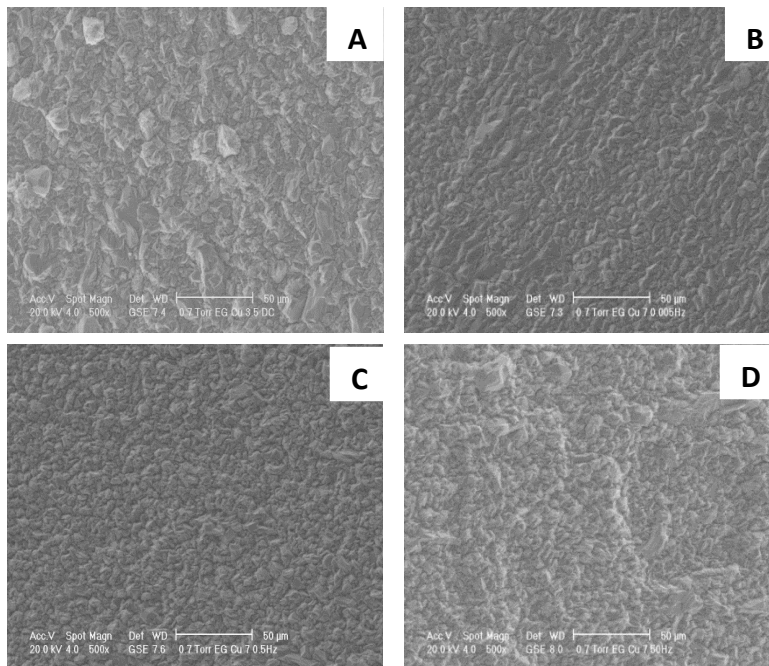


**Figure 3.19** SEM images of Cu film on brass substrate deposited from 0.5 M  $\text{CuCl}_2 \cdot 2\text{H}_2\text{O}$  in ethaline at 80 °C applying a) direct current b) pulse current at frequency of 0.005 Hz c) pulse current at 0.5Hz d) pulse current at 50Hz

As shown in Figure 3.19, Cu layer deposited with pulse current shows much lower roughness and finer grains compared to that deposited with direct current. The resulting surfaces obtained with frequencies of 0.005 Hz, 0.5 Hz and 50 Hz were rather similar. The present investigation indicates that pulse current favors the formation of finer and more regular grains and inhibits the occurrence of side reactions. The grain refinement should be attributed to the off-time allowing the Cu adatoms have enough time to move to the surface of substrate and look for the lowest energy sites and a higher instantaneous current density become possible during deposition process

Due to the mass transfer investigated previously, pulse current can effectively reduce the concentration gradient near the surface of the cathode electrode during off-time and replenish the  $\text{Cu}^{2+}$  which has been consumed in the course of on-time. By this way, pulse deposition can decrease the side reaction of the solvent effectively by complementing the reducible electrolytes near the electrode area. This acts similar as a well-know effect of pulse plating concerning the reduction of evolution of hydrogen in aqueous solutions<sup>[22]</sup>.

Pulse plating is widely used in electrodeposition from aqueous solutions for several decades to improve deposits while it is still quite new in field of ionic liquids. To our knowledge, few papers deal with pulse plating from ionic liquids, especially from deep eutectic solvents. From our study in this section, we can conjecture that pulse plating can serve with important impact in ethaline system especially when the process is characterized by low efficiency.

### **3.7 Conclusions**

A detailed and systematic study on the electrodeposition of Cu layers in a deep eutectic solvent. Physical properties such as conductivity and viscosity are insensitive to neither exposure to natural environment nor the addition of metal salt. Copper salts with different anions generated same complexed form in the same solvent with  $[\text{CuCl}_4]^{2-}$  in ethaline and  $[\text{Cu}(\text{NH}_3)_4]^{2+}$  in reline. The mass transfer in these solvents is diffusion controlled and be enhanced by elevating operation temperature and concentration of metallic salts. Due to almost 10 times difference between the reduction current in ethaline and reline, electrodeposition parameters were optimized and 0.5 M,

80 °C and conducting in ethaline were employed for consideration of better appearance and morphology. Pulse current was applied to deposit copper layer with great improvement on current efficiency from 56% up to 98% at 50 Hz. The main cause of the very low current efficiency was proved to be mass transport limitation that pulse current can avoid.

### 3.8 References

- [1] F. Endres, S. Z. El Abedin, *Physical Chemistry Chemical Physics*, 8 (2006) 2101-2116.
- [2] M.R. Ali, M.Z. Rahman, S. SankarSaha, *Journal of Electrochemistry*, 20 (2014) 139-145.
- [3] D. Yue, Y. Jing, J. Sun, X. Wang, Y. Jia, *Journal of Molecular Liquids*, 158 (2011) 124-130.
- [4] J.O.M.Bockris, A.K.N. Reddy, *Modern Electrochemistry*, Plenum Press, New York, 1970.
- [5] H.-C. Chang, J.-C. Jiang, W.-C. Tsai, G.-C. Chen, S.H. Lin, *Chemical Physics Letters*, 427 (2006) 310-316.
- [6] K.E. Ttaib, Ph.D thesis, University of Leicester, 2010..
- [7] A.P. Abbott, *ChemPhysChem*, 5 (2004) 1242-1246
- [8] C. Amuli, M. Elleb, J. Meullemeestre, M. Schwing, F. Vierling, *Inorganic Chemistry*, 25 (1986) 856-861.
- [9] A.D. McLaren, S. Pearson, *Journal of Polymer Science*, 4 (1949) 408-408.
- [10] V. Lagana, Process for treating flue gas, patent WO/1999/061136, 1999.
- [11] A.S. Ismail, S.Z. El Abedin, O. Höfft, F. Endres, *Electrochemistry Communications*, 12 (2010) 909-911.
- [12] M. Galiński, A. Lewandowski, I. Stępnia, *Electrochimica Acta*, 51 (2006) 5567-5580.
- [13] W. Simka, D. Puszczuk, G. Nawrat, *Electrochimica Acta*, 54 (2009) 5307-5319.
- [14] S. Zein El Abedin, F. Endres, *ChemPhysChem*, 7 (2006) 58-61.

- [15] R. Greef, R. Peat, L.M. Peter, D. Pletcher, J. Robinson, *Instrument Methods in Electrochemistry*, Ellis Horwood Limited, Chichester, 1990.
- [16] W. Yang, H. Cang, Y. Tang, J. Wang, Y. Shi, *Journal of Applied Electrochemistry*, 38 (2007) 537-542.
- [17] C. Jagadeeswara Rao, K.A. Venkatesan, K. Nagarajan, T.G. Srinivasan, P.R. Vasudeva Rao, *Electrochimica Acta*, 54 (2009) 4718-4725.
- [18] A.P. Abbott, K.J. McKenzie, *Physical Chemistry Chemical Physics*, 8 (2006) 4265-4279.
- [19] K. Haerens, E. Matthijs, K. Binnemans, B.V.d. Bruggen, *Green Chemistry*, 11 (2009) 1357-1365.
- [20] E.R. Parnham, E.A. Drylie, P.S. Wheatley, A.M.Z. Slawin, R.E. Morris, *Angewandte Chemie International Edition*, 45 (2006) 4962-4966.
- [21] W.-C. Tsai, C.-C. Wang, Y.-Y. Wang, *Journal of The Electrochemical Society*, 150 (2003) C267-C272.
- [22] D. Landolt, A. Marlot, *Surface and Coatings Technology*, 169-170 (2003) 8-13.

## **4 Electrodeposition of Tin from Deep Eutectic Solvent based on mixture of Choline Chloride and Ethylene Glycol**

In this chapter, the electrochemical and transport properties of tin in DES and resultant morphology of the deposits prepared under different parameters was studied. Optimized current density for more efficient deposition process and better coverage on substrate was investigated. Meanwhile, the effect of nicotinic acid (NA) on the deposition process was studied since the adoption of additive in the deep eutectic solvents is still in an initial stage. Electrochemical methods were applied to investigate the deposition process and scanning electron microscopy was used to observe the surface morphology of deposited layers.

## 4.1 Voltammetric behavior

Ethaline and reline were prepared and stored as described in the third chapter. Complete dissolution of tin salt ( $\text{SnCl}_2 \cdot 2\text{H}_2\text{O}$ ) was aided by gentle stirring for 10 min under a nitrogen atmosphere by continuous purging into the bath. The solvents after complete dissolution of tin salts at room temperature formed a colorless liquid. After preparation, the electrolyte was stored in an airtight glass bottle to minimize the interaction between the melt and air. Before each measurement, the solutions were de-aerated with nitrogen to decrease the possible oxidation of stannous ions.

All electrochemical measurements were conducted using the same instrument as that in previous chapter. Cyclic voltammetry measurement was carried out at scan rate of 20 mV/s at 80 °C. The cell set-up consists of three electrodes, brass electrode (diameter 2 mm) as working electrode, a Pt wire as quasi-reference and a Pt plate as counter electrode which were placed inside a thermostatic jacket. Instead of Pt plate (6 cm<sup>2</sup>) as in condition of Cu deposition, smaller size of brass was used as working electrode here for higher sensitivity and lower interference from background noise. The electrodes were polished until mirror-like surfaces were obtained and cleaned by ultrasound for 10 min in distilled water and acetone and then dried with N<sub>2</sub> prior to each experiment.

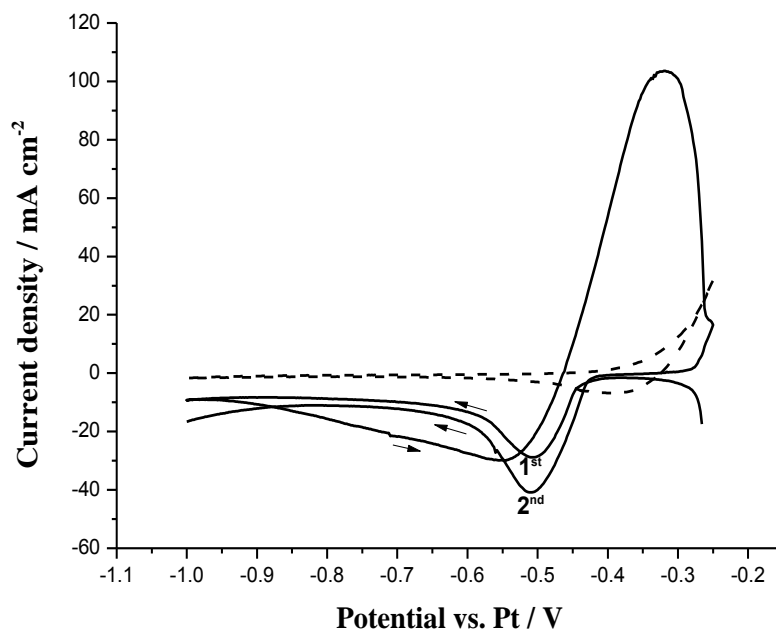


**Figure 4.1** Cyclic voltammograms of neat ethaline (dashed line) and ethaline containing 0.3 M SnCl<sub>2</sub>·2H<sub>2</sub>O (solid line) at a brass electrode at 80 °C

The cyclic voltammograms of the neat ethaline and ethaline containing 0.3 M SnCl<sub>2</sub>·2H<sub>2</sub>O electrolyte at 80 °C are shown in Figure 4.1. The scanning starts from open circuit potential to negative direction and the first/second cycles were recorded for comparison. As shown in Figure 4.1 (dashed line), the electrochemical window of the neat ethaline on brass electrode displays a cathodic potential limit of more negative than -1 V and an anodic potential limit of -0.30 V. From Figure 4.1 (solid line), we observe that the addition of SnCl<sub>2</sub>·2H<sub>2</sub>O induced a pair of well-defined peaks corresponding to the reduction and oxidation of tin since they are

absent in the tin free DES. The reduction of Sn(II) initiates at -0.42 V and reach a maximum at -0.51V at first cycle.

In the reverse scan a ‘current loop’ (hysteresis) was observed. Such a current loop is indicative of an overpotential driven nucleation/growth process that is associated with the electrodeposition of a metal onto a metal<sup>[1]</sup>. In the second cycle, the reduction current is higher than that recorded in the first cycle and the induction of reduction has been slightly moved to positive direction. The fact proves that depositing metal on foreign substrates requires a larger over potential to be applied in order to initiate the nucleation but less negative potential for the growth for the deposit<sup>[2]</sup>. The anodic scan of neat ethaline displayed an oxidation wave from -0.4 V, which is attributed to the oxidation of ethylene glycol on brass working electrode and the oxidation of brass<sup>[2]</sup>. The sizeable oxidation peak after the addition of 0.3M SnCl<sub>2</sub> · 2H<sub>2</sub>O shows the oxidation of Sn deposits at -0.32 V vs. Pt. The shape of the peak is similar with that observed with glassy carbon in the same solvent by S. Salome<sup>[3]</sup>. The reduction of tin occurs in more negative potential when a saturated ChCl calomel reference electrode was applied.

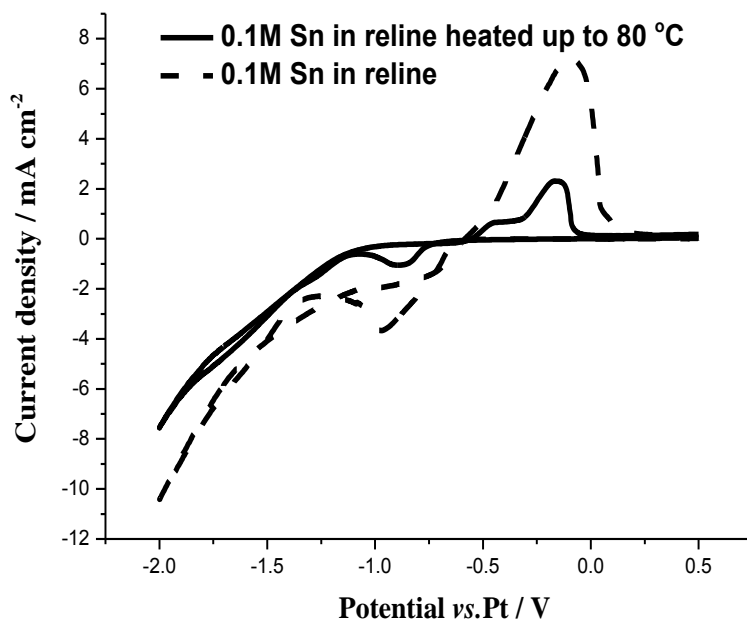


**Figure 4.2** Cyclic voltammograms of 0.1 M Sn(II) in reline measured in room temperature(dashed line) and at 80 °C (solid line)

Reline was also studied for Sn deposition at elevated temperature for improved mass transfer. However, after heated up to 80 °C, reline containing tin salts changed from colorless to milky yellow totally. In addition, the mixture turned to turbid instead of transparent which we assume due to the occurrence of white precipitation. By comparing cyclic voltammograms in Figure 4.2, we can clearly see that concentration of reducible  $\text{Sn}^{2+}$  decreased significantly after the solvent was heated. Even in the anodic scan after the reduction process, a new peak appeared before the oxidation of Sn(0). This is can be ascribed to the existence of complexation form between  $\text{Sn}^{2+}$  and  $\text{NH}_3$  which is released from heated urea as explained below.

Since there is no similar study available up to now, we can propose some possibilities from chemical point of view. By comparing the different thermal stability of ethaline and reline which both contain Sn salt, accelerating effect on oxidation in presence of urea in the system should be considered as a priority reason. Upon heated up, reline can decompose at 125 °C<sup>[4]</sup>. However Liao et al.<sup>[5]</sup> stated that the decomposition can take place at 80 °C in presence of transition metals and low content of water. This proved that the presence of impurities will decrease the decomposition temperature of this solvent. Liberated ammonia, NH<sub>3</sub>, can be generated in situ from partial decomposition of urea. This will lead to white precipitation according to the following reaction:



The resulting product is not stable in alkaline solution which can be easily oxidized by atmospheric oxygen:  $2\text{Sn}(\text{OH})_2 + 2\text{H}_2\text{O} + \text{O}_2 \rightarrow 2\text{Sn}(\text{OH})_4$  which will undergo another reversible reaction:  $\text{Sn}(\text{OH})_4 + 4\text{NH}_4^+ + 6\text{Cl}^- \leftrightarrow [\text{SnCl}_6]^{2-} + 4\text{NH}_3 + 4\text{H}_2\text{O}$ . The non-conducting behavior of  $[\text{SnCl}_6]^{2-}$  reduced the electroactive property of final mixture and certain content of  $\text{Sn}(\text{OH})_2$  and  $\text{Sn}(\text{OH})_4$  reduced the transparency.

Due to the instability of Sn salts in reline upon warm up and even electrochemical decomposition after continuous electrolysis<sup>[6]</sup>, we would like to interrupt the study of tin deposition from reline and carry on subsequent research of alloy only in ethaline.

## 4.2 Chronoamperometric investigations

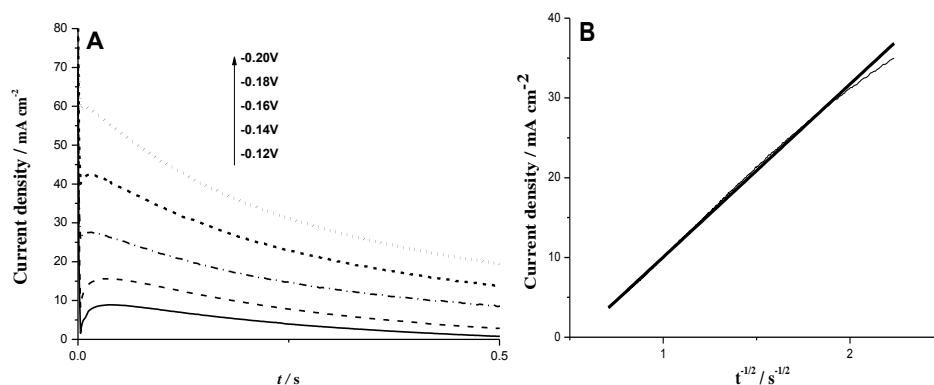


**Figure 4.3** (A) Chronoamperograms of Sn deposition on brass electrode in 0.3 M SnCl<sub>2</sub>·2H<sub>2</sub>O at different potentials under 80 °C. (B) Representations of  $j$  vs.  $t^{-1/2}$  and linear fitting at -0.20 V.

The chronoamperometric experiments were carried out to study the Sn nucleation/growth process on brass electrode by stepping the potential from a value where no reduction of Sn(II) takes place to progressively more negative values where nucleation would be initiated, as shown in Figure 4.3(A). Same cell setup was used as that in cyclic voltammetry study. All measurements were carried out at 80 °C.

After the double layer discharge the current rapidly increases until a current maximum,  $j_m$ , is reached at time  $t_m$ , from which it decreases. This is a typical nucleation/growth process<sup>[1, 7]</sup>. When the applied potential becomes more negative, the rate of formation and growth of Sn nuclei increase, which result in higher  $j_m$  and reduced  $t_m$ .

The transients merged to a constant current at longer time therefore the data could be fitted to Cottrell equation:  $i = \frac{nFAc_j^0\sqrt{D_j}}{\sqrt{\pi t}}$  where  $i$  is the current

measured,  $n$  represents the electrons reduced of one molecule of analyte,  $F$  equals to  $96485\text{C/mol}$ ,  $A$  is the planar area of electrode,  $c_j^0$  is the initial concentration of reducible species in solvents,  $t$  is the time process lasts and  $D_j$  is diffusion coefficient of species. This equation describes the case which is diffusion controlled and can be used to estimate the value of diffusion coefficient from the slope of the curve.

As shown in Figure 4.3(B),  $i-\sqrt{t}$  is a curve passing the origin suggesting the deposition was controlled by diffusion<sup>[8]</sup>. The estimated value for the diffusion coefficient of tin species  $4.32 \times 10^{-6} \text{ cm}^2 \text{ s}^{-1}$ . This diffusion coefficient value is in the same order as that reported for Sn species in aqueous solutions<sup>[9]</sup> but larger than those reports in different RTILs<sup>[3, 10, 11]</sup>. S. Ghosh et al.<sup>[12]</sup> reported that  $\text{Sn}^{2+}$  diffusivities was  $1.96 \times 10^{-7} \text{ cm}^2 \text{ s}^{-1}$  in ethaline containing 0.05M Sn salts at 23 °C, which shows one magnitude lower value than that in this case because of difference in conducting temperature and concentration

Deposition of metals to foreign substrates usually takes place via two types of three-dimensional nucleation process which are called instantaneous and progressive nucleation. The first one refers to the situation in which all nuclei are formed immediately after the potential is applied, and in the latter case the number of nuclei increases gradually with deposition time. The theoretical transits of instantaneous and progressive nucleation can be represented by two following equations respectively where  $i_m$  and  $t_m$  represent the current coordinate values of the nucleation peak<sup>[13]</sup>:

$$\text{IN-3D} \left( \frac{i}{i_m} \right)^2 = \frac{1.9542}{t/t_m} \left[ 1 - \exp \left( -1.2564 \frac{t}{t_m} \right) \right]^2 \quad (1)$$

$$\text{PN-3D} \left( \frac{i}{i_m} \right)^2 = \frac{1.2254}{t/t_m} \left\{ 1 - \exp \left[ -2.3367 \left( \frac{t}{t_m} \right)^2 \right] \right\}^2 \quad (2)$$

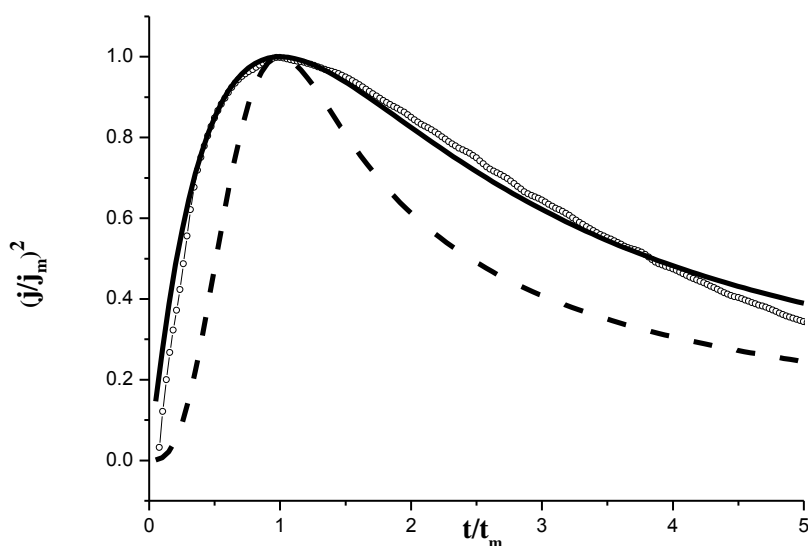


**Figure 4.4** Experimental transients in dimensionless form considering a 3D model for ( ° ° ° ) 0.3 M  $\text{SnCl}_2 \cdot 2\text{H}_2\text{O}$ , and theoretical transients for instantaneous (solid line) and progressive (dashed line)

The comparison of the experimental plots with the theoretical curves is shown in Figure 4.4. The experimental results suggest instantaneous three-dimensional nucleation as described in equation 1 in this case. This approach has been extensively used to analyse the electrodeposition of metals in ionic liquids as Ni and Al<sup>[14, 15]</sup>. Similar result was observed on a GC electrode in  $\text{AlCl}_3\text{-EMICl}$ <sup>[16]</sup> and on W and GC electrodes in  $\text{ZnCl}_2\text{-EMICl}$ <sup>[17]</sup>, respectively. However Tachikawa and co-workers suggested the progressive nucleation on a Pt electrode in  $\text{BMPNTf}_2$ <sup>[11]</sup>.

### 4.3 Potentiostatic deposition

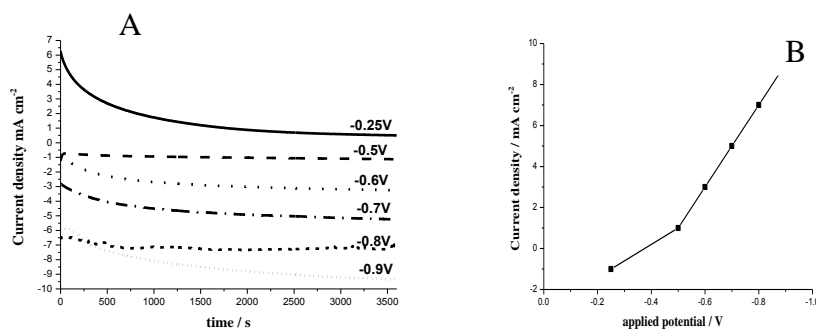


**Figure 4.5** (A) Resulting current density vs. time during potentiostatic deposition at fixed potentials (B) relationship between current and potentials

Potentiostatic deposition was carried out at 80 °C in static condition on brass foil (area=10 cm<sup>2</sup>) for its low roughness and fine reflection. Figure 4.5 shows the effect of reduction potential on the current response in ethaline containing 0.3 M SnCl<sub>2</sub>. A well linear relationship between the reduction current and applied potential in the range of -0.5V to -0.9V can be observed. The results indicate that deposition process can be accelerated effectively by increasing potential drops.

## 4.4 Influence of agitation speed

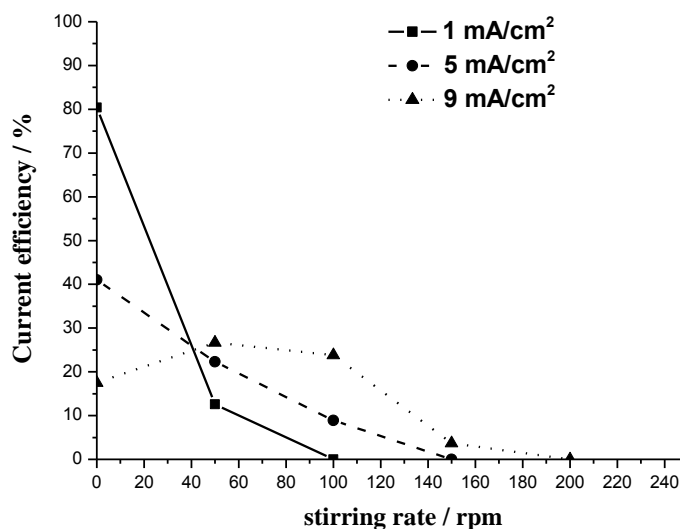


**Figure 4.6** Resulting current efficiency of deposition processes as a function of agitation speed carried out in ethaline containing 0.3 M SnCl<sub>2</sub> at current density of 1 mA/cm<sup>2</sup>, 5 mA/cm<sup>2</sup> and 9 mA/cm<sup>2</sup>

Influence of varied stirring rate on resulting deposition process was studied under galvanically applying various current densities. As shown in Figure 4.6, generally, resulting current efficiency decreased with increasing agitation rate until it reached zero. The agitation speed range which supported non-zero current efficiency at current density of 9 mA/cm<sup>2</sup> (5 mA/cm<sup>2</sup>) is larger than that of 1 mA/cm<sup>2</sup>.

Higher applied current will help to form steeper concentration profile near electrode in the solvent and this can be regarded as stronger driving force accelerating mass transfer of reducible species. More mass of metallic species can be reduced under this condition. However, agitation in the

system of DES can perform two different forms: when the rate is lower than a certain point, the mass transfer will be enhanced by the increased agitation generating more deposits; when the rate is higher than a critical point, the reduced particles will be removed by agitation because of their poor adhesion to electrode surface. The stronger agitation is, the more mass will be removed by stirring. By observing the changing trend of current efficiency influenced by agitation, we can assume that during reduction process carried out with low current density ( $1 \text{ mA/cm}^2$ ), the tin anions driven by stirring is not sufficient for reduction process and furthermore agitation tends to decrease the concentration of tin anions adjacent working electrode. As a result, occurrence of possible side-reaction increases and the resulting current efficiency decreases. While higher current density is applied ( $9 \text{ mA/cm}^2$ ), there is a counterbalance effect between mass transfer influenced by stirring and applied currents. Higher reduction current will bring more tin anions to the working electrode while agitation with speed over a critical point will act a removal effect on the electroactive species in front of electrode. So a trend of increase and then decrease with an optimized condition can be reached at 50 rpm under  $9 \text{ mA/cm}^2$ .

From visual observation during experimental process, we can also find that because of poor adhesion between substrate and tin layer, more loose deposit formed in electrolyte near working electrode which would be removed by drying after preparation. This effect turns to be more severe when higher current density is applied. So as a result, the weighted deposit is supposed to be lower than actual reduced mass which decrease the value of final current efficiency. Moreover, the faster agitation speed is, more loosen deposit would be formed in solvent.

## 4.5 Morphology characterization

The galvanic deposition was carried out between two parallel vertical electrodes immersed in a cell warmed by thermostatic jacket. The tin deposition was performed on brass foil (area=10 cm<sup>2</sup>). A surface cleaning treatment of the brass substrate was conducted by ultrasound cleaning in acetone and deionized water rinsing and dried with flowing N<sub>2</sub>. A graphite plate was employed as anode to avoid any impurity produced into the bath. Deposition time was calculated using applied current densities (1, 3, 5, 7, 9 mA/cm<sup>2</sup>) to obtain 4μm thick deposit.

The final deposits were sequentially rinsed with deionized water and dried with a flow of air. Surface morphology of Sn deposits was characterized by Scanning Electron Microscopy (Philips XL 30 ESEM).

Since current efficiency of deposition process is sensitive to agitation from our observation, static condition was used to for easier control and maintaining the same environment. Current efficiency decreases with the applied currents in the order of 1 mA/cm<sup>2</sup> (80.38%) ~ 3 mA/cm<sup>2</sup> (53.89%) ~ 5 mA/cm<sup>2</sup> (41.00%) ~ 7 mA/cm<sup>2</sup> (35.99%) ~ 9 mA/cm<sup>2</sup> (17.50%). So after calculation according to Faraday's law, time needed to deposit 4μm thick deposit is 13.5min (1 mA/cm<sup>2</sup>) ~ 6.7 min (3 mA/cm<sup>2</sup>) ~ 5.3 min (5 mA/cm<sup>2</sup>) ~ 4.3 min (7 mA/cm<sup>2</sup>) ~ 10.7 min (9 mA/cm<sup>2</sup>). For more efficient deposition process and more distinguished parameter, the morphology comparison of tin deposits was carried out between the deposits prepared with current density of 3 mA/cm<sup>2</sup> and 7 mA/cm<sup>2</sup> as displayed in Figure 4.7.

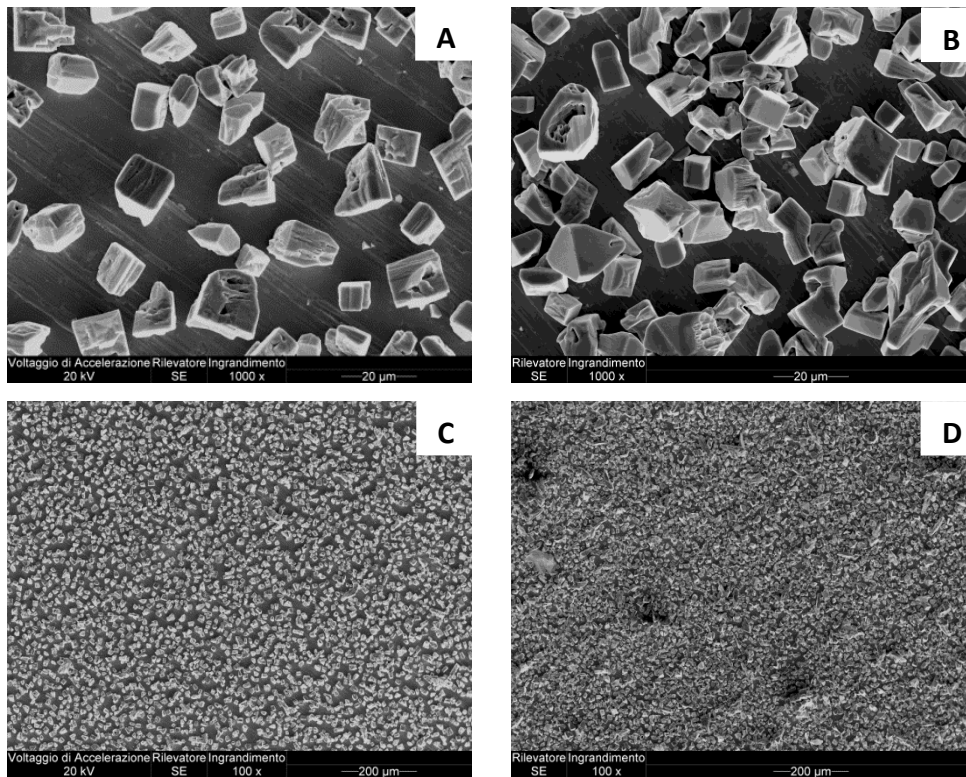


**Figure 4.7** SEM images of tin deposits obtained galvanically on brass electrode at (A)  $3 \text{ mA/cm}^2$  and (B)  $7 \text{ mA/cm}^2$  for 1800 s in  $0.3 \text{ M SnCl}_2 \cdot 2\text{H}_2\text{O}$ . (C) and (D) are corresponding images of (A) and (B) in lower magnification.

The Figure 4.7 shows that the deposits obtained cannot cover the entire surface with crystals overlapping and on top of which few parallelepiped crystallites are visible. Cubic and cuboid-shaped crystallites grow perpendicularly from the electrode surface randomly and average size can be hardly estimated because of the irregular shapes. Increasing deposition current improves the coverage of grains on the substrate, meanwhile reduces the average grain size from optical observation.

In spite of important information obtained by SEM, no quantitative description of layer roughness is available due to its limitations. In this work laser confocal microscopy was used to measure the roughness of the tin deposit on the cathode surface in a laboratory-scale tin electrorefining cell. 3D surface profiles were analyzed by means of Laser Confocal Microscopy (Nikon A1), multiple stack image capture and volume reconstruction. To enhance surface topography, images were collected by exciting with a laser beam at 488 nm and collecting emission signal at 525 nm, after staining the samples with fluorescein.

This method offers the distinct advantage of eliminating defocused images rather than creating a blur of that image<sup>[18]</sup>. The principle of confocal scanning optical microscopy used to measure the surface roughness was introduced by Lange et al.<sup>[19]</sup>.

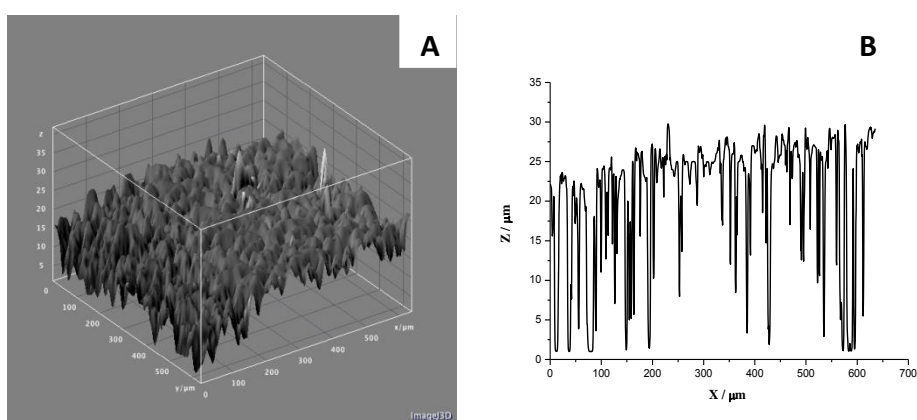


**Figure 4.8** (A) The reconstructed images of tin deposited at  $7 \text{ mA/cm}^2$  for 1800 s in  $0.3 \text{ M SnCl}_2 \cdot 2\text{H}_2\text{O}$  (B) Depth profile of the cross section

For better coverage of deposit on the substrate as well as higher deposition efficiency among various current densities studied,  $7 \text{ mA/cm}^2$  was chosen to study the surface morphology. From topographic images reconstructed from a series of optical sections shown in Figure 4.8(A),

comprehensive mapping of deposit can be presented showing morphology such as valleys and peaks. Figure 4.8(B) portrays the line depth profile gained from the cross section. More information may be taken from any position of the profile image from left to right side for average calculation. We can see the depth of ditches from top of tin layer to surface of substrate can be estimated around  $25\mu\text{m}$  which is quite close to grain diameter shown in SEM image.

Generally the deposits prepared with higher currents shows lower roughness compared with those deposited at lower ones, which can be roughly measured by a surface profilometer (MarSurf PS1). This is the same from the process carried out in aqueous solutions where higher currents are beneficial to refined grains<sup>[20]</sup>. Also it's the also true for results obtained for the deposition from conventional ionic liquids<sup>[21]</sup>.

## **4.6 Effect of nicotinic acid additive on the Sn deposition**

The electrodeposition of metals has been widely practiced in aqueous solutions with a wide range of additives<sup>[22-25]</sup>. A detailed description of the influence of organic additives on the microstructure of metal deposits is given by Fischer<sup>[26]</sup>. In contrast, few additives have been attempted in ionic liquids. Some famous additives like thiourea, ethylene diamine, ammonia and coumarin work well in producing uniform and bright metal coatings from ionic liquids<sup>[1, 7, 27-30]</sup>. Among them H. Yang states nicotinic acid (NA) serves as a very effective brightener producing highly uniform and smooth Ni deposits from choline chloride-urea eutectic based ionic liquid<sup>[1]</sup>.

However, no parallel work has been carried out in electrodeposition of tin with NA from ethylene glycol-choline chloride deep eutectic solvent. So it is unknown if the same effect can be expected.

#### 4.6.1 Voltammetric behavior

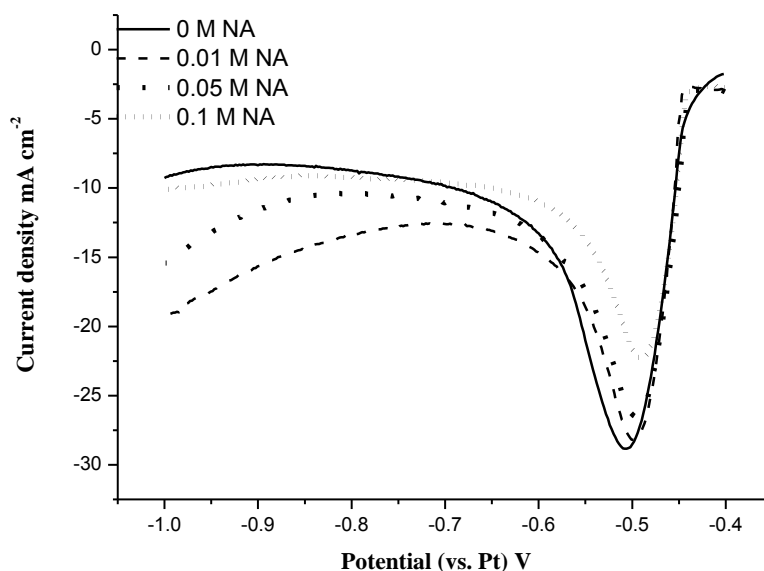


**Figure 4.9** Linear stripping voltammograms of Sn(II) in ethaline containing 0.3 M  $\text{SnCl}_2 \cdot 2\text{H}_2\text{O}$  with 0 M (solid line), 0.01 M (dashed line), 0.05 M (dotted line) and 0.1 M (short dotted line) nicotinic acid on a brass electrode at 80 °C.

To observe the effect of different concentrations of NA on the electrochemical behavior of Sn(II), linear stripping voltammetry was scanned negatively in ethaline containing 0.3 M  $\text{SnCl}_2 \cdot 2\text{H}_2\text{O}$  with 0, 0.01, 0.05, 0.1 M NA are shown in Figure 4.9. Each voltammogram was

recorded on a fresh brass electrode surface and was performed at a scan rate of 20 mV/s. Before each measurement, different amount of nicotinic acid was added into fresh prepared DES and aided with stirring for 10 min for complete dissolution. It is obvious that the addition of NA produces an inhibition of Sn deposition current and a slight shift of reduction potential towards positive potential. This NA effect increases with the NA concentration.

Brighteners can function in two ways to block nucleation and inhibit crystal growth: one is to decrease the reduction potential by complexing with metal ions and the other one is to blocking the active sites by adsorption on the electrode surface<sup>[31]</sup>. These mechanisms may also applicable in ILs. In recent studies, the addition of ethylene diamine into ethylene containing 0.45 M CuCl<sub>2</sub> suppressed underpotential deposition of Cu and led to finer grains and smoother surface<sup>[30]</sup>. In contrast, ethylene diamine in same solvent containing 0.3 M ZnCl<sub>2</sub> acted to promote the reduction of zinc<sup>[29]</sup>.

Considering the complexing properties of NA with other metal ions the formation of tin-NA, which has more positive reduction potential in this case, should be taken into consideration to explain experimental results<sup>[1, 32-34]</sup>. However, the onset of reduction is shifted anodically by 10 mV, suggesting that the presence of NA acts to promote the reduction of tin. This is opposite effect to that observed for the corresponding experiment with Ni<sup>[1]</sup>. This implies that nicotinic acid does not ligate the Sn species in solution since the replacement of chloride by nicotinic acid in the coordination sphere would be expected to make the tin phase more stable and hence more difficult to be reduced. The increased nucleation loop under 0.01 M, 0.05 M can be associated to the promotion effect of NA in the

solvent. In the meanwhile, the inhibition effect of NA on the tin deposition reaction is also probably related to the adsorption of the additive molecules. Adsorption of NA in free-metal ion electrolyte on different substrates has been studied by Auger and SERS spectroscopies<sup>[35, 36]</sup>. The residual NA subtracting that acts with Sn can absorb on the brass surface causing the diminishing crystal growth rate indicated from both reduction and oxidation charge under the peak. It is therefore clear that nicotinic acid is not behaving in a similar manner to brighteners in aqueous electrolytes.

#### 4.6.2 Chronoamperometric study

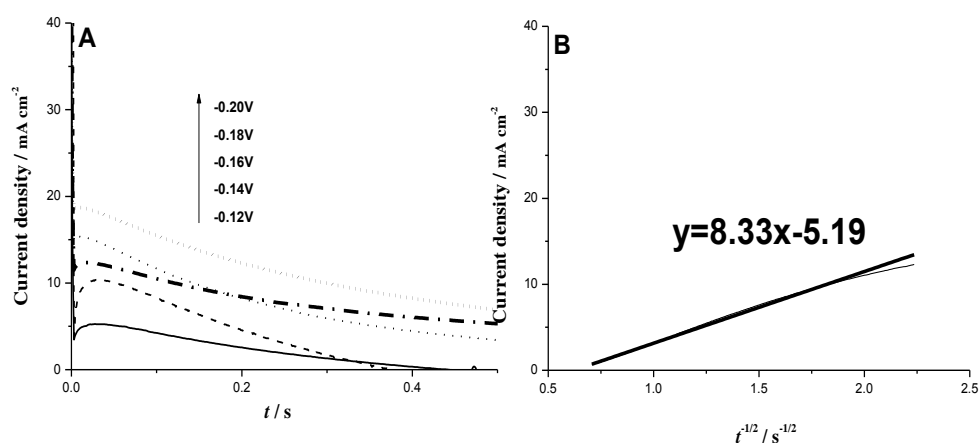


**Figure 4.10** (A) Chronoamperograms of Sn deposition on brass electrode in 0.3 M SnCl<sub>2</sub>·2H<sub>2</sub>O + 0.1 M nicotinic acid at different potentials under 80 °C and (B) representations of  $j$  vs.  $t^{-1/2}$  and linear fitting at -0.20V.

The results obtained in presence of nicotinic acid show no obvious change in  $t_m$  but great decline in  $j_m$  when compared to NA free solution, which suggest that the formation of tin nuclei was hindered and agree with the result obtained by cyclic voltammograms. The estimated value for the

diffusion coefficient of tin species in presence of nicotinic acid was  $5.34 \times 10^{-7} \text{ cm}^2 \text{ s}^{-1}$ . The value of D decreased almost 10 times after the addition of NA. This value in presence of NA shows lower diffusion rate than aqueous solution<sup>[9]</sup> but similar with those in RTILs<sup>[3, 10, 11]</sup>.

Also, it can be observed that curve of Cottrell equation does not go through the origin in this case which states this process is not purely controlled by diffusion.

### 4.6.3 Surface morphology

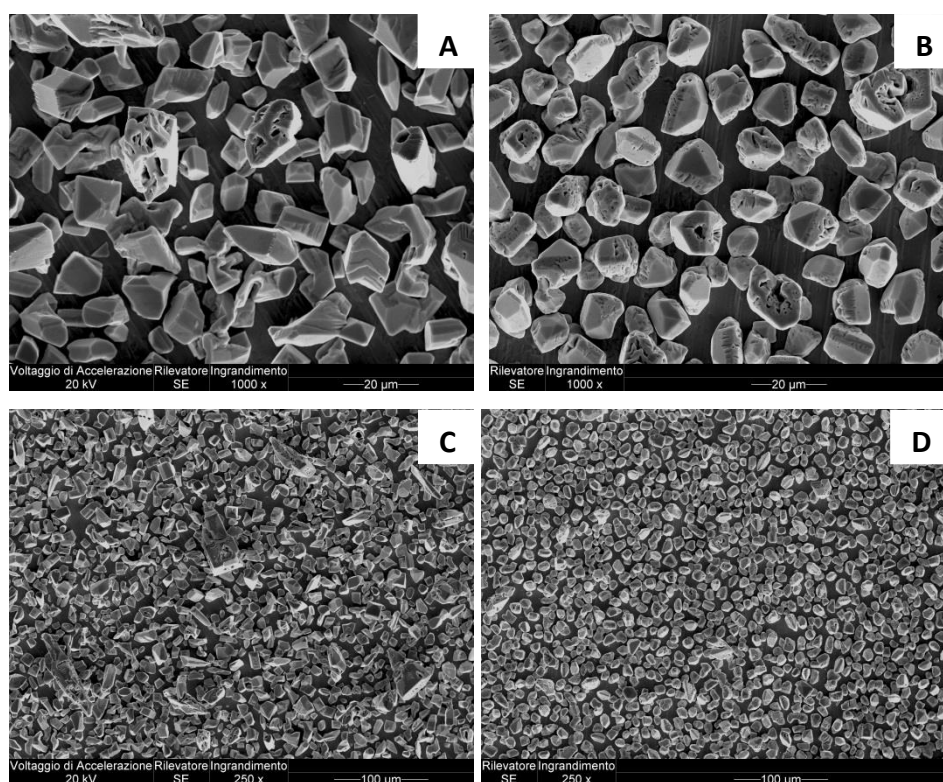


**Figure 4.11** SEM images of tin deposits obtained galvanically on brass electrode at  $7 \text{ mA/cm}^2$  for 1800 s in (A)  $0.3 \text{ M SnCl}_2 \cdot 2\text{H}_2\text{O} + 0.01 \text{ M NA}$ , (B)

*0.3M SnCl<sub>2</sub> 2H<sub>2</sub>O+0.1 M NA, (C) and (D) are corresponding images of (A) and (B) in lower magnification.*

Figure 4.11 shows the addition of 0.01M NA into the solvent suggests no obvious effect on the deposit which matches the neglectable change in electrochemical response. However 0.1M NA acted a more effective brightener in Sn deposition by improvement on crystal size and shape. The grains show more even size and free of shape corners, which slightly elevated the surface coverage. We can assume that increase concentration of NA can decrease the size of spherical crystals and make the surface morphology more compact.

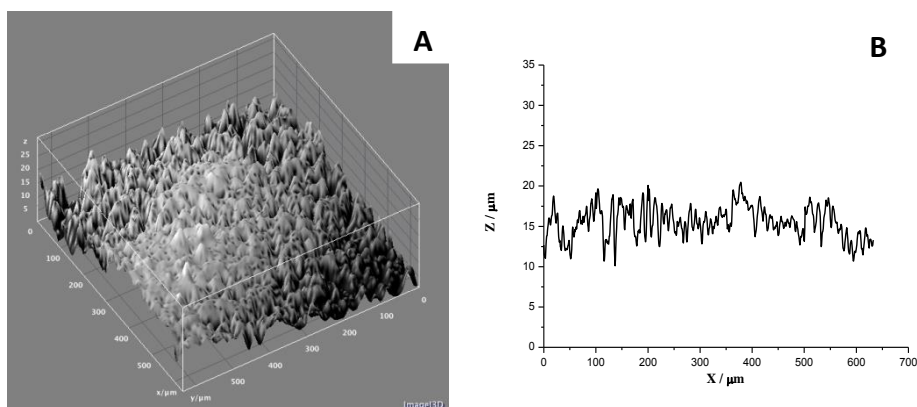


**Figure 4.12**(A) The reconstructed images of tin deposited at  $7 \text{ mA/cm}^2$  for 1800 s in  $0.3 \text{ M SnCl}_2 \cdot 2\text{H}_2\text{O} + 0.1 \text{ M NA}$  (B) Depth profile of the cross section

From the comparison from topographic images in absence and presence of 0.1 M NA, we can see that the addition of nicotinic acid can reduce the roughness of the surface obviously shown in Figure 4.12(B). It can effectively decrease the height between valleys and peaks of deposited

grains. The attached nicotinic acid can inhibit continuous growth of tin grains in vertical direction and instead it helped tin nucleation occurs in a more adjacent planes. The appearance of numerous tiny concaves between heaves in Figure 4.12(A) can be regarded as the places where additive comes into play. With the same deposition time in the same deposition current density, the layer obtained in presence of nicotinic acid shows lower roughness than the one without additive. This can be reasonable since certain amount of tin tend to grow in places of valleys and result in layers with higher solidity. Although the improvement on the refinement of grains size with the addition of nicotinic acid in DES is not so great as that in aqueous solution, the action effect of additives is still worth investigation in future.

## **4.7 Conclusions**

Poor stability of reline when warmed up tends to generate the occurrence of stannic ions, which make it unsuitable for Sn involved deposition. This section has demonstrated that in the electrodeposition of tin from deep eutectic solvent composed by choline chloride and ethylene glycol. The electrodeposition of tin on brass at 80 °C follows an instantaneous three-dimensional nucleation and was controlled by diffusion. The deposition leads to the formation of Sn cluster that do not cover the surface completely. Increasing current density will improve the coverage of tin grains on substrate with slight decrease in grain size. Addition of nicotinic acid can be applied as a brightener to refine the grain size of tin deposits and smooth the surface of layers.

## 4.8 References

- [1] H. Yang, X. Guo, N. Birbilis, G. Wu, W. Ding, *Applied Surface Science*, 257 (2011) 9094-9102.
- [2] A.H. Whitehead, M. Pözlner, B. Gollas, *Journal of the Electrochemistry Society*, 157 (2010) D328-D334.
- [3] S. Salomé, N.M. Pereira, E.S. Ferreira, C.M. Pereira, A.F. Silva, *Journal of Electroanalytical Chemistry*, 703 (2013) 80-87.
- [4] K. Matsumoto, R. Hagiwara, *Journal of Fluorine Chemistry*, 128 (2007) 317-331.
- [5] J.-H. Liao, P.-C. Wu, Y.-H. Bai, *Inorganic Chemistry Communications*, 8 (2005) 390-392.
- [6] D. Yue, Y. Jia, Y. Yao, J. Sun, Y. Jing, *Electrochimica Acta*, 65 (2012) 30-36.
- [7] N.M. Pereira, P.M.V. Fernandes, C.M. Pereira, A. Fernando Silva, *Journal of the Electrochemistry Society*, 159 (2012) D501-D506.
- [8] F.G. Cottrell, *Z. Physical Chemistry*, 42 (1903) 385-431.
- [9] E. Gomez, E. Gaus, F. Sanz, E. Valles, *Journal of Electroanalytical Chemistry*, 465 (1999) 63-71.
- [10] T.-I. Leong, Y.-T. Hsieh, I.W. Sun, *Electrochimica Acta*, 56 (2011) 3941-3946.
- [11] N. Tachikawa, N. Serizawa, Y. Katayama, T. Miura, *Electrochimica Acta*, 53 (2008) 6530-6534.
- [12] S. Ghosh, K. Ryder, S. Roy, *Transaction of the IMF*, 92 (2014) 41-46.
- [13] J.J. Lee, B. Miller, X. Shi, R. Kalishi, K.A. Wheeler, *Journal of the Electrochemistry Society*, 148 (2001) C183-C190.

- [14] O. Mann, W. Freyland, *Journal of Physical Chemistry C*, 111 (2007) 9832-9838.
- [15] T. Jiang, M. Chollier Brym, J.G. Dubé, A. Lasia, G.M. Brisard, *Surface and Coatings Technology*, 201 (2006) 1-9.
- [16] X.-H. Xu, C.L. Hussey, *Journal of the Electrochemical Society*, 140 (1993) 618-626.
- [17] J.-F. Huang, I.W. Sun, *Journal of The Electrochemical Society*, 150 (2003) E299-E306.
- [18] G.S. Kino, T.R. Corl, *Applied Physics Letters*, 6 (1990) 28-31.
- [19] D.A. Lange, H.M. Jennings, S.P. Shan, *Journal of Materials Science*, 28 (1993) 3879-3884.
- [20] A.M. Rashidi, A. Amadeh, *Surface and Coatings Technology*, 202 (2008) 3772-3776.
- [21] K. Ki-Sub, K. Sang hyun, P. Sun-Mi, K. Wan-Kyu, K. Jeong Won, *Journal of the Korean Physical Society*, 57 (2010) 1639-1643.
- [22] S. Vitkova, V. vanova, I. Raichevsky, *Surface and Coatings Technology*, 86 (1996) 226-231.
- [23] F.J. Barry, V.J. Cunnane, *Journal of Electroanalytical Chemistry*, 537 (2002) 151-163.
- [24] N. Pewnim, S. Roy, *Electrochimica Acta*, 90 (2013) 498-506.
- [25] E. Gaus, J. Torrent-Burgués, *Journal of Electroanalytical Chemistry*, 575 (2005) 301-309.
- [26] H. Fischer, *Elektrolytische Abscheidung und. Elektrokristallisation von Metallen*, Springer Verlag Berlin-GSttingen-Heidelberg, 1954.

- [27] Y.L. Zhu, Y. Katayama, T. Miura, *Electrochimica Acta*, 85 (2012) 622-627.
- [28] R. Fukui, Y. Katayama, T. Miura, *Electrochimica Acta*, 56 (2011) 1190-1196.
- [29] A.P. Abbott, J.C. Barron, G. Frisch, K.S. Ryder, A.F. Silva, *Electrochimica Acta*, 56 (2011) 5272-5279.
- [30] C.D. Gu, Y.H. You, X.L. Wang, J.P. Tu, *Surface and Coatings Technology*, 209 (2012) 117-123.
- [31] A.P. Abbott, K.J. McKenziea, *Physical Chemistry Chemical Physics*, 8 (2006) 4265-4279.
- [32] L. Bonou, M. Eyraud, R. Denoyel, Y. Massiani, *Electrochimica Acta*, 47 (2002) 4139-4148.
- [33] A.L. Portela, G.I. Lacconi, M.L. Teijelo, *Journal of Electroanalytical Chemistry*, 495 (2001) 169-172.
- [34] F. Endres, M. Bukowski, R. Hempelmann, H. Natter, *Angewandte Chemie International Edition*, 42 (2003) 3428-3430.
- [35] N. Batina, D.G. Frank, J.Y. Gui, B.E. Kahn, *Electrochimica Acta*, 34 (1989) 1031-1044.
- [36] J. Barthelmes, G. Pofahl, W. Plieth, *Journal of Physical Chemistry*, 96 (1992) 1055-1060.

## **5 Electrodeposition of Copper-Tin from Deep Eutectic Solvent based on mixture of Choline Chloride and Ethylene Glycol**

This chapter focused on the study of the co-deposition of Cu-Sn alloys under the optimized conditions. The metals ions are given in their simplest forms,  $\text{Cu}^{2+}$  ions and  $\text{Sn}^{2+}$  ions. The influence of liquid formulation, i.e. the ratio of metal ions in solution on the composition of the alloy formed was investigated. The study on the different deposition kinetics of Cu and Sn was carried out separately and finally pulse current was used to improve the microstructure and composition of deposited layers.

## 5.1 Cyclic Voltammetry

The eutectic solvent (ethaline) was prepared as previously mentioned. Tin chloride dihydrate [ $\text{SnCl}_2 \cdot 2\text{H}_2\text{O}$ ] and copper chloride [ $\text{CuCl}_2$ ] (all Aldrich,  $\geq 98\%$ ) were used as received without further treatment. Solvents containing various concentrations of metal salts (0.2 M  $\text{SnCl}_2 \cdot 2\text{H}_2\text{O}$ , 0.3 M  $\text{SnCl}_2 \cdot 2\text{H}_2\text{O}$ , 0.2 M  $\text{CuCl}_2$ , 0.05 M  $\text{CuCl}_2$ , 0.2 M  $\text{SnCl}_2 \cdot 2\text{H}_2\text{O}$  + 0.2 M  $\text{CuCl}_2$ , 0.3 M  $\text{SnCl}_2 \cdot 2\text{H}_2\text{O}$  + 0.05 M  $\text{CuCl}_2$ ) were prepared after complete dissolution at 80 °C and stored in airtight glasses before using.

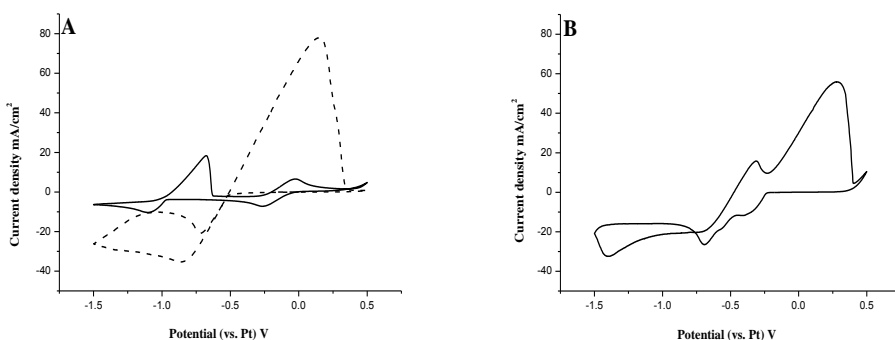


**Figure 5.1** (A) Voltammograms (20 mV/s) for a Pt electrode (0.8 cm<sup>2</sup>) immersed in ethaline containing 0.2M  $\text{CuCl}_2$  (solid line) or 0.2M  $\text{SnCl}_2$  (dashed line). (B) Voltammograms (20 mV/s) for a Pt electrode (0.8 cm<sup>2</sup>) immersed in ethaline containing 0.2M  $\text{CuCl}_2$  and 0.2M  $\text{SnCl}_2$

Cyclic voltammetry was used to define the redox properties of Cu-Sn alloy deposition processes. It was carried out using the same instrument as previous study. The cell set-up and preparation of electrodes are the same as previous chapter except that Pt plate with planar area of 0.8 cm<sup>2</sup> was used here as working electrode. Figure 5.1(A) shows the CV curves of pure Cu and Sn on a Pt disc electrode in ethaline. Figure 5.1(B) shows the mixture of

0.2M Cu and 0.2M Sn in DES. It can be clearly seen from Figure 5.1(A), the reduction charge of  $\text{Sn}^{2+}$  is significantly higher than that of  $\text{Cu}^+$  or  $\text{Cu}^{2+}$ , despite in the same concentration. As suggested by Table 5.1, even the cathodic charge of  $\text{Sn}^{2+}$  is slightly higher than the total charge of  $\text{Cu}^+$  and  $\text{Cu}^{2+}$  reduction.

Figure 5.1(B) shows the cyclic voltammetry of an equimolar mixture (0.2 M) of  $\text{CuCl}_2$  and  $\text{SnCl}_2$  in ethaline. Three reduction processes can be distinguished from the partially overlapped peaks initiated at -0.25V. The most positive one of these at -0.35V shows the  $\text{Cu}^{2+}$  reduction dominating process. The peak at -0.7V shows the deposition of a Sn rich phase. The unobvious peak between the above two can be ascribed to the reduction of  $\text{Cu}^+$ , which has been discussed in detail by A. Alhaji<sup>[1]</sup>. The total cathodic charge of the mixed Cu/Sn salts was close to the sum of solo Cu and solo Sn reduction. The occurrence of the peak at -1.4V can be supposed to the accelerated Cu nucleation on Sn underlayer from the previous scan, which will be explained in detail in 5.2. The positively shift of Cu/ $\text{Cu}^+$  oxidation peak from -0.75V in DES containing only Cu to -0.35V in that containing both Cu and Sn salts can be regarded as an evidence of formation of alloy

As we all know, electrodeposition of Cu-Sn alloys in aqueous solution turns to be difficult because of great difference (around 0.5V) between the reduction potentials of  $\text{Cu}^{2+}$  and  $\text{Sn}^{2+}$  in absence of additive. Suitable complexing agent has to be searched to unify the potential positions, which is indispensable to the codeposition. While herein the potential gap between these two has been reduced to less than 0.2V even with partially overlapping. This makes the occurrence of codeposition of Cu and Sn become possible without any additive.

	Q <sub>c</sub> (mC)	Q <sub>a</sub> (mC)
Pure Cu	3.57	5.86
Pure Sn	3.73	36.2
1:1 Cu:Sn	8.42	20.03

**Table 5.1** Comparison of total cathodic and anodic charge density of Cu-Sn alloy (0.2M Cu + 0.2M Sn) with pure Cu (0.2M) and pure Sn (0.2M) in ethaline.

## 5.2 Chronocoulometry

Chronocoulometry is one classical electrochemical technique used to measure charge as a function of time. Abbott et al applied chronocoulometry of Cu on a Pt disc electrode in 0.01M CuCl<sub>2</sub> from ethaline and suggested that metal growth was diffusion controlled [2].

In the current study, the same concentration of metal salts (0.2M CuCl<sub>2</sub> or 0.2M SnCl<sub>2</sub>) was used and the chronocoulometric response of a Cu (1.77 mm<sup>2</sup>) and Sn (2 mm<sup>2</sup>) disc electrode was measured. Chronocoulometry plots that compare depositions on different substrates at applied potential of -0.65V and -0.8V was shown in Figure 5.2. Tin is supposed to grow faster than copper due to a larger over-potential which can be found in cyclic voltammetry. In contrast, at -0.6 V copper grows in comparable kinetics with Sn, which we can assume tin also follows reported instantaneous mechanism of copper deposition in this DES<sup>[1]</sup>. While at more negative potential of -0.8 V, copper response on copper substrate is lower than tin on two substrates. From these results, we could assume that copper growth is

not so sensitive to potential drop compared to tin. Under both conditions, copper growth on tin substrate shows the fastest kinetics than the others showing that codeposition has even faster response than separate metal. The plots of charge versus  $t^{1/2}$  are linear for Cu or Sn on Cu or Sn substrates over longer times suggesting the processes are not purely diffusion controlled.

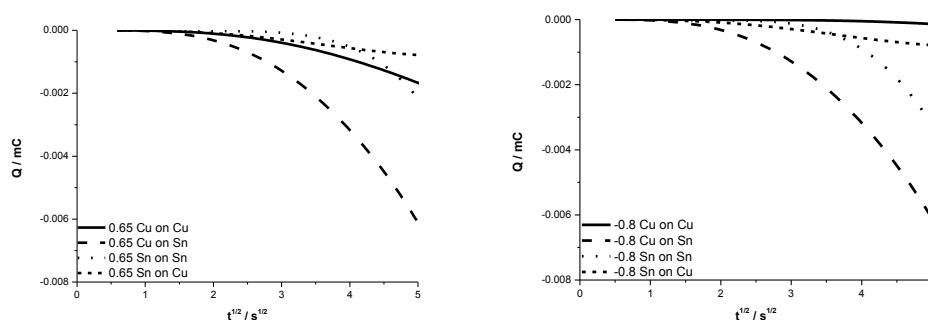


**Figure 5.2** Chronocoulometry for  $0.2M$   $CuCl_2$  or  $0.2M$   $SnCl_2$  from ethaline (A) at  $-0.65V$  and (B) at  $-0.8V$  using a Cu or Sn disc as working electrode as stated.

Chronocoulometry plots at different electrodeposition potentials from  $-0.65V$  to  $-0.8V$  are recorded and shown in Figure 5.3 for Cu on Cu and Sn on Sn. The chronocoulometry response for the deposition of copper and tin shows that the change in charge density of tin on tin is larger than for copper on copper and it is also more potential dependent. This suggests that the tin content in the alloy will depend not only the solution composition but also the applied potential in greater extent than copper. However in this case which both metals are deposited, the resultant copper content will be decided by not only the reduction potential but also the metal which has already been deposited. This leads to a complex model of alloy deposition to analysis.

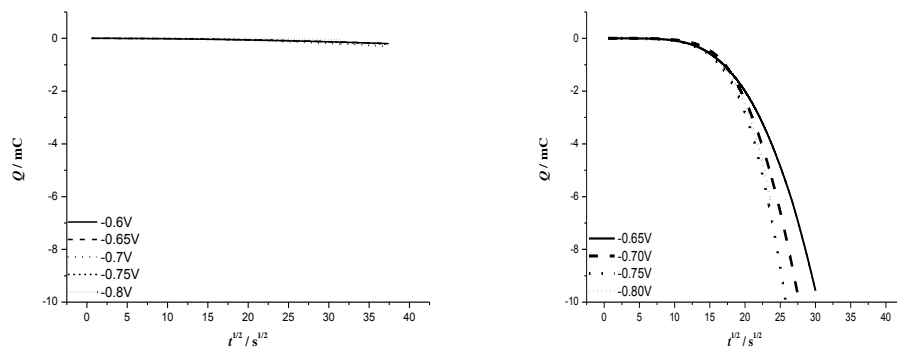


**Figure 5.3** Chronocoulometry for (A)  $0.2M$   $CuCl_2$  on  $Cu$  working electrode and (B)  $0.2M$   $SnCl_2$  on  $Sn$  working electrode at different applied potentials

## 5.3 Electrodeposition from ethaline containing 0.2 M $\text{CuCl}_2$ +0.2 M $\text{SnCl}_2 \cdot 2\text{H}_2\text{O}$

### 5.3.1 Galvanostatic deposition

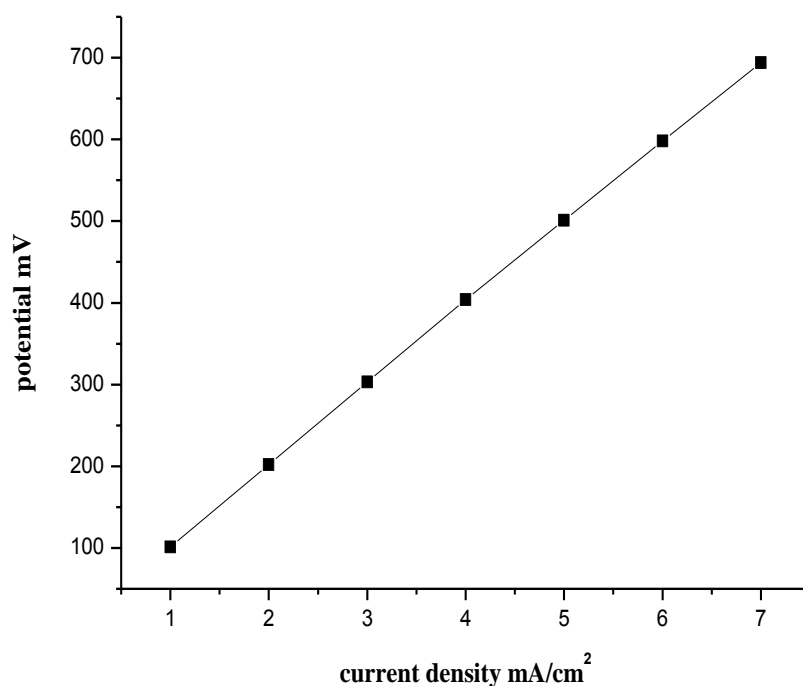


*Figure 5.4* The potential-current curve recorded during galvanostatic electrodeposition experiments on steel plates in ethaline containing 0.2M  $\text{CuCl}_2$  and 0.2M  $\text{SnCl}_2$  at 80 °C.

Galvanostatic deposition was carried out under stirring conditions (300 rpm) in a cell at 80 °C warmed by thermostatic jacket. The alloys were deposited on steel substrate which was etched in 10v%  $\text{H}_2\text{SO}_4$  for 10 min

followed by rinsing and ultrasonic cleaning in acetone before using. Graphite was employed as counter electrode and Pt wire was used as reference in this case. Deposition time was calculated depending applied current density to obtain around 5  $\mu\text{m}$  thick deposits. The final deposits were sequentially rinsed with deionized water and dried with a flow of air.

The potentials recorded during galvanostatic experiments at different current densities (from 1  $\text{mA}/\text{cm}^2$  to 7  $\text{mA}/\text{cm}^2$ ) are seen in Figure 5.4. It revealed that the depositing potential increases significantly when the applied current increased. It's almost a linear relationship between the out-coming potential and deposition currents,

### 5.3.2 Surface morphology and composition of deposit

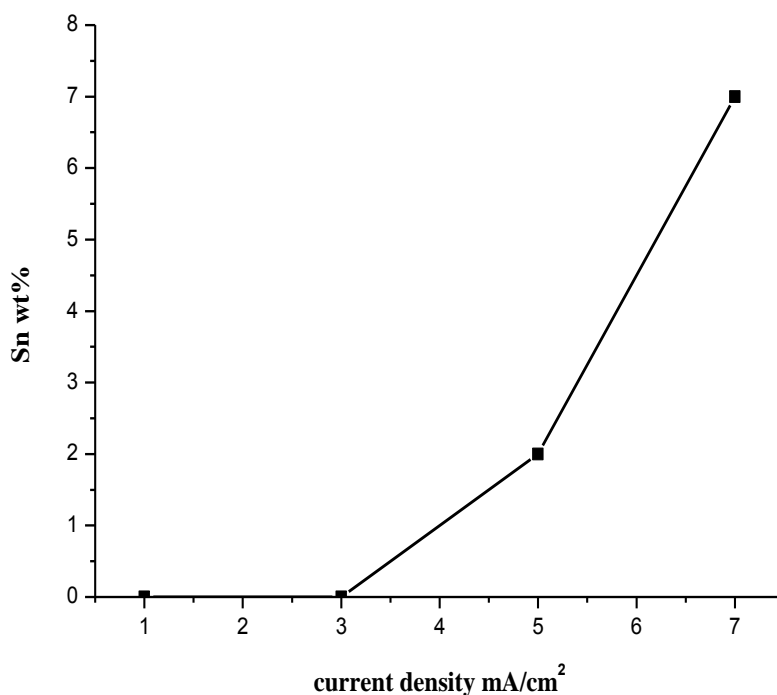


*Figure 5.5 Tin content as a function of current density for the deposits prepared on steel plates in ethaline containing 0.2M CuCl<sub>2</sub> and 0.2M SnCl<sub>2</sub> at 80 °C*

Figure 5.5 shows the weight percentage of tin as a function of current density and it can be seen that tin can be deposited only when applied current is higher than 3 mA/cm<sup>2</sup>. Increasing the current density yields increased content of tin in the deposits. However since the layers start to show black powdery deposit when applied current is higher than 7 mA/cm<sup>2</sup>,

the maximum of tin content which can be obtained under this condition with homogeneous surface will be approximately 7 wt%.

As discussed in previous section, Cu shows faster deposition kinetic than Sn under certain potentials and turns to be opposite when the potential moves to more negative direction. From the relationship between current density and potential, we can conclude that resultant potentials here are generally more positive than -0.7V under which condition copper shows faster deposition kinetics than tin. This means that with the same applied current on the bath containing both salts, copper should be easier to be deposited than tin. This agrees with composition analysis, copper tends to be reduced more easily than tin.

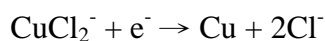
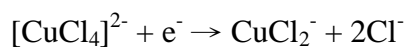
Meanwhile, current efficiency was calculated by comparing the actual and theoretical weight deposited according to Faraday's law. The results are out of our expectations: 246% (1 mA/cm<sup>2</sup>) ~ 153% (2 mA/cm<sup>2</sup>) ~ 135% (3 mA/cm<sup>2</sup>) ~ 165% (4 mA/cm<sup>2</sup>) ~ 126% (5 mA/cm<sup>2</sup>) ~ 157% (6 mA/cm<sup>2</sup>) ~ 166% (7 mA/cm<sup>2</sup>). From the element analysis, neglectable oxide exists in the layer. Since no similar results have been reported so far and these results have been confirmed by at least three repetitions, we can propose possible reactions occur in the eutectic during deposition process.

From the study on separate addition of copper or tin in ethaline which was carried out by S. Ghosh et.al<sup>[3]</sup> lately, comparable diffusion coefficient for Cu<sup>2+</sup> and Sn<sup>2+</sup> species were observed in ethaline.

Possible reactions in system containing only copper salt can occur like:

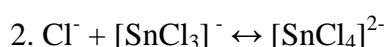
1.  $\text{Cl}^- + \text{CuCl}_2 \leftrightarrow [\text{CuCl}_3]^-$
2.  $\text{Cl}^- + [\text{CuCl}_3]^- \leftrightarrow [\text{CuCl}_4]^{2-}$

In addition, copper was reduced through a two-step mechanism as followed and the first electron exchange is reversible:

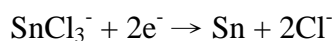


It was also proved that Cu(I) complexes can be stable in this solvent at certain level<sup>[4]</sup>.

Sn speciation formed in the solvent is supposed to be like:



Tin was reduced via a two electron transfer route from  $\text{SnCl}_3^-$  ligand which is an irreversible process:



We can assume that complexation may occur between the existing species of copper and tin. Such as  $[\text{CuCl}_3]^-$  with  $[\text{SnCl}_3]^-$ ,  $\text{CuCl}_2^-$  with  $[\text{SnCl}_3]^-$ , which resulted in intermetallic complexes with reduced activation energy. The applied potential generates the co-deposition of both copper and tin in this case.

Due to the activation gap between the oxidation of  $\text{Sn}^{2+}$  and  $\text{Cu}^{2+}$ , replacement reaction may happen between reduced Sn and  $\text{Cu}^{2+}$  which generates two portion of  $\text{Cu}^+$ . Due to the limited stability of  $\text{Cu}^+$  species in this solvent, auto-reduction may occur and reduced Cu can be obtained.

This proposal can be confirmed by the reduced current efficiency when the solvent containing 0.3 M  $\text{SnCl}_2$  and 0.05 M  $\text{CuCl}_2$  was used in the following study. Because of almost one magnitude difference between the concentrations of these two salts, complexity formed decreased greatly compared to previous bath composition. Co-deposition of the two metals happens in lower extent resulting in decreased replacement.

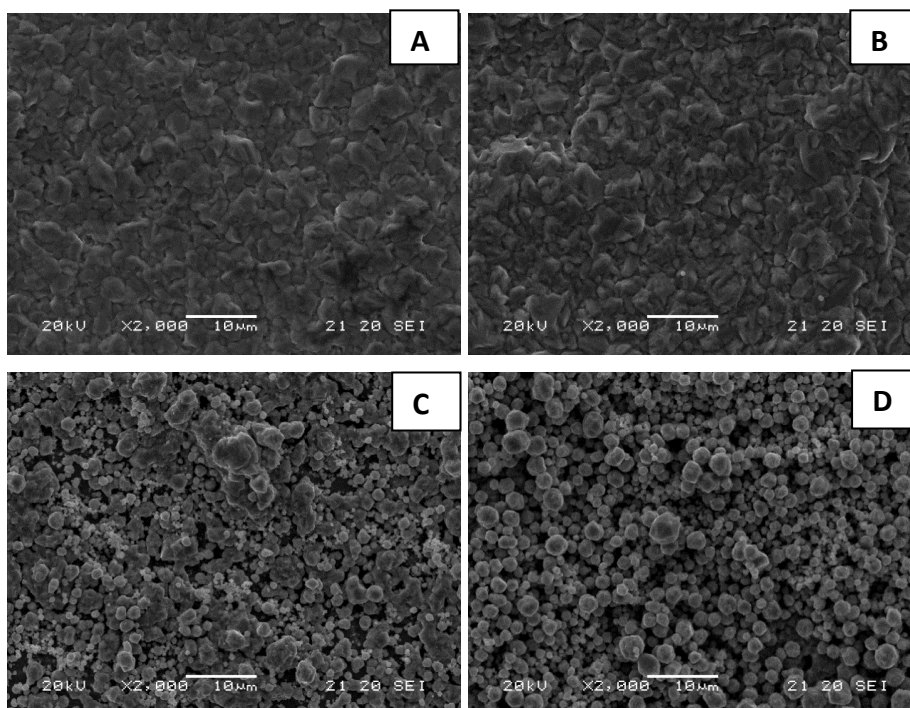


**Figure 5.6** SEM images of deposits obtained during galvanostatic electrodeposition experiments on steel plates in ethaline containing 0.2 M  $\text{CuCl}_2$  and 0.2 M  $\text{SnCl}_2$  at 80 °C at current densities of (A) 1  $\text{mA}/\text{cm}^2$ , (B) 3  $\text{mA}/\text{cm}^2$ , (C) 5  $\text{mA}/\text{cm}^2$  and (D) 7  $\text{mA}/\text{cm}^2$ .

Figure 5.6 shows the surface morphology of deposits prepared at currents corresponding to Figure 5.5. It can be seen that the layer prepared at 1 or 3  $\text{mA}/\text{cm}^2$  is rather compact which is typical for pure Cu film. When Sn starts to be deposited in the alloy, grains tend to grow in vertical direction and aggregate in larger size even though tin content is as low as 2 wt%. With the further increasing of tin content in the film, at higher currents, grains show more regular shape and overlap on each other. The anomalous growth pattern results in a porous morphology and loose microstructure.

## 5.4 Electrodeposition from ethaline containing 0.1 M CuCl<sub>2</sub>+0.3 M SnCl<sub>2</sub>·2H<sub>2</sub>O

For the consideration of corrosion resistance and mechanical properties, layer containing higher content of tin is required. As known, composition of deposited films is highly dependent on the composition of metallic species in the bath. As a result, bath containing 0.3 M SnCl<sub>2</sub> and 0.1 M CuCl<sub>2</sub> was adopted to adjust the composition of layers deposited.

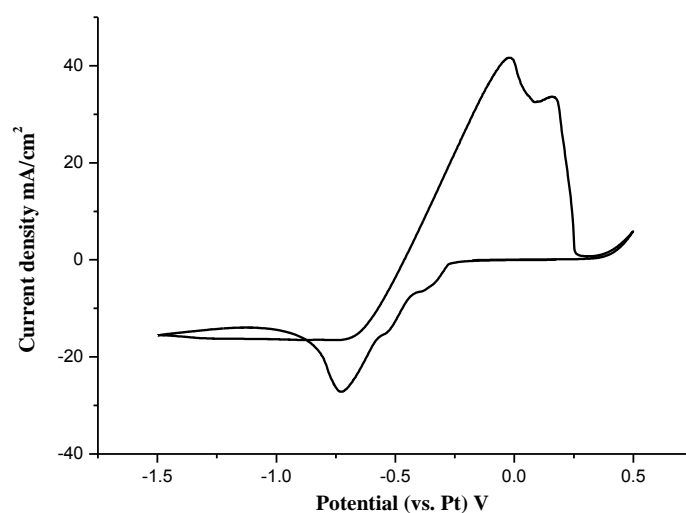


**Figure 5.7** Voltammograms (20 mV/s) for a Pt electrode (0.8 cm<sup>2</sup>) immersed in ethaline containing 0.1 M CuCl<sub>2</sub> and 0.3 M SnCl<sub>2</sub>

Cyclic voltammogram recorded in ethaline containing 0.3 M SnCl<sub>2</sub> and 0.1 M CuCl<sub>2</sub> shows three peaks for reduction process which is similar to bath with equal concentration of metallic salts 0.2 M. The three peaks locate around -0.35 V, -0.5 V and -0.75 V.

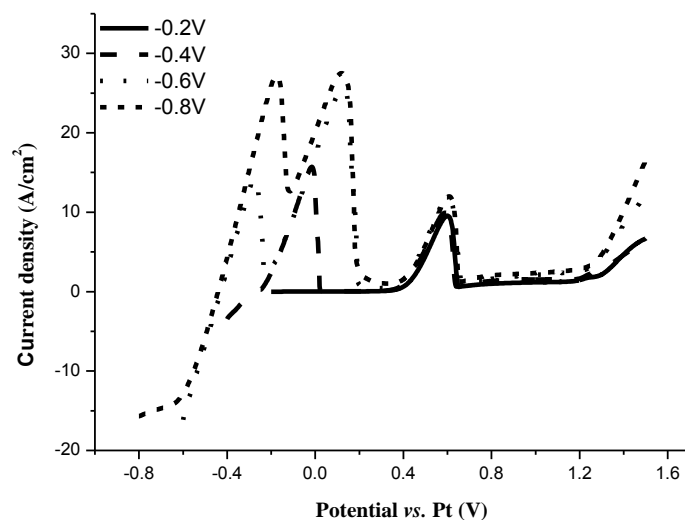


**Figure 5.8** Stripping voltammograms (20 mV/s) of deposits obtained at indicated potentials for 10 s on a Pt electrode in ethaline containing 0.1 M  $\text{CuCl}_2$  and 0.3 M  $\text{SnCl}_2$

Anodic stripping experiments were used to analyze the formation of Cu-Sn deposits, using the same cell setup as in cyclic voltammetry. Figure 5.8 shows the linear stripping curves for the deposits grown potentiostatically fixed at different potentials for 10s. The stripping of deposit formed at -0.2V shows only one anodic peak at 0.5V which correlates to electrochemical decomposition of solvent, that is, oxidation of  $\text{Cl}_3^-$  ions in the solution<sup>[5]</sup>. This indicates that nothing has been deposited at -0.2 V vs. Pt. With decrease of reduction potential to -0.4V, a new oxidation peak appeared around 0V which is typical for copper stripping in this solvent from previous study. When the deposits were grown at -0.6V or -0.8V, an

additional oxidation process takes place around  $-0.3\text{V}$  which is mostly related to stripping of alloy.

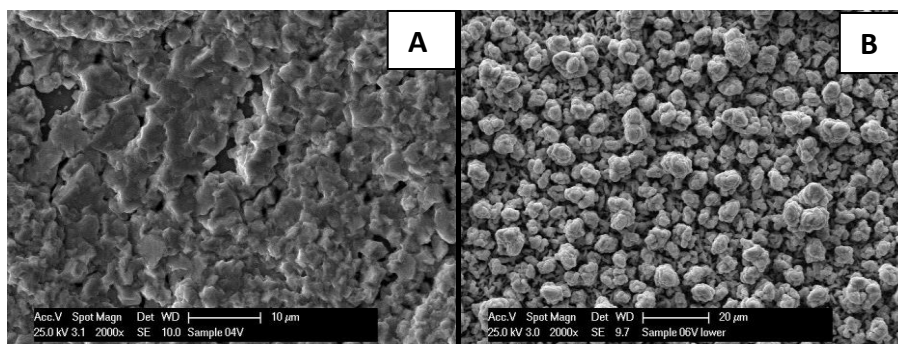


**Figure 5.9** SEM images of deposits obtained during potentiostatic electrodeposition experiments on steel plates in ethaline containing  $0.1\text{ M CuCl}_2$  and  $0.3\text{ M SnCl}_2$  at  $80\text{ }^\circ\text{C}$  at potentials of (A)  $-0.4\text{V}$  and (B)  $-0.6\text{V}$  vs. Pt

Potentiostatic deposition with longer time duration was carried out at above mentioned potentials. Metal can be hardly deposited at  $-0.2\text{V}$  and layer obtained at  $-0.8\text{V}$  shows inhomogeneous color distribution which cannot be regarded as a coating. The morphology of layers prepared at  $-0.4\text{V}$  and  $-0.6\text{V}$  are shown in Figure 5.9. As we can see, reduction process carried out at  $-0.4\text{V}$  resulted in plate-shaped films with obvious pores and cracks. However, completely different pattern on microstructure can be generated using  $-0.6\text{V}$  as reduction potential. Grains grow vertically from substrate and not join with each other. Vacancies can be shown in surrounding space of each grain and shows agreement with the growth kinetically faster than 3D instantaneous growth as studied previously. The significantly different morphology between the deposits prepared at  $-0.4\text{ V}$  and  $-0.6\text{ V}$  can be ascribed to the different reduction currents which are  $2\text{ mA/cm}^2$  and  $5\text{ mA/cm}^2$ . This also increases Sn content from  $9.37\text{wt}\%$  Sn at  $-0.4\text{V}$  to  $27.89\text{wt}\%$  at  $-0.6\text{ V}$  which can be seen from the EDXS analysis in

Figure 5.10. The signal of Fe can be attributed to the presence of steel substrate.

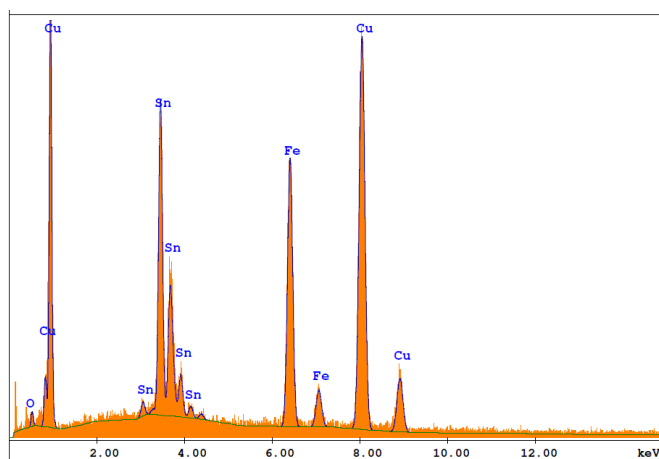


**Figure 5.10** EDS mapping of film deposited from ethaline at  $-0.6V$  containing  $0.1 M CuCl_2$  and  $0.3 M SnCl_2$  at  $80\text{ }^\circ C$  at a current density of  $5\text{ mA/cm}^2$

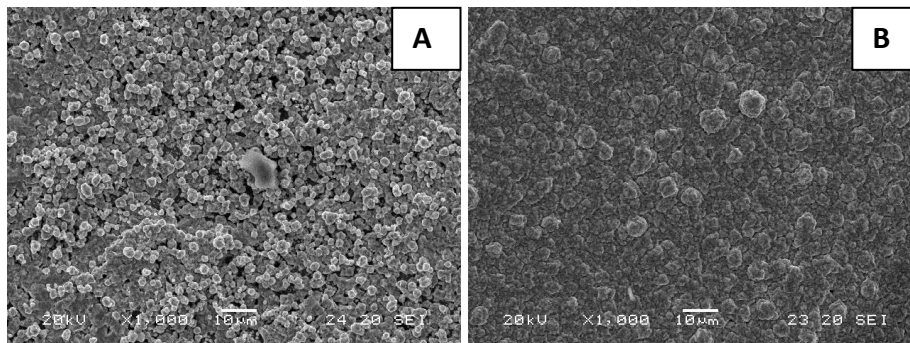


**Figure 5.11** SEM images of deposit obtained from ethaline containing  $0.1 M CuCl_2$  and  $0.3 M SnCl_2$  at  $80\text{ }^\circ C$  at current densities of (A)  $1\text{ mA/cm}^2$  and (B)  $4\text{ mA/cm}^2$

It is possible to control the composition of the deposit by carefully controlling the applied potential to produce different deposition kinetics but this method of kinetic control is notoriously unreliable due to varied

operation parameters. More often in practical applications, current is controlled to achieve required deposits. As shown in Figure 5.11, deposition current density was fixed at  $1 \text{ mA/cm}^2$  and  $4 \text{ mA/cm}^2$ . The grains grown at  $1 \text{ mA/cm}^2$  showed a spherical shape with an average size around several microns in Figure 5.11(A). Grains tend to grow in loosen stereoscopic structure which forms porous surface. When the current density increased to  $4 \text{ mA/cm}^2$ , grown grains tend to connect together. The film can cover the substrate and shows compact morphology with bigger grains distributed on surface.

## 5.5 Electrodeposition from ethaline containing 0.05 M $\text{CuCl}_2$ + 0.3 M $\text{SnCl}_2 \cdot 2\text{H}_2\text{O}$

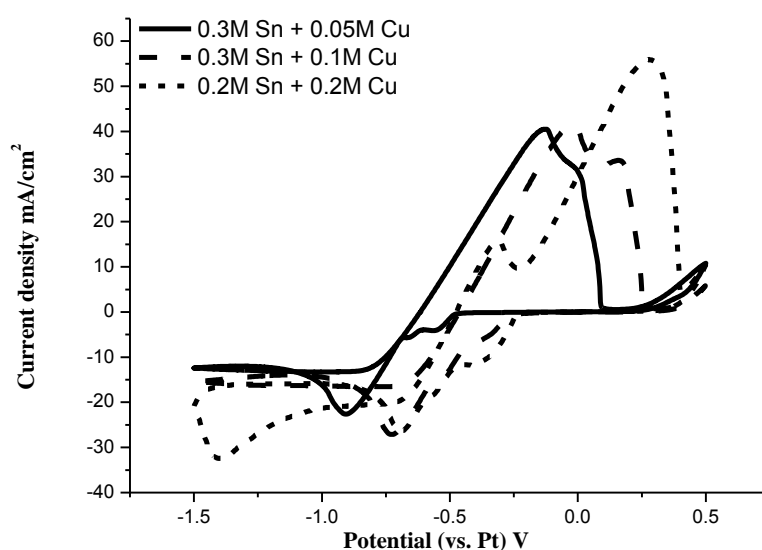


**Figure 5.12** Voltammograms ( $20 \text{ mV/s}$ ) for a Pt electrode ( $0.8 \text{ cm}^2$ ) immersed in ethaline containing metallic salts at different ratio

To deposit layers which contain more tin for better physical and chemical properties, solvents dissolved 0.3 M SnCl<sub>2</sub> and 0.05 M CuCl<sub>2</sub> was further studied. Compared to solvent containing 0.1 M or 0.2 M CuCl<sub>2</sub>, the reduction of Cu rich phase occurs in negatively shifted potentials and in much lower current density. In the meanwhile, oxidation currents of deposits followed the first negative scan exhibited different ratio on the two oxidation processes. The shift in the Cu<sup>2+/+</sup> potential is larger than that would be predicated using the Nernst Equation. It has been recently investigated that the Cu<sup>2+/+</sup> couple shows an ideal Nernstian behavior up to 1 mol/kg. This means a change in Cu<sup>2+</sup> concentration from 0.2 mol/kg to 0.05 mol/kg should result in a shift in redox potential of 36mV. The shift of redox potential observed in Figure 5.12 is larger than that predicted and could result from a number of reasons.

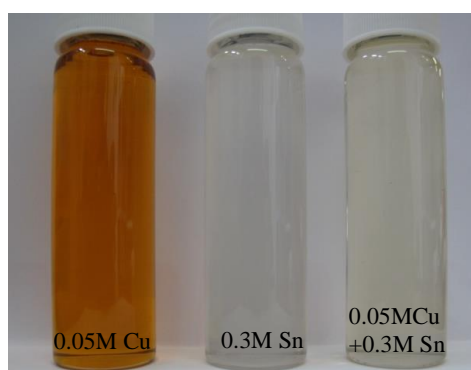
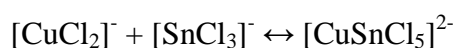


**Figure 5.13** Photos of solvent containing different metallic salts

As observed from the photos of ethaline containing different concentration of metallic species in Figure 5.13, the co-existence of both CuCl<sub>2</sub> and SnCl<sub>2</sub> altered the color of resulting mixtures. This agrees the guess made previously on the complexation formed between copper and tin species in this solvent. Co-complex may occur between existing speciation like following:



### 5.5.1 Galvanostatic deposition

Current density ranging from 1 mA/cm<sup>2</sup> to 5 mA/cm<sup>2</sup> was used to study its influence on composition and morphology of deposits. Reduction current at 1 mA/cm<sup>2</sup> generated homogeneous microstructure as shown in Figure 5.14 with 7.36 wt% Sn. Grains tend to grow into irregular shapes.

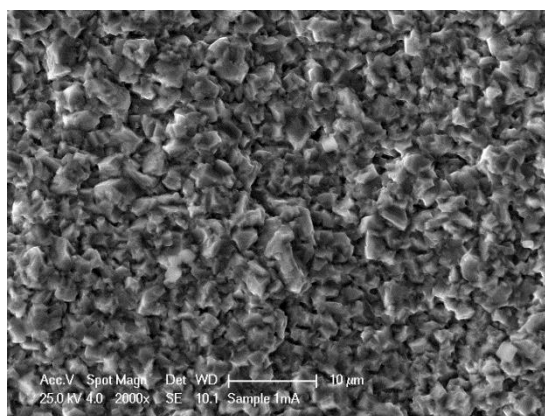


**Figure 5.14** SEM image of deposit obtained from ethaline containing 0.05 M CuCl<sub>2</sub> and 0.3 M SnCl<sub>2</sub> at current density of 1 mA/cm<sup>2</sup>

The films deposited at current density higher than 1 mA/cm<sup>2</sup> split into two significantly different morphologies in the same panel. The upper of deposit is rich in copper while the lower part contains more tin. As shown in Figure 5.15, upper parts of deposits obtained at 2, 3 and 4 mA/cm<sup>2</sup> present different morphologies while lower parts have more similar grain pattern in varied size. The tin content corresponding to the three tops are 12.48, 18.34

and 14.68wt%; meanwhile bottom parts contain 28.07, 26.98 and 26.91wt% Sn in observed area, respectively.

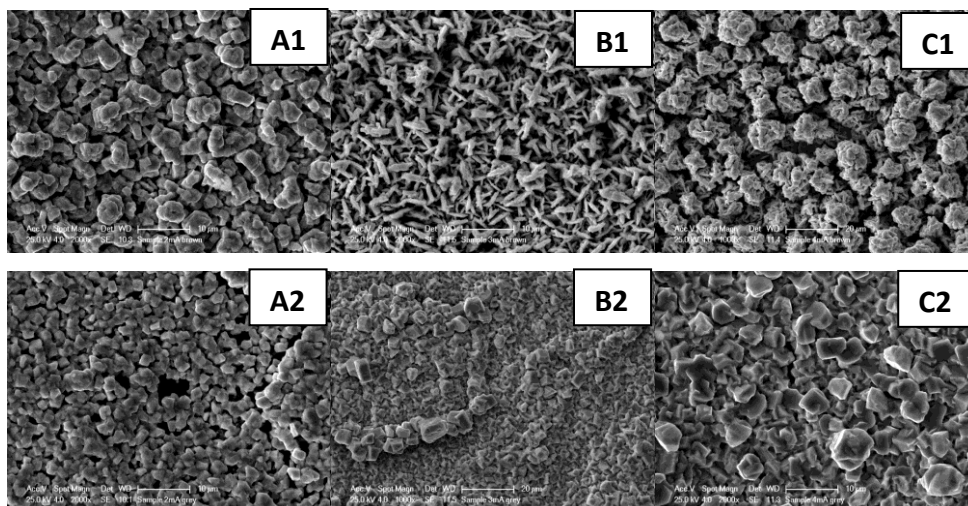


**Figure 5.15** SEM image of deposit obtained from ethaline containing 0.05 M  $\text{CuCl}_2$  and 0.3 M  $\text{SnCl}_2$  at current density of (A)  $2 \text{ mA/cm}^2$  (B)  $3 \text{ mA/cm}^2$  and (C)  $4 \text{ mA/cm}^2$ , in which first line indicates upper part and second line refers to bottom part of deposits.

The difference between the surfaces deposited on positions with various vertical heights can be ascribed to the distinct mass transfer induced by mechanical agitation. Since magnetic stirrer works in the bottom part of the round cell, the lower part of solvent displays higher kinetics in mass transfer for complementing the species of electrodeposition. On the other hand, solvent flow higher horizontally presents much slower mass transfer which leads to insufficient supply of metallic species. This reduction on driving force is beneficial to the copper enrichment in layers.

Current density higher than  $5 \text{ mA/cm}^2$  will generate a layer of black powder on surface of substrate. As seen in Figure 5.16, extremely irregular

shaped grains spread on the whole substrate including hexagonal cuboids, frilled pleats and small granules. Besides, stronger Fe signal can be observed in EDXS analysis due to the porous film deposited. For a compromise of composition and maximum current to obtain a homogeneous visual appearance,  $4 \text{ mA/cm}^2$  was chosen as suitable current density for subsequent deposition.



**Figure 5.16** SEM image of deposit obtained from ethaline containing 0.05 M  $\text{CuCl}_2$  and 0.3 M  $\text{SnCl}_2$  at current density of  $5 \text{ mA/cm}^2$

## 5.5.2 Pulse deposition

Pulse current was applied to improve the homogeneity of layers as well as the morphology. Different frequencies were attempted to study its influence on the resulting behaviors of deposited layers. Since average current of pulse mode was maintained as  $4 \text{ mA/cm}^2$  and duty cycle was set as 50%, peak current of pulse on-time was  $8 \text{ mA/cm}^2$  and duration of whole electrodeposition process remains the same as direct mode.

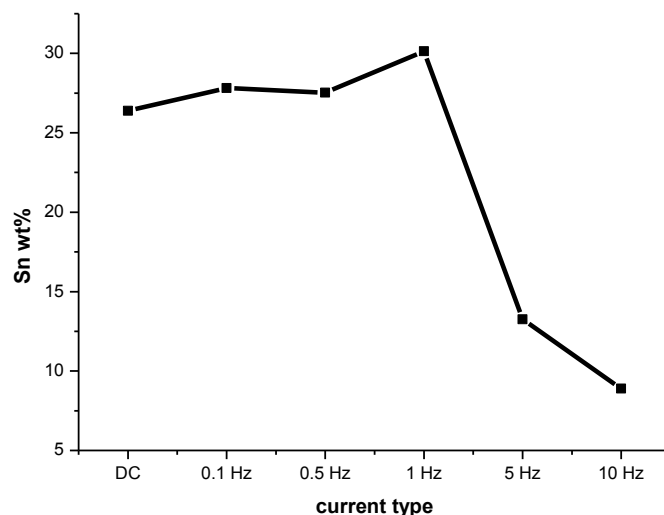


**Figure 5.17** Composition of layers deposited at direct and pulse currents ( $I_{av}=4 \text{ mA/cm}^2$ ) with different frequencies from ethaline containing  $0.05 \text{ M CuCl}_2$  and  $0.3 \text{ M SnCl}_2$

As shown in Figure 5.17, Sn content in the deposits slightly increases when pulse current with frequencies not higher than 1Hz were used. However, 5 Hz and 10 Hz decreased the tin in the layer dramatically. Since there is no similar study revealing the mechanism so far, possible explanations can be proposed. Due to the relatively slower mass transfer in DES, low frequencies of pulse current can be considered as an effective tool to supply metallic sources during off-time. In-time complement can be achieved every time when on-time starts, so more stable bath composition generates higher tin content in deposits. Nevertheless, higher values in frequencies associated with rapid conversions of currents cannot work properly in DES due to the low flow kinetics. Insufficient time for double

layer charging during on-time together with too rapid turns for ions supply during off-time will lead to a lower peak current compared to the value we set. As a result, it is not surprising that 5 Hz and 10 Hz result in layers richer in copper. We can assume that, pulse current works in a different way in ionic liquids compared with aqueous solutions and high frequencies are not applicable in this case.

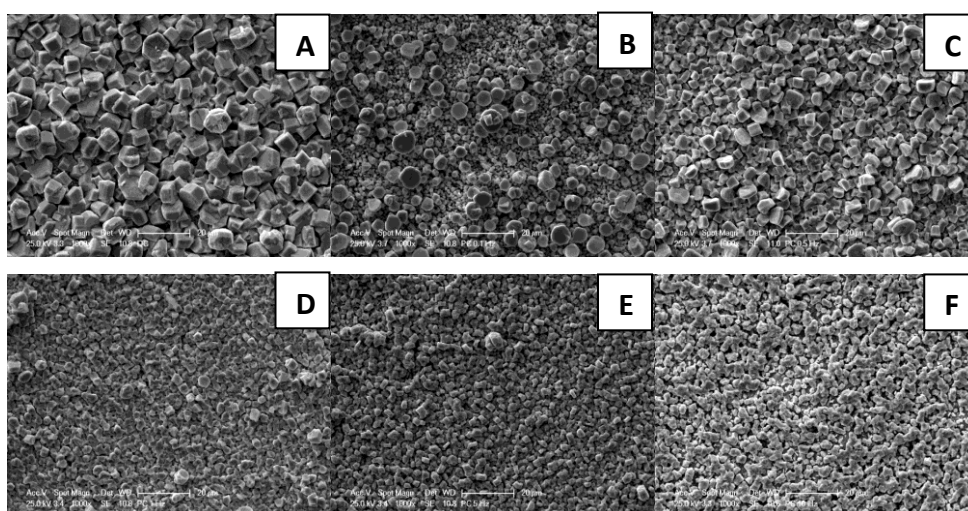


**Figure 5.18** SEM image of deposit obtained from ethaline containing 0.05M  $\text{CuCl}_2$  and 0.3M  $\text{SnCl}_2$  using different current modes of (A) DC (B) PC 0.1 Hz (C) PC 0.5 Hz (D) PC 1 Hz (E) PC 5 Hz (F) PC 10 Hz.

Surface morphology of films deposited with pulse current at different frequencies was compared with that using direct current, shown in Figure 5.18. Obvious refinement of grain size can be identified. Grains tend to grow into smaller size and more compact pattern. The layers prepared at 10Hz shows higher porosity compared to others.

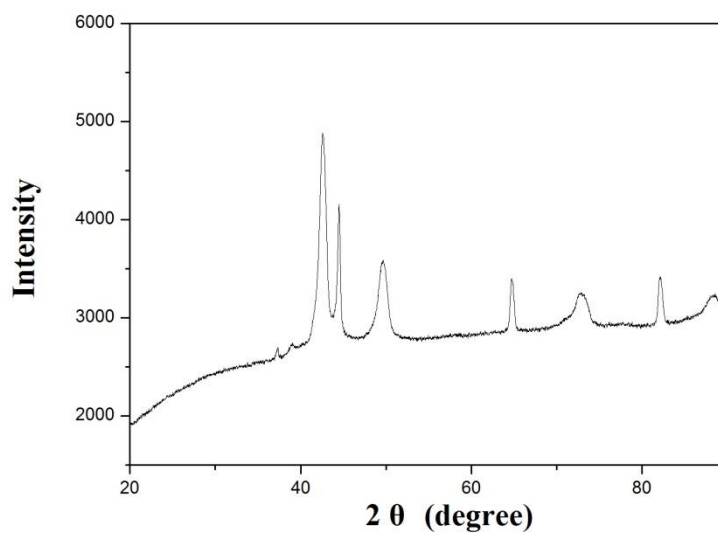


**Figure 5.19** XRD spectra of deposit prepared with pulse current at 10 Hz

Microstructure of film deposited with 10Hz pulse current was studied using XRD in Figure 5.19. In the spectrum, the peaks located at  $2\theta$  equals to  $43^\circ$ ,  $65^\circ$  and  $82^\circ$  come from reflection of the iron substrate. The observed bronze phase fits the data of a cubic structure, space group Fm-3m, lattice parameter  $3.667 \text{ \AA}$ , and crystallite size  $206 \text{ \AA}$ .

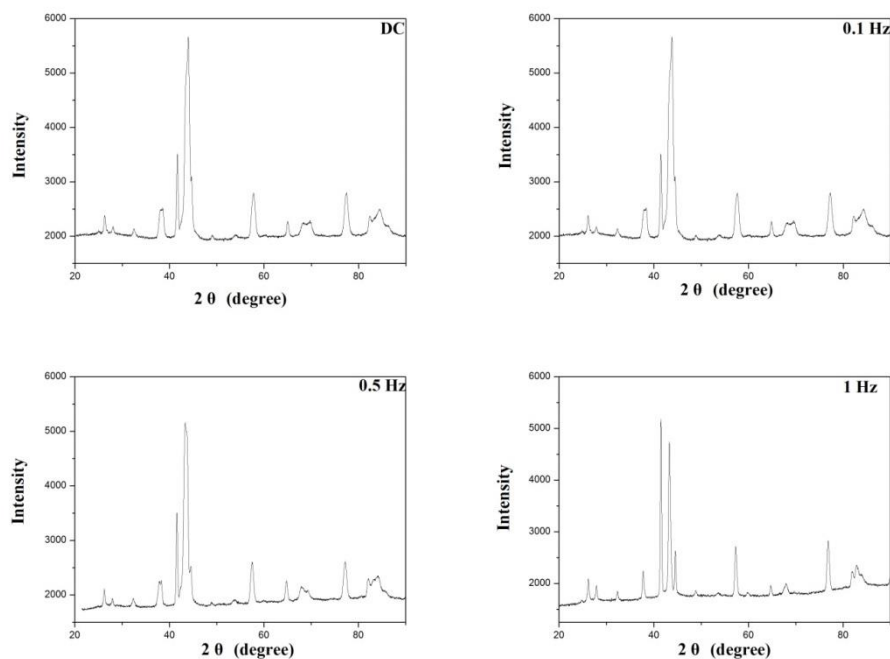


*Figure 5.20 XRD spectra of deposit prepared with direct current and pulse current at different frequencies*

The microstructure of DC deposited film and those deposited with 0.1 Hz, 0.5 Hz and 1 Hz were compared in Figure 5.20. They have the same crystal structure which indicates the existence of tin, copper with  $\text{Cu}_6\text{Sn}_5$  and  $\text{Cu}_3\text{Sn}$  intermetallics. The relative intensity of iron reflection changes because of varied thickness of sample film. The peaks between  $40^\circ$  and  $45^\circ$  can be ascribed to the codeposition of Cu,  $\text{Cu}_6\text{Sn}_5$  and  $\text{Cu}_3\text{Sn}$  while peaks at  $57^\circ$  and  $77^\circ$  come from the Sn deposit. The intensity of tin peaks decreased in order of  $1 \text{ Hz} > \text{DC} > 0.5 \text{ Hz} > 0.1 \text{ Hz}$  which generally agrees with the result obtained from EDXS analysis.

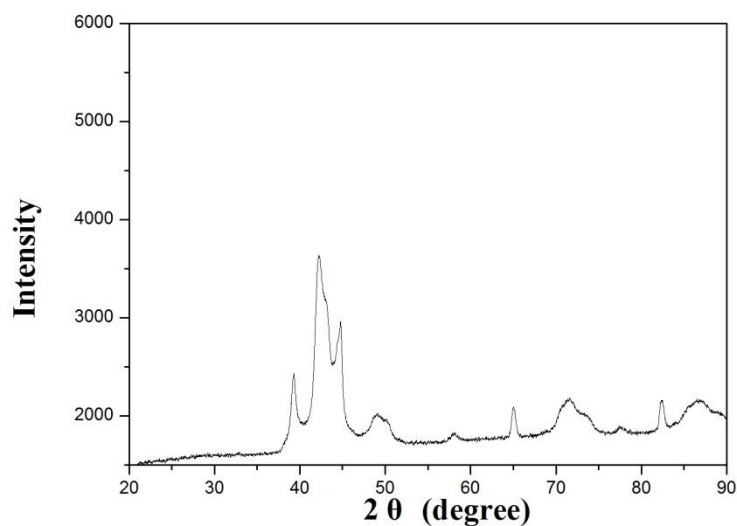


**Figure 5.21** XRD spectra of deposit prepared with pulse current at 5Hz

The diffraction pattern of film deposited at 5 Hz exhibits similar response compared with those observed from samples prepared from described MSA based aqueous bath in second chapter. This suggests that comparable microstructure results can be achieved from DES and aqueous solutions.

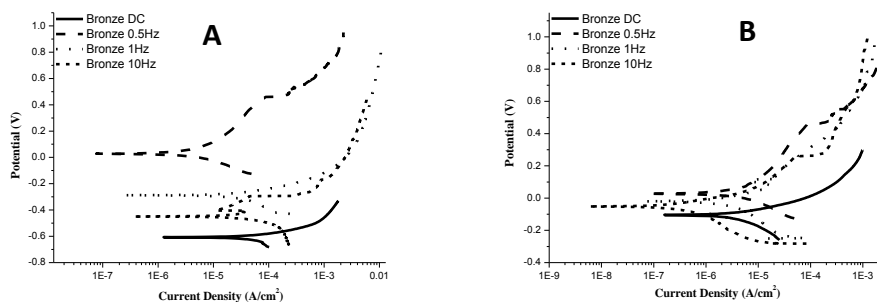


**Figure 5.22** Polarization curves of bronze films deposited on (A) steel plate and (B) Cu underlayer in 0.1 M NaCl solution

To check the corrosion behavior, coatings were deposited on both steel substrate and Cu underlayer to study their electrochemical response by performing potentiodynamic polarization measurement in 0.1 M NaCl solution similar to the study reported in chapter 2. Two different substrates were used: one is steel and other one is Cu underlayer with thickness of 5  $\mu\text{m}$  coated on steel from aqueous bath before alloy deposition. For better clarity, curves of 1 Hz, 0.5 Hz and 0.1 Hz are represented for pulse prepared samples. As shown in Figure 5.22(A), deposits on steel substrate can hardly display any passivation behavior. Corrosion potentials decreased in the order of 0.5 Hz > 1 Hz > 10 Hz > DC and anodic current of layer prepared with 0.5 Hz is lower than others. This doesn't totally follow the tin content in the layer which indicates that composition is not the only element which influences the corrosion property. On the other hand, bronze coatings deposited on copper underlayer exhibit much close corrosion potentials which can be due to the reduced porosity from more compact substrate in this case. In addition, samples deposited with pulse current display quasi-passivation behavior and lower anodic currents than direct current deposited sample. From the above results, we can conclude that pulse current can be beneficial to better corrosion resistance.

## 5.6 Conclusions

In this part of our study, codeposition of copper and tin was investigated in ethaline solvent at 80°C. The simultaneous deposition of copper and tin shows faster kinetic than separate metal. Deposition from solvent dissolved equal molar metallic species was carried out and maximum tin content in layer was as low as 7 wt%. Deposit with ideal composition and visual

appearance can be obtained by applying  $4 \text{ mA/cm}^2$  as deposition current from ethaline containing  $0.3 \text{ M SnCl}_2$  and  $0.05 \text{ M CuCl}_2$ . The tin content can be as high as around 27 wt% which displays silver white colour. Pulse current is beneficial to well-patterned grains and better corrosion resistance while frequencies higher than 1Hz are not feasible in this case for consideration of stable composition of coatings.

## 5.7 References

- [1] A. Alhaji, PhD thesis, Department of Chemistry, University of Leicester, Leicester, 2011.
- [2] A. P. Abbott, K. El Ttaib, G. Frisch, K. J. McKenzie and K. S. Ryder, *Physical Chemistry Chemical Physics*, 11 (2009) 4269-4277.
- [3] S. Ghosh, K. Ryder, S. Roy, *Transaction of the IMF*, 92 (2014) 41-46.
- [4] D. Lloyd, T. Vainikka, L. Murtomaki, K. Kontturi, E. Ahlberg, *Electrochimica Acta*, 56 (2011) 4942-4948.
- [5] K. Haerens, E. Matthijs, K. Binnemans, B. Van der Bruggenb, *Green Chemistry*, 11 (2009) 1357-1365.

## **6 Conclusions and future work**

### **6.1 Conclusions**

As an environmentally friendly replacement of nickel undercoat, bronze can be commonly found on eyeglass frames, knock handles, bells and many other decorative applications since it is a sturdy and durable metal when well cared for. In order to be applied, bronze must fulfill some characteristic as color, brightness and corrosion resistance.

Electrodeposition has been proved to be an easy and economical way to prepare bronze. However, most of commercial baths for bronze coatings induce inconvenience during preparation and waste treatment. This work has been focused on the development of co-deposition of copper and tin alloys from non-toxic baths and the optimization of electrodeposition parameters. Two different baths were tested: an aqueous solution based on methanesulfonic acid and deep eutectic solvent of choline chloride and ethylene glycol. The former one was an industrial product not optimized for decorative application and used under room temperature. This bath avoids the risk of cyanide contained bath during operation and treatment. The bath and the deposition parameters have been studied and optimized so that the resultant coatings from this electrolyte have been successfully applied on decorative metallic articles with satisfying physical and chemical properties. These bronze coatings show comparable luster and corrosion resistance with commercial nickel coatings. However, bronze possesses safer skin contact property.

The effect of anode material as well as deposition current was studied in relation to lifetime of the bath and composition of the alloy. Insoluble anode

was used to substitute commercial copper anode for longer working life of the bath. This can effectively reduce the occurrence of tin oxidation which would lead to poor deposit quality in practical production. Layers obtained in this case show comparable physical properties as Ni layer and those deposited from cyanide based baths. Successful scale up can be realized finally to achieve satisfying bronze coatings on irregular shaped articles.

The deposition bath based on deep eutectic solvent was prepared from simple mixture of chemicals without addition of complexing agents. Separate deposition behavior of copper and tin from this eutectic solvent was studied first and copper-tin alloys were deposited successfully. The use of deep eutectic solvent as deposition electrolyte presents less negative influence to environment as well as longer working duration. Recycling of deposition bath by adding metallic salts and removing impurities can be realized on industrial scale in some companies. This turns to be a more economical way after certain operation cycles compared with aqueous solutions.

Since deposition from DES is quite new research field, it was important to characterize the DES from a physical and electrochemical point of view first and considering the deposition of each metal separately. Two different DES was evaluated from the beginning: ethaline (2:1 Choline chloride and ethylene glycol) and reline (2:1 choline chloride and urea).

Electrochemical characterization of the deposition bath and the relationship between deposition parameter and deposited layer were conducted to determine the deposition mechanism as well as optimize the process.

Different from previous study on copper deposition from ethaline, solubility limit was reached here under warmed condition to have higher

deposition rate. Typical appearance of copper deposit can be observed when deposited on various substrates in this condition and compact microstructure can be obtained without adding any agents. Reline shows much lower deposition rate and obvious decomposition when heated up. This indicates that thermo-stability is necessary when carrying out operation under this temperature. The deposition efficiency was found to be low under DC condition, but the application of a pulse current lead to an improvement.

Tin was deposited only from ethaline. The deposition was difficult resulting in rough surface and non-compact layers. Nicotinic acid, which is a common grain refiner in aqueous solutions, did not bring obvious improvement to the tin microstructure which indicates that the working mechanism of additive is totally different in these systems. Certain studies have proved that reaction mechanism of additives is not the same between aqueous solutions and ionic liquids which makes the investigation on the new system challenging.

Co-deposition of copper and tin was finally investigated and it was found the alloy deposition has much faster growth rate than separate metal. Alloy composition depends on both metal concentration ratio in deposition bath and applied current. Acceptable films, from both chemical and morphological point of view, can be obtained from bath which is rich in tin by applying optimized currents. These bronze coatings show lower lusters than those prepared from aqueous solutions since they do not contain additive.

Even after improvement on deposition rate by optimizing operation conditions, lower growth rate of bronze coatings can be observed in these deep eutectic solvents than in aqueous solutions. Longer time is needed to deposit equal thickness of bronze in this condition.

Pulse current with various frequencies was employed to improve the quality of deposited films. As known in the field of aqueous solutions, pulse current has been proved to be a useful tool for enhancement of metallic coating properties and a considerable number of theoretical models have been induced to explain the way pulse alters the process of electrodeposition. However, this technique just started find application in the study of ionic liquids. On one hand, pulse current acts as an effective grain refiner compared to the direct current deposition. The pulse current induced a microstructural change which led finer grain size with a flat and homogeneous surface. On the other hand, frequency range which can produce the desired results turns to cover the lower values than in that feasible in aqueous solutions. This may due to the relatively higher viscosity and resulting lower mass transfer in deep eutectic solvents. In this case of copper-tin codeposition, exchange reaction occurs during the off-time of pulse cycles, which will generate increased copper content in the deposited layers. Speciation formed in the bath containing both copper and tin salts were investigated by electrochemical techniques and possible complexations were proposed. Mixed controlled mechanism was observed for the metallic concentrations studied in this work, instead of diffusion controlled previously found in ethaline containing lower concentration of copper salt.

By carrying out characterization on the films deposited from both solvents on the steel and copper substrates, it can be found that similar crystalline of bronze phase were obtained as well as analogous corrosion resistance properties. Meanwhile, improved microstructure from pulse set-up brings obvious enhanced properties. The corrosion resistance was

affected by the composition of the films and the synergic effect of the employed substrate.

## **6.2 Future work**

The study demonstrated that bronze can be deposited from DES with proper chemical composition to be applied as decorative coating. Corrosion protection was comparable to coatings deposited from aqueous solution. Brightness has not been improved yet since the study did not focus on use of additives. Future work should study and optimize additives for the deposition of a bright layer. Being a new field of research, this kind of electrolyte is still under continuous development and improvement and different brighteners should be taken into account, considering the deposition mechanism and kinetic differs from the ones in aqueous solution.

Moreover a long term stability of the bath and its component should be evaluated as also the upscaling and use of anodes.